

Alma Mater Studiorum – Università di Bologna

DOTTORATO DI RICERCA IN

Ingegneria Elettrotecnica

Ciclo XXVIII

Settore Concorsuale di afferenza: 09/E2

Settore Scientifico disciplinare: ING-IND/33

INSULATION COORDINATION IN MODERN DISTRIBUTION NETWORKS

Presentata da: Ing. Fabio Tossani

Coordinatore Dottorato

Relatore

Prof. Domenico Casadei

Prof. Carlo Alberto Nucci

Esame finale anno 2016

| | |
|---|-----|
| Introduction | 3 |
| 1. Lightning Induced Overvoltages on Multiconductor Lines | 5 |
| 1.1. Lightning Electromagnetic Pulse Appraisal..... | 5 |
| 1.2. Lightning Electromagnetic Pulse Coupling to Multi-Conductor Lines | 9 |
| 1.2.1. The Agrawal, Price and Gurbaxani model..... | 9 |
| 1.2.2. The LIOV Code..... | 10 |
| 1.2.3. Fields and Overvoltages due to a Stroke Location Close to the Line | 12 |
| 1.3. Transient Ground Resistance of Multiconductor Lines..... | 19 |
| 1.3.1. Inverse Laplace Transform of Sunde's Logarithmic Formula - The Series Expression..... | 19 |
| 1.3.2. Inverse Laplace Transform of Sunde's Logarithmic Formula - The Integral Expression..... | 32 |
| 1.3.3. Inverse Laplace Transform of Sunde's Integrals..... | 38 |
| 1.4. The Response of Multi-Conductor Lines to Lightning-Originated Electromagnetic Pulse | 43 |
| 2. Statistical Evaluation of the Lightning Performance of Distribution Networks..... | 58 |
| 2.1. The Lightning Performance of Overhead Distribution Lines..... | 58 |
| 2.2. The Influence of Direct Strikes on the Lightning Performance of Overhead Distribution Lines | 63 |
| 2.3. The Effect of the Channel Base Current Waveform on the Lightning Performance of Overhead Distribution Lines..... | 73 |
| 2.4. Lightning Performance of a Real Distribution Network with Focus on Transformer Protection..... | 89 |
| 3. Conclusion | 106 |
| 4. Appendix 1 - Inverse Laplace transform of Ground Impedance Matrix - case 1: Sunde's Logarithmic formula..... | 108 |
| 5. Appendix 2 - Inverse Laplace transform of Ground Impedance Matrix - case 2: Sunde's Integral formula..... | 110 |
| 6. References | 117 |

Introduction

Lightning is a major cause of faults on typical overhead distribution lines. These faults may cause momentary or permanent interruptions on distribution circuits. Power-quality concerns have created more interest in lightning, and as a consequence improved lightning protection of overhead distribution lines against faults is being considered as a way to reduce the number of momentary interruptions and voltage sags (*IEEE Std 1410-2010*, 2011).

For the above reasons, the problem of lightning protection of overhead and buried power lines has been reconsidered in recent years due to the proliferation of sensitive loads and the increasing demand by customers for good quality in the power supply (*Nucci et al.*, 2012). This leads to specific requirements concerning insulation and protection coordination, which need also to take into account the presence of distributed generation and of the evolving topology/structure of the smart grid.

Another aspect that deserves proper attention is that in modern distribution networks there is an increasing number of distribution system operators interested in changing the earthing method from solidly grounded to resonant one. This makes it crucial to distinguish single-phase to ground faults from other types of faults. In addition to that, the increasing development and wider interconnection of smart grids leads to more complex network structure and dynamic behaviors.

The appropriate analysis of the response of distribution networks against Lightning Electro Magnetic Pulse (LEMP) requires therefore the availability of more accurate models of LEMP-illuminated lines with respect to the past in order to reproduce the real and complex configuration of distribution systems including the presence of shield wires and of their groundings, as well as that of surge arresters and distribution transformers.

From the distribution system operator point of view, the above models represent a fundamental tool for achieving the estimate of the number of protective devices and of their most appropriate location in order to guarantee a given minimum number of flashovers and outages per year. When dealing with real networks, such an optimization could require huge computational efforts due to the vast number of power components and feeders present in real power systems. This thesis thoroughly analyzes many of the possible engineering

simplifications that, without losing accuracy, can be adopted in the statistical evaluation of the lightning performance of distribution networks in order to limit computational times.

The structure of this thesis is the following:

Chapter one begins with a brief description of the expression adopted in this thesis for the evaluation of the lightning electromagnetic pulse (LEMP). The calculation of the induced voltages is performed by using the LIOV code (Lightning induced overvoltages) which is based on the coupling model by *Agrawal et al* (1980). Particular attention is devoted to the effect of the ground conductivity on the LEMP and on the line parameters. In this regard, this thesis proposes two new analytical expressions for the evaluation of the inverse Laplace transform of the ground impedance matrix elements of a multiconductor overhead line. The first expression is the inverse Laplace transform of Sunde's logarithmic formula (*Sunde, 1968*) and is given in two equivalent forms. The second expression is the inverse Laplace transform of the general integral expression given by *Sunde* (1968). The mathematical derivation of the latter is then extended to the classical case of a multiconductor buried line (*Pollaczek, 1926*) taking into account also the displacement currents (*Sunde, 1968*).

Chapter two is devoted to the statistical evaluation of the lightning performance of distribution networks. The analysis begins with the case of a straight line and discusses the effect of the lightning base channel waveform and of the taking into account of direct strikes on the lightning performance. Finally, a procedure able to evaluate the lightning performance of a real medium-voltage distribution network, which includes a number of lines, transformer stations and surge protection devices is developed and proposed for the analysis of some real cases. Such a procedure allows inferring the characteristics of the statistical distributions of lightning-originated voltages at any point and at any phase of the network. The analysis aims at assessing the expected mean time between failures of MV/LV transformers caused by both direct and indirect lightning strikes. A heuristic technique has been specifically developed to reduce the computational effort despite the non-linear response of the network equipped with surge arresters.

Chapter three concludes the thesis and summarizes the main results.

1. Lightning Induced Overvoltages on Multiconductor Lines

1.1. Lightning Electromagnetic Pulse Appraisal

The expressions in time domain of the electromagnetic field radiated by a vertical dipole of length dz' at a height z' along the lightning channel, assumed as an antenna over a perfectly conducting plane, have been derived by *Master & Uman* (1983) by solving Maxwell's equations in terms of retarded scalar and vector potentials:

$$\begin{aligned}
 dE_r(r, z, t) &= \frac{dz'}{4\pi\epsilon_0} \left[\frac{3r(z-z')}{R^5} \int_0^t i(z', \tau - R/c) d\tau + \right. \\
 &\quad \left. + \frac{3r(z-z')}{cR^4} i(z', t - R/c) + \right. \\
 &\quad \left. + \frac{r(z-z')}{c^2 R^3} \frac{\partial i(z', t - R/c)}{\partial t} \right] \\
 dE_z(r, z, t) &= \frac{dz'}{4\pi\epsilon_0} \left[\frac{2(z-z')^2 - r^2}{R^5} \int_0^t i(z', \tau - R/c) d\tau + \right. \\
 &\quad \left. + \frac{2(z-z')^2 - r^2}{cR^4} i(z', t - R/c) + \right. \\
 &\quad \left. - \frac{r^2}{c^2 R^3} \frac{\partial i(z', t - R/c)}{\partial t} \right] \\
 dB_\varphi(r, z, t) &= \frac{\mu_0 dz'}{4\pi} \left[\frac{r}{R^3} i(z', t - R/c) \right. \\
 &\quad \left. + \frac{r}{cR^2} \frac{\partial i(z', t - R/c)}{\partial t} \right]
 \end{aligned} \tag{1.1}$$

where

- $i(z', t)$ is the current along the channel obtained from the return-stroke current model;
- c is the speed of light;
- R is the distance of the electric dipole from the observation point;

and the geometrical factors are given in Figure 1-1.

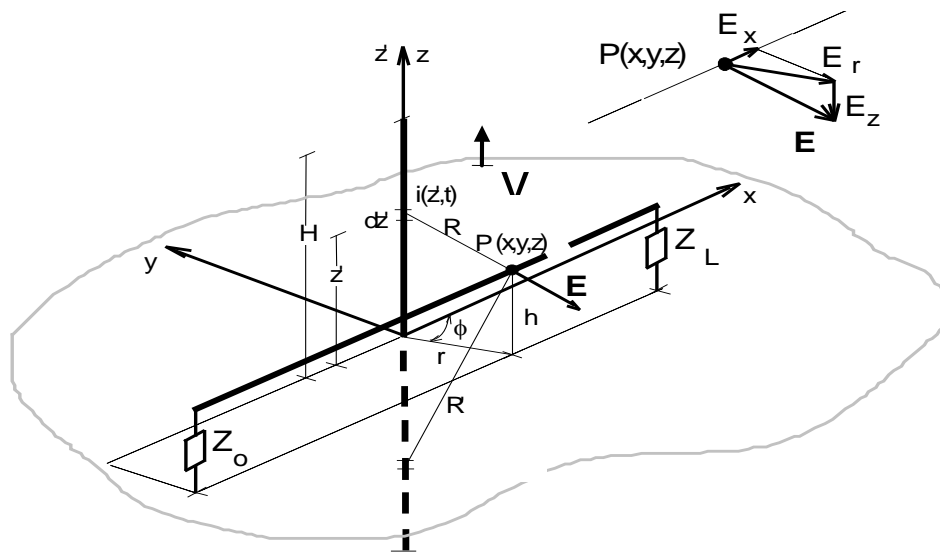


Figure 1-1 – Return Stroke channel

By integrating expressions (1.1) along the channel one obtains the electromagnetic exciting field. The current distribution, as a function of height and time, is given by the so called return-stroke model (*Nucci et al.*, 1990), (*Rakov & Uman*, 1998).

For distances not exceeding a few kilometers, the perfect ground conductivity assumption is a reasonable approximation for the vertical component of the electric field and for the azimuthal component of the magnetic field (*Zeddani & Degauque*, 1990). This can be explained considering that the contributions of the source dipole and of its image to these field components add constructively and, consequently, small variations in the image field due to the finite ground conductivity will have little effect on the total field. On the other hand, the horizontal component of the electric field is appreciably affected by finite ground conductivity. Indeed, for such a field component, the effects of the two contributions subtract, and small changes in the image field may lead to appreciable changes in the total horizontal field (*Rubinstein*, 1996). Although the intensity of the horizontal field component is generally much smaller than that of the vertical one, within the context of certain coupling models it plays an important role in the coupling mechanism (*Master & Uman*, 1984; *Cooray & De la Rosa*, 1986; *Rubinstein et al.*, 1989; *Diendorfer*, 1990; *Ishii et al.*, 1994) and, hence, an accurate calculation method has to be chosen for it.

The exact solution for the problem of an oscillating hertzian dipole over a finite ground is due to *Sommerfeld* (1909) and in terms of magnetic vector potential is given by (*Sommerfeld*, 1949)

$$dA_z(j\omega, r, z) = \frac{\mu_0 I(z', j\omega) dz'}{4\pi} \left(\frac{e^{\frac{j\omega}{c}R}}{R} + \frac{e^{\frac{j\omega}{c}R'}}{R'} - \int_0^\infty \frac{2\mu_E}{n^2\mu + \mu_E} J_0(\lambda r) e^{-\mu(z'+z)} \frac{\lambda}{\mu} d\lambda \right) \quad (1.2)$$

where, $k^2 = \omega^2 \mu_0 \epsilon_0$

$$k_E^2 = \omega^2 \epsilon_0 \epsilon_r \mu + \omega j \mu \sigma$$

$n^2 = k_E^2 / k^2$ and

$$\mu = \sqrt{\lambda^2 - k^2} \quad (1.3)$$

$$\mu_E = \sqrt{\lambda^2 - k_E^2} \quad (1.4)$$

where $I(j\omega)$ is the current of the dipole in the frequency domain, ω is the angular frequency, J_0 is the Bessel function of the first kind of order zero, and $j^2 = -1$. The first two terms in (1.2) are the components of the magnetic vector potential in case of perfect ground; the latter is the Sommerfeld integral, which is present only in case of lossy ground.

The non-null components of the electromagnetic field in the frequency domain due to the dipole can be obtained from the magnetic vector potential by

$$\begin{aligned} E_r(j\omega, r, z) &= \frac{j\omega}{k^2} \frac{\partial^2 A_z}{\partial r \partial z} \\ E_z(j\omega, r, z) &= \frac{j\omega}{k^2} \left(\frac{\partial^2 A_z}{\partial z^2} + k^2 A_z \right) \\ H_\phi(j\omega, r, z) &= -\frac{1}{\mu_0} \frac{\partial A_z}{\partial r} \end{aligned} \quad (1.5)$$

Performing this operation one obtains the electromagnetic field in frequency domain for $z > 0$.

The fields in case of ideal ground can be directly transformed in time domain and are given by (1.1). In case of lossy ground, the following contributions should be added to (1.1):

$$\begin{aligned}
dE_r(j\omega, r, z) &= -j \frac{I(j\omega) dz'}{2\pi\omega\epsilon_0} \int_0^\infty \frac{\mu_E}{n^2\mu + \mu_E} J_1(\lambda r) e^{-\mu(z'+z)} \lambda^2 d\lambda \\
dE_z(j\omega, r, z) &= -j \frac{I(j\omega) dz'}{2\pi\omega\epsilon_0} \int_0^\infty \frac{\mu_E}{n^2\mu + \mu_E} J_0(\lambda r) e^{-\mu(z'+z)} \frac{\lambda^3}{\mu} d\lambda \\
dH_\phi(j\omega, r, z) &= -\frac{I(j\omega) dz'}{2\pi} \int_0^\infty \frac{\mu_E}{n^2\mu + \mu_E} J_1(\lambda r) e^{-\mu(z'+z)} \frac{\lambda^2}{\mu} d\lambda
\end{aligned} \tag{1.6}$$

The total electric and magnetic field is obtained by summing the time-domain contribution of each dipole, taking into account the time delays associated with finite speed of propagation of return stroke front and the electromagnetic fields in air. Recently (*F. Delfino, Procopio, and Rossi 2008; F. Delfino et al. 2008*) numerical techniques that can be utilized to perform these integrals rapidly and efficiently have been developed. However, when the evaluation of the LEMP for a large number of observation points is needed (e.g. when assessing the induced voltages in a real network or in statistical procedures) the calculation of the horizontal field using the exact Sommerfeld integrals is inefficient from the point of view of computer-time. Many simplified expressions exist, and the most commonly adopted one is that proposed independently by Cooray and Rubinstein (*Cooray, 1992; Rubinstein, 1996*) and discussed by *Wait (1997)*. The Cooray-Rubinstein expression is given by

$$E_r(r, z, j\omega) = E_{rp}(r, z, j\omega) - cB_{\phi p}(r, z=0, j\omega) \cdot \frac{\gamma_o}{\gamma} \tag{1.7}$$

where

- $\gamma_o = \omega\sqrt{\mu_o\epsilon_o}$
- $\gamma = \gamma_o\sqrt{\epsilon_r\epsilon_o - \frac{j\sigma}{\epsilon_o\omega}}$
- σ is the ground conductivity;
- $E_{rp}(r, z, j\omega)$ e $B_{\phi p}(r, z=0, j\omega)$ are the radial component of the electric field and the azimuthal component of the magnetic field evaluated as the ground was a perfect conductor

and c is the speed of light in vacuum.

The second term in (1.7) is known in the literature as ‘*surface impedance*’ expression. The surface impedance expression is in good agreement with the Sommerfeld integrals solution for distances not closer than 50 m from the stroke location for $\sigma = 0.01$ S/m, 200 m for $\sigma =$

0.001 S/m (100 m if only the peak is concerned) and approximately 600 m for 0.0001 S/m. The error can be significant if this expression is adopted for smaller distances (Cooray, 2010).

1.2. Lightning Electromagnetic Pulse Coupling to Multi-Conductor Lines

The approach adopted in this thesis stands on the transmission line theory. The basic assumptions of this approximation are that the response of the line is quasi-transverse electromagnetic (quasi-TEM) and that the transverse dimension of the line is smaller than the minimum significant wavelength. The line is represented by a series of elementary sections which is illuminated progressively by the incident electromagnetic field so that longitudinal propagation effects are taken into account. Different and equivalent coupling models based on the use of the transmission-line approach have been proposed in the literature (e.g., see *C. D. Taylor et al. 1965; Agrawal et al. 1980; Rachidi 1993*). The Agrawal model presents the notable advantage of taking into account in a straightforward way the ground resistivity in the coupling mechanism and it is the only one that has been thoroughly tested and validated using experimental results (*Nucci & Rachidi, 2003; Paolone et al., 2009*).

1.2.1. The Agrawal, Price and Gurbaxani model

The coupling equations according to the Agrawal et al. model are given by (*Agrawal et al., 1980*)

$$\frac{\partial}{\partial x} [v_i^s(x, t)] + [L'_{ij}] \frac{\partial}{\partial t} [i_i(x, t)] = [E_x^e(x, h_i, t)] \quad (1.8)$$

$$\frac{\partial}{\partial x} [i_i(x, t)] + [C'_{ij}] \frac{\partial}{\partial t} [v_i^s(x, t)] = 0 \quad (1.9)$$

where

- $[E_x^e(x, h_i, t)]$ is the vector of the horizontal component of the incident electric field (calculated in absence of the line conductors) along the x axis at the conductor's height h_i where the sub-index i denotes the particular wire;

- $[L'_{ij}]$ and $[C'_{ij}]$ are the matrices of the line per-unit-length inductances and capacitances respectively;
- $[i_i(x,t)]$ is the line current vector;
- $[v_i^s(x,t)]$ is the scattered voltage vector, from which the total voltage vector $[v_i(x,t)]$ can be evaluated as

where

$$[v_i(x,t)] = [v_i^s(x,t)] - \left[\int_0^{h_i} E_z^e(x,z,t) dz \right] \quad (1.10)$$

- $E_z^e(x,z,t)$ is the vertical component of the incident electric field (calculated in absence of the line conductors).

Let us assume that the line is terminated on linear terminations represented by the matrices $[Z_{0,ij}]$ and $[Z_{L,ij}]$. The boundary conditions are given by

$$[v_i^s(0,t)] = -[Z_{0,ij}][i_i(0,t)] + \left[\int_0^{h_i} E_z^e(0,z,t) dz \right] \quad (1.11)$$

$$[v_i^s(L,t)] = [Z_{L,ij}][i_i(L,t)] + \left[\int_0^{h_i} E_z^e(L,z,t) dz \right] \quad (1.12)$$

1.2.2. The LIOV Code

In the literature, several approaches have been proposed for the evaluation of the lightning electromagnetic pulse (LEMP) response of distribution networks (e.g., *Nucci et al. (1994)*, *Orzan et al. (1996)*, *Høidalen (2003)*, *Perez et al. (2007)*, *Andreotti et al. (2015)*, *Thang et al. (2015)*, and references therein).

In this thesis the LIOV-EMTP-RV code is adopted for the calculation of the induced voltages. LIOV (“Lightning-induced overvoltages”) (*Nucci & Rachidi, 2003*), (*Borghetti et al., 2004*), (*Napolitano et al., 2008*) is a computer code which allows for the calculation of lightning-induced overvoltages on multiconductor overhead lines above a lossy soil as a function of line

geometry, lightning current wave shape and stroke location, return-stroke velocity and soil resistivity.

LIOV has been developed in the framework of an international collaboration involving the University of Bologna, the Swiss Federal Institute of Technology and the University of Rome La Sapienza. LIOV has been experimentally validated by means of tests carried out on reduced scale setups with NEMP (Nuclear Electromagnetic Pulse) simulators (*Borghetti et al., 2004*), LEMP (Lightning Electromagnetic Pulse) simulators (*Piantini et al., 2007*) and full scale setups illuminated by artificially initiated lightning (*Paolone et al., 2009*).

In order to analyze the response of realistic configurations such as an electrical medium and low-voltage distribution network to a LEMP excitation, the presence of specific line terminations or line discontinuities (e.g. surge arresters) is to be properly taken into account. To deal with the problem of lightning-induced voltages on complex systems, different interfacing methods between LIOV and EMTP were developed (*Nucci et al., 1994*), (*Borghetti et al., 2004*), (*Napolitano et al., 2008*).

For the LEMP-to-line coupling solution, LIOV adopts the Agrawal *et al.* model, under the assumption that the response of the line is TEM (or quasi-TEM if the effect of the line losses is accounted in the surge propagation). The Agrawal *et al.* transmission line equations are solved by means of a one-dimensional Finite Difference Time Domain (FDTD) technique (*Nucci et al., 1994*), (*Borghetti et al., 2004*), (*Napolitano et al., 2008*). In particular, a second order FDTD scheme is adopted, according to which the line length is discretized in a finite number of nodes, at which scattered voltages, currents and the horizontal component of the external electromagnetic field are evaluated at each time step (*Paolone et al., 2001*), (*Nucci & Rachidi, 2003*), (*Borghetti et al., 2004*), (*Napolitano et al., 2008*).

1.2.3. Fields and Overvoltages due to a Stroke Location Close to the Line

The presence of objects nearby distribution lines may cause indirect overvoltages due to very close lightning return strokes. In these cases, the evaluation of the LEMP by using the Cooray-Rubinstein approach may lead to significant errors. Furthermore, when calculating the incident voltage, the numerical evaluation of integral (1.10) is necessary, due to the height-dependence of the integrand. In the following, the analysis of fields and overvoltages due to a return stroke close to a distribution line is presented.

Figure 1-2 and Figure 1-4 show the vertical component of the electric field at a distance $r = 10$ m from the lightning channel for a typical first stroke and subsequent stroke respectively. The comparison is performed at different heights above an ideal ground, showing that the vertical component of the electric field is strongly dependent on the height z (h in the figures). The mean value is also reported. In Figure 1-3 and Figure 1-5 the same comparison is shown but at a distance $r = 20$ m from the lightning channel and in Figure 1-6 and Figure 1-7 at a distance $r = 50$ m; it is clear that, as r increases, the vertical component tends to be constant with height. One can conclude that, if the stroke position is close to a line, the vertical component of the electric field has to be integrated along the coordinate z in (1.10). When the stroke distance is greater or equal 50 m, considering the vertical electric field constant with height is a good approximation.

TABLE 1-1 – PARAMETERS ASSUMED FOR THE RETURN STROKE CURRENTS

| | I_{01} (kA) | τ_{11} (μ s) | τ_{12} (μ s) | n_1 | I_{02} (kA) | τ_{21} (μ s) | τ_{22} (μ s) | n_2 |
|-------------------|---------------|------------------------|------------------------|-------|---------------|------------------------|------------------------|-------|
| First stroke | 28 | 1.8 | 95 | 2 | - | - | - | - |
| Subsequent stroke | 10.7 | 0.25 | 2.5 | 2 | 6.5 | 2 | 230 | 2 |

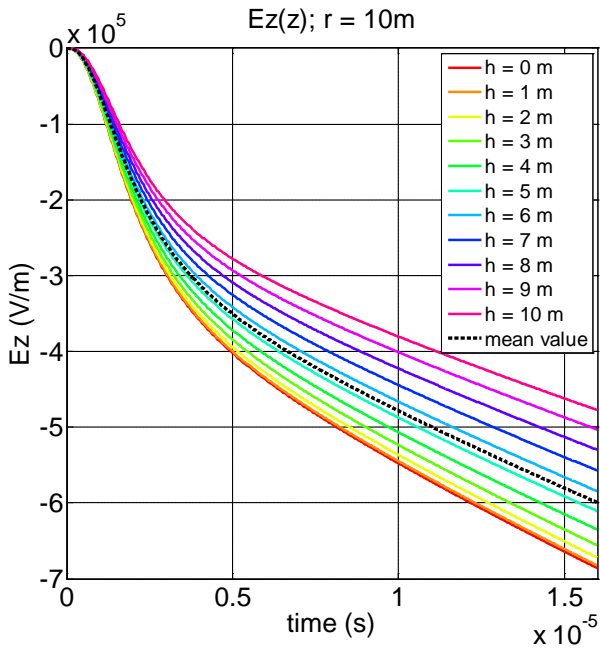


Figure 1-2 – Vertical component of the electric field for $r = 10$ m, at different heights above ideal ground. Channel base current typical of first strokes.

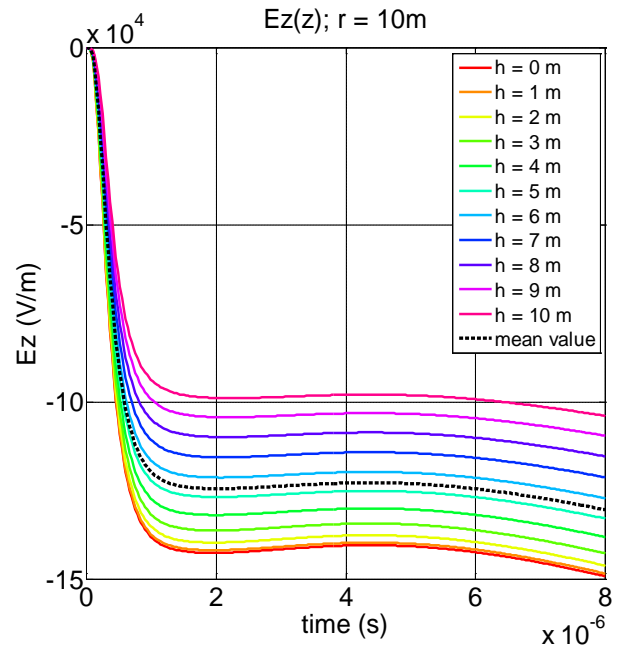


Figure 1-4 – Vertical component of the electric field for $r = 10$ m, at different heights above ideal ground. Channel base current typical of subsequent strokes.

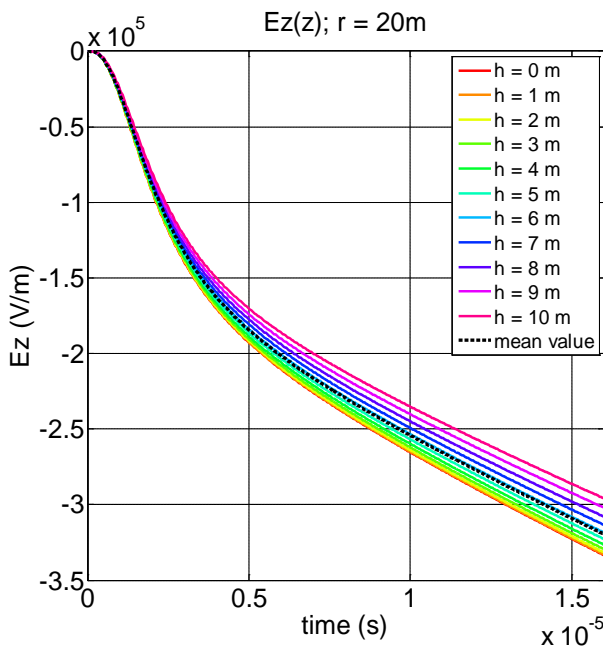


Figure 1-3 – Vertical component of the electric field for $r = 20$ m, at different heights above ideal ground. Channel base current typical of first strokes.

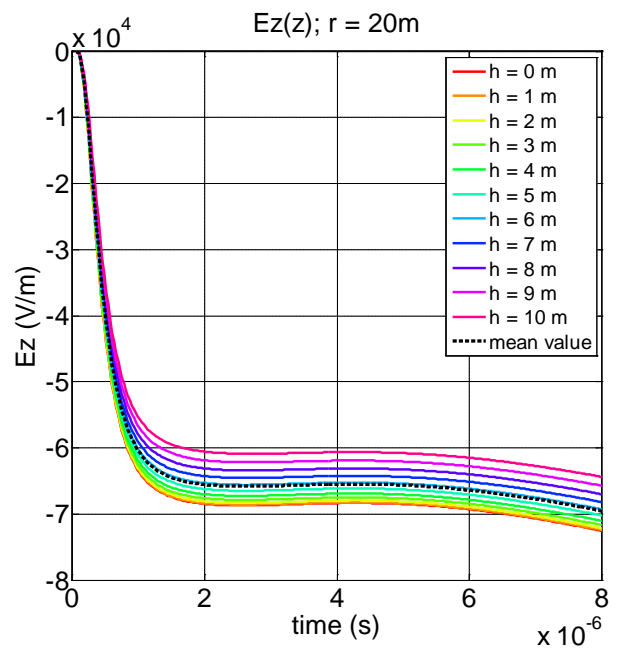


Figure 1-5 – Vertical component of the electric field for $r = 20$ m, at different heights above ideal ground. Channel base current typical of subsequent strokes.

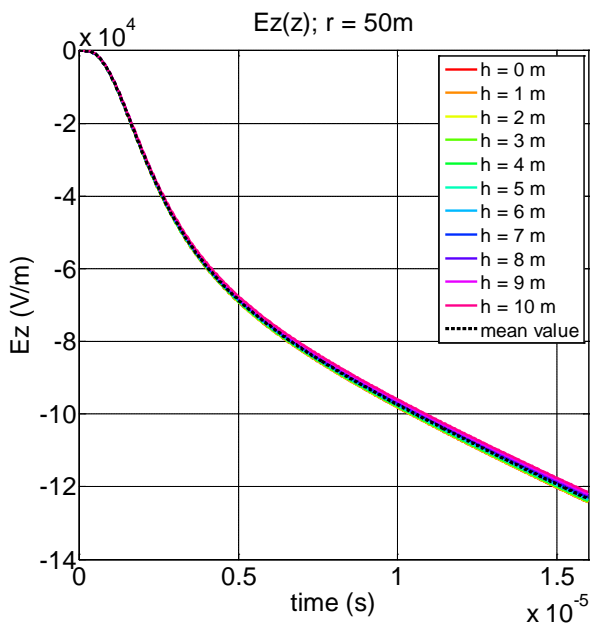


Figure 1-6 – Vertical component of the electric field for $r = 50$ m, at different heights above ideal ground. Channel base current typical of first strokes.

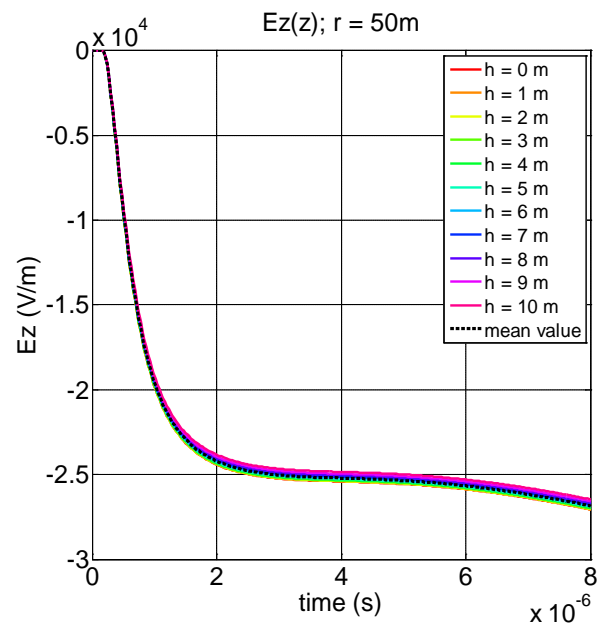


Figure 1-7 – Vertical component of the electric field $r = 50$ m, at different heights above ideal ground. Channel base current typical of subsequent strokes.

The accurate evaluation of the horizontal component of the electric field in the vicinity of the lightning channel can be performed by using Sommerfeld integrals or a FEM model such as the one described in (Borghetti et al., 2013), which is in very good agreement with the solution of Sommerfeld integrals. A time-domain formula for the calculation of the horizontal electric field in the vicinity of the lightning channel has been present in (Barbosa & Paulino, 2010).

In Figure 1-8, the radial component of the electric field for $r = 10$ m, at $z = 10$ m above a lossy ground ($\sigma_g = 1$ mS/m, $\epsilon_r = 10$) due to a first stroke current is shown; the black line refers to the FEM solution, which can be assumed as benchmark, the red one is calculated by using the Cooray-Rubinstein (CR) formula and the blue one by Barbosa et. al formula. The comparison is also reported in Figure 1-10 for the case of a subsequent stroke. The comparison is then repeated for $r = 20$ m and $r = 50$ m. As already mentioned, the CR formula can lead to significant errors if used for the evaluation of the horizontal field in the vicinity of the lightning channel (distance lower than 50 m). The formula by Barbosa and colleagues is, instead, in better agreement with the benchmark solution.

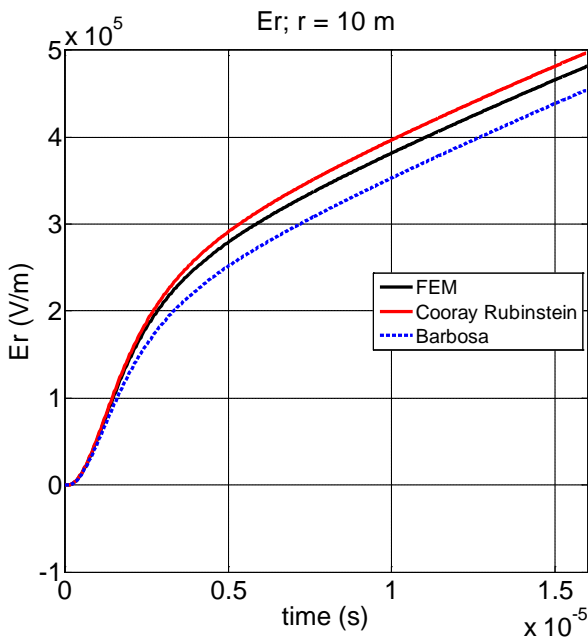


Figure 1-8 – Radial component of the electric field for $r = 10$ m, at $z = 10$ m above a lossy ground ($\sigma_g = 1$ mS/m, $\epsilon_r = 10$). Channel base current typical of first strokes.

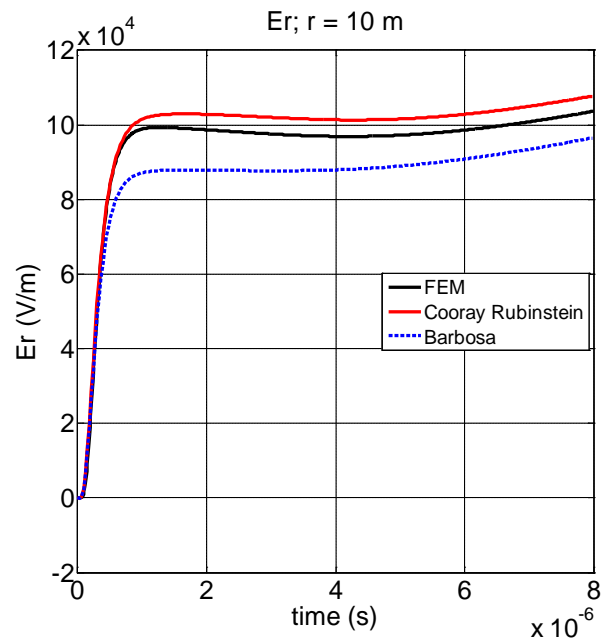


Figure 1-10 – Radial component of the electric field for $r = 10$ m, at $z = 10$ m above a lossy ground ($\sigma_g = 1$ mS/m, $\epsilon_r = 10$). Channel base current typical of subsequent strokes.

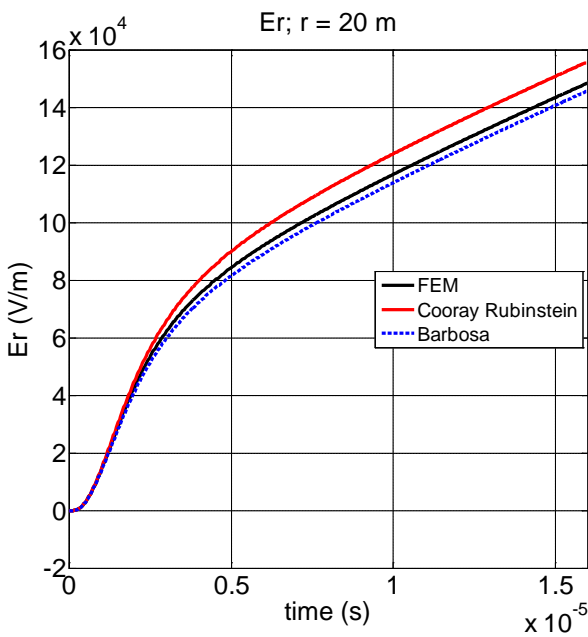


Figure 1-9 – Radial component of the electric field for $r = 20$ m, at $z = 10$ m above a lossy ground ($\sigma_g = 1$ mS/m, $\epsilon_r = 10$). Channel base current typical of first strokes.

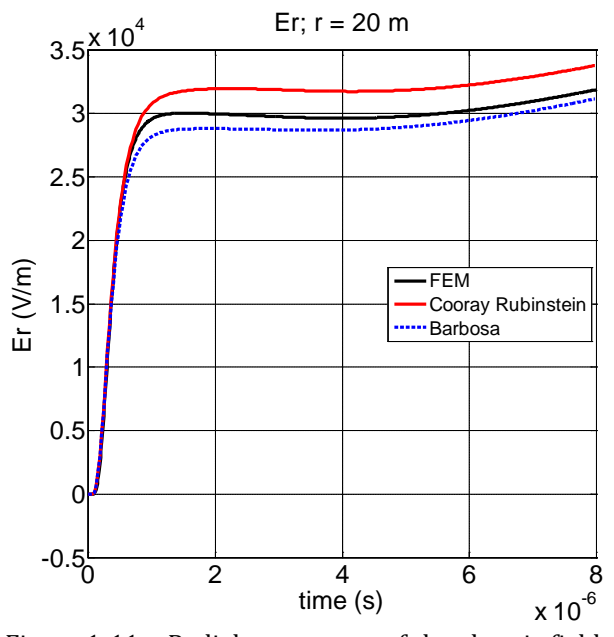


Figure 1-11 – Radial component of the electric field for $r = 20$ m, at $z = 10$ m above a lossy ground ($\sigma_g = 1$ mS/m, $\epsilon_r = 10$). Channel base current typical of subsequent strokes.

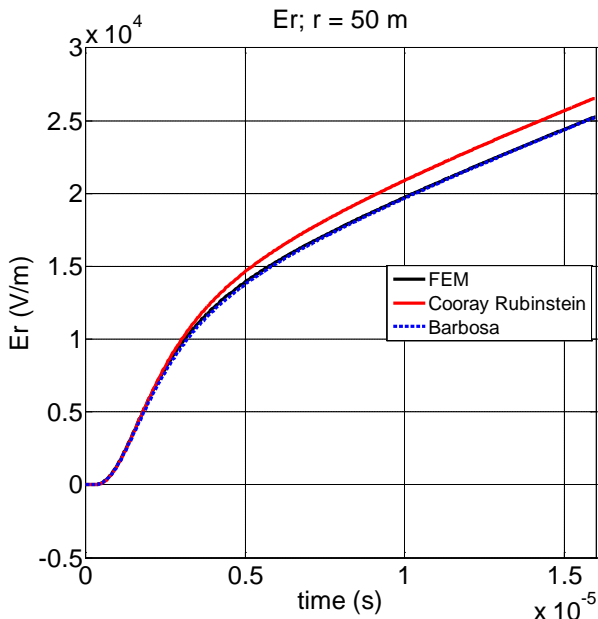


Figure 1-12 – Radial component of the electric field for $r = 50$ m, at $z = 10$ m above a lossy ground ($\sigma_g = 1$ mS/m, $\epsilon_r = 10$). Channel base current typical of first strokes.

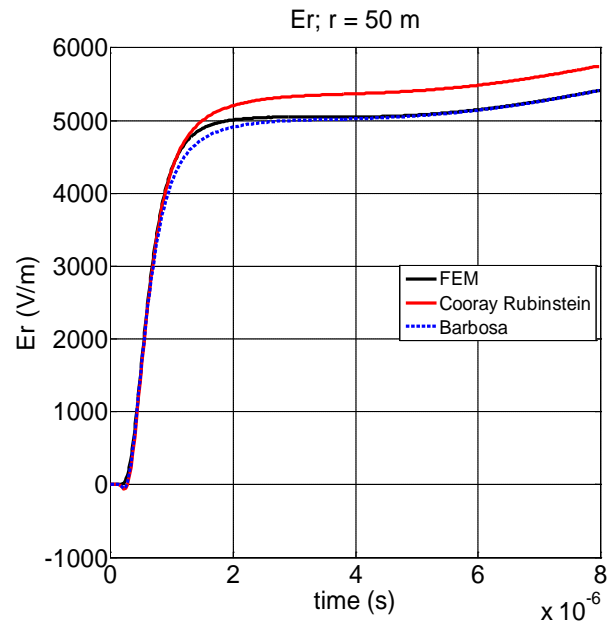


Figure 1-13 – Radial component of the electric field for $r = 50$ m, at $z = 10$ m above a lossy ground ($\sigma_g = 1$ mS/m, $\epsilon_r = 10$). Channel base current typical of subsequent strokes.

Let us now consider the geometry reported in Figure 1-14, namely a 1-km long, 10-m high single conductor line with matched terminations.

In Figure 1-15, the comparison between the overvoltages at the mid-point of the line calculated different approaches discussed in this section is reported. The stroke distance from the line is $d = 10$ m and the ground is characterized by $\sigma_g = 1$ mS/m and $\epsilon_r = 10$. The comparison is performed again for the two different return stroke current considered and for the three distances between the line and the stroke location (namely 10, 20 and 50 m). The overvoltages calculations are performed by using the LIOV code with the different fields provided as input. Considerations similar to the ones done for the horizontal electric field apply. As expected, the importance of integrating the vertical field along the z coordinate is noticeable when the distance from the line is lower than 50 m.

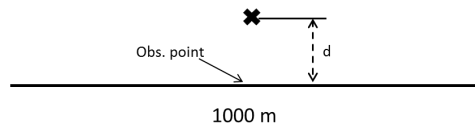


Figure 1-14 – Considered geometry

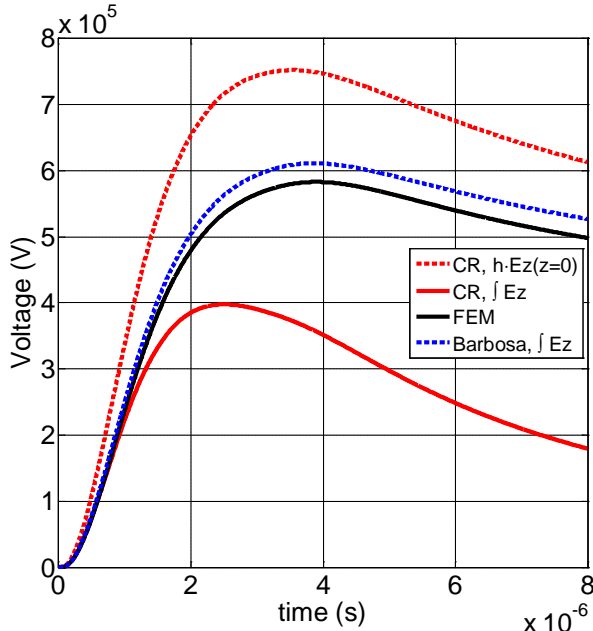


Figure 1-15 – Overvoltage at point in front of the stroke location. Stroke distance from the line: $d = 10$ m. Lossy ground with $\sigma_g = 1$ mS/m and $\epsilon_r = 10$. Channel base current typical of first strokes.

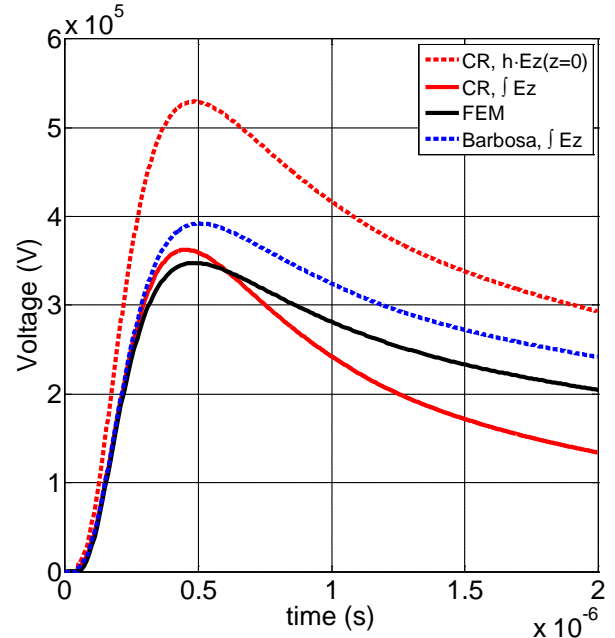


Figure 1-17 – Overvoltage at point in front of the stroke location. Stroke distance from the line: $d = 10$ m. Lossy ground with $\sigma_g = 1$ mS/m and $\epsilon_r = 10$. Channel base current typical of subs. strokes.

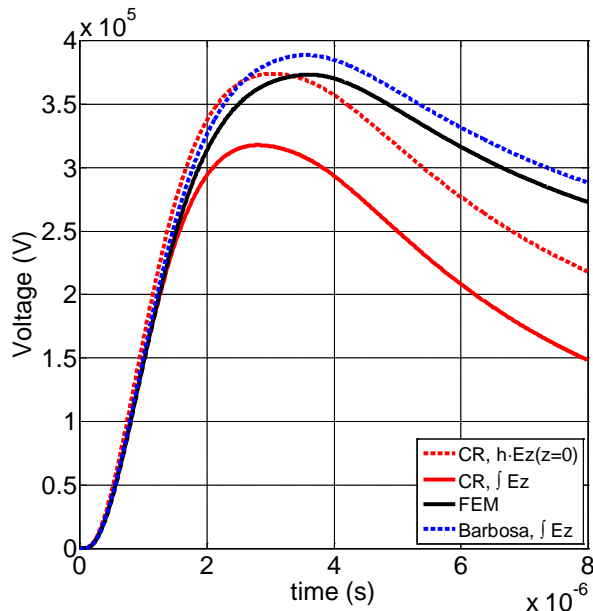


Figure 1-16 – Overvoltage at point in front of the stroke location. Stroke distance from the line: $d = 20$ m. Lossy ground with $\sigma_g = 1$ mS/m and $\epsilon_r = 10$. Channel base current typical of first strokes.

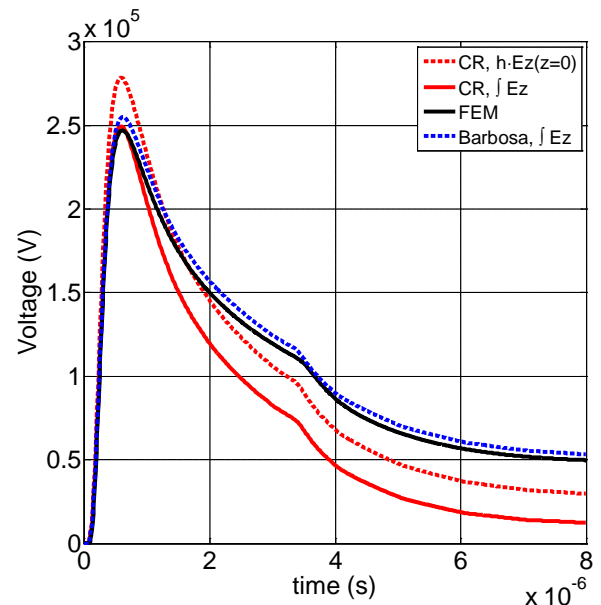


Figure 1-18 – Overvoltage at point in front of the stroke location. Stroke distance from the line: $d = 20$ m. Lossy ground with $\sigma_g = 1$ mS/m and $\epsilon_r = 10$. Channel base current typical of subsequent strokes.

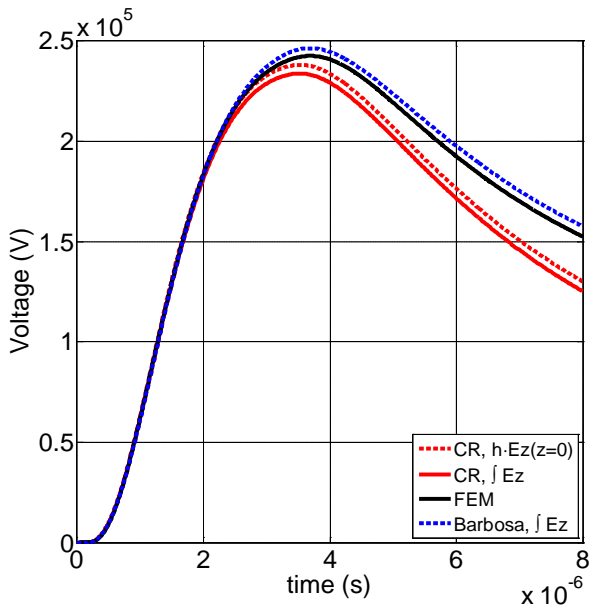


Figure 1-19 – Overvoltage at point in front of the stroke location. Stroke distance from the line: $d = 50$ m. Lossy ground with $\sigma_g = 1$ mS/m and $\epsilon_r = 10$. Channel base current typical of first strokes.

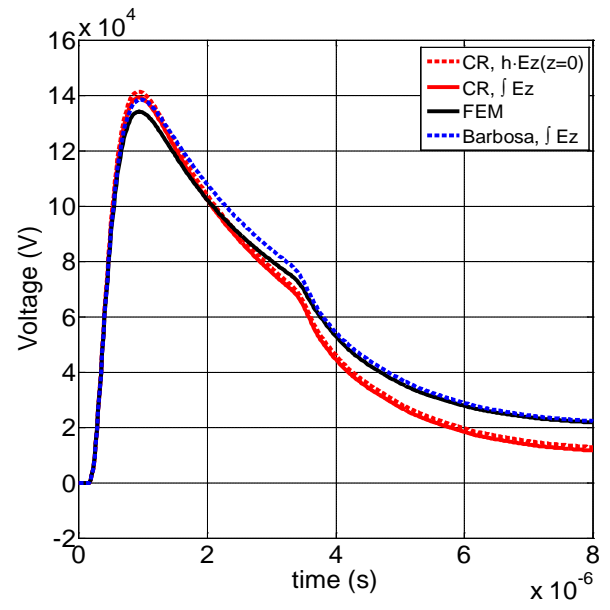


Figure 1-20 – Overvoltage at point in front of the stroke location. Stroke distance from the line: $d = 50$ m. Lossy ground with $\sigma_g = 1$ mS/m and $\epsilon_r = 10$. Channel base current typical of subsequent strokes.

1.3. Transient Ground Resistance of Multiconductor Lines

The effect of losses on the surge propagation along a multiconductor line illuminated by an external electromagnetic field has been treated in quite a few papers by representing the ground losses as an additional longitudinal term in the coupling equations e.g., (*Rachidi et al.*, 1996, 1999, 2003): the so-called ground impedance in the frequency domain, or its time-domain counter-part, the transient ground resistance. Several expressions for the terms of the ground impedance matrix have been proposed e.g., (*Sunde*, 1968; *Carson*, 1926; *Pollaczek*, 1931; *Vance*, 1978; *Gary*, 1976) and, within the limits of the transmission line approximation (TL), the most accurate one is considered the one derived by *Sunde* (1968). Indeed, it can be shown that the general, more rigorous, expressions derived using scattering theory reduce to the Sunde approximation under the transmission line theory assumption (*Tesche et al.*, 1997). So far, analytical expressions for the inverse Fourier transform of the Sunde formula are not available in the literature, thus, the elements of the ground transient resistance matrix in time domain have to be, in general, evaluated adopting a numerical inverse Fourier transform algorithm. A low-frequency approximation for the ground impedance is the well-known expression derived by *Carson* (1926) and its analytical inverse Fourier transform has been first derived by *Timotin* (1967) for the case of a single conductor line, and then extended to a multiconductor line by *Orzan* (1997). The expressions of *Timotin* and *Orzan* feature a singularity at $t = 0$ for the transient ground resistance matrix elements. *Rachidi et al.* (2003) showed that the singularity is due to the low frequency approximation of the Carson formula. Such singularity is indeed absent in the case of the Sunde formula, according to which the ground transient resistance tends to an asymptotic value when t tends to zero. Combining the asymptotic behavior of the transient ground resistance at early times and the *Timotin/Orzan* expressions for the late times, *Rachidi et al.* (2003) proposed an improved analytical formula for the transient ground resistance matrix elements. The *Rachidi et al.* formula, however, does not accurately reproduce the transition between the early time and the late time region where its time-derivative exhibits a discontinuity.

1.3.1. Inverse Laplace Transform of Sunde's Logarithmic Formula – The Series Expression

In this section, a novel approach for calculating the transient ground resistance matrix is presented. This approach, compared with the previous formula of *Rachidi et al.* (2003), is able to reproduce in a more accurate way both the early time and the late time response of the transient

ground resistance. Such an approach stands on the analytical solution of the inverse Laplace transform of the Sunde logarithmic expression (Sunde, 1968), which is not affected by any singularity at the early times, but presents some complexities relevant to its implementation for late times. It will be shown that the proposed analytical formula for the transient ground resistance matrix can be implemented in a straightforward way in computer codes for the evaluation of transients in multiconductor lines.

It is worth mentioning that recently, the frequency dependence of soil parameters has been accounted in lightning electromagnetic transients by using different empirical formulas (Lima & Portela, 2007; Visacro & Alipio, 2012; Akbari et al., 2013; Silveira et al., 2014), an issue that in this thesis is disregarded.

Let us consider the power line geometry presented in Figure 1-21. The configuration assumed is a uniform overhead multiconductor transmission line above a finitely conducting ground characterized by its conductivity σ_g and its relative permittivity ϵ_{rg} . The diameter of each conductor measures 1 cm.

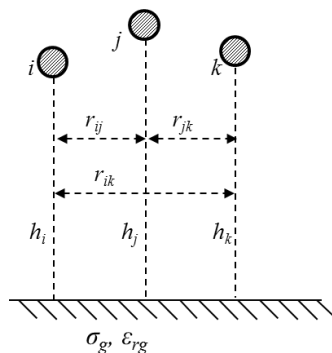


Figure 1-21 – Definition of the geometry

The Sunde expression for mutual ground impedance between two conductors i and j is (Sunde, 1968)

$$Z'_{g,ij} = \frac{j\omega\mu_0}{\pi} \int_0^{\infty} \frac{e^{-(h_i+h_j)x}}{\sqrt{x^2 + \gamma_g^2} + x} \cos(r_{ij}x) dx \quad (1.13)$$

where h_i , h_j and r_{ij} are the geometrical parameters defined in Figure 1-21 and γ_g is the wave propagation constant defined as

$$\gamma_g = \sqrt{j\omega\mu_0(\sigma_g + j\omega\epsilon_0\epsilon_{rg})} \quad (1.14)$$

Applying a low-frequency approximation ($\sigma_g \gg \omega \varepsilon_0 \varepsilon_{r_g}$), (1.13) reduces to the well-known Carson expression (Carson, 1926)

$$Z'_{g,ij} = \frac{j\omega\mu_0}{\pi} \int_0^{\infty} \frac{e^{-(h_i+h_j)x}}{\sqrt{x^2 + j\omega\sigma_g\mu_0 + x}} \cos(r_{ij}x) dx \quad (1.15)$$

As shown in (Rachidi et al., 1999), for typical overhead power lines and for ground conductivities of about 0.01 S/m, Carson approximation might fail at frequencies beyond a few MHz, and even at lower frequencies for poorer ground conductivity. As a result, the general expression (1.13) should be used to obtain more accurate results for the analysis of fast transients (such as nuclear electromagnetic pulse, lightning, and intentional electromagnetic interferences).

The time domain transient ground resistance matrix elements are defined as

$$\xi'_{g,ij}(t) = F^{-1} \left\{ \frac{Z'_{g,ij}(\omega)}{j\omega} \right\} \quad (1.16)$$

The inverse Fourier transform of the main diagonal elements of Carson ground impedance matrix derived by Timotin (1967) is

$$\xi'_{g,ii}(t) = \frac{\mu_0}{\pi\tau_{g,ii}} \left[\frac{1}{2\sqrt{\pi}} \sqrt{\frac{\tau_{g,ii}}{t}} + \frac{1}{4} e^{\frac{\tau_{g,ii}}{t}} \operatorname{erfc} \left(\sqrt{\frac{\tau_{g,ii}}{t}} \right) - \frac{1}{4} \right] \quad (1.17)$$

in which $\tau_{g,ii} = h_i^2 \mu_0 \sigma_g$ and erfc is the complementary error function. In (Orzan, 1997), the author extended the Timotin expression to the case of a multiconductor line; the general term $\xi'_{g,ij}$ is

$$\begin{aligned} \xi'_{g,ij}(t) = & \frac{\mu_0}{\pi T_{ij}} \left[\frac{1}{2\sqrt{\pi}} \sqrt{\frac{T_{ij}}{t}} \cos(\theta_{ij}/2) \right. \\ & + \frac{1}{4} \exp\left(\frac{T_{ij}}{t} \cos \theta_{ij}\right) \cos\left(\frac{T_{ij}}{t} \sin \theta_{ij} - \theta_{ij}\right) \\ & \left. - \frac{1}{2\sqrt{\pi}} \sum_{n=0}^{\infty} a_n \left(\frac{T_{ij}}{t}\right)^{\frac{2n+1}{2}} \cdot \cos\left(\frac{2n-1}{2} \theta_{ij}\right) - \frac{\cos \theta_{ij}}{4} \right] \end{aligned} \quad (1.18)$$

with

$$\hat{h}_{ij} = \left(\frac{h_i + h_j}{2} + j \frac{r_{ij}}{2} \right) \quad (1.19)$$

$$T_{ij} e^{j\theta_{ij}} = \hat{h}_{ij}^2 \mu_0 \sigma_g \quad (1.20)$$

$$\text{and } a_n = \frac{2^n}{1 \cdot 3 \cdots (2n+1)}.$$

As Carson approximation presents a singularity at high frequency (*Rachidi et al.*, 1999), the Timotin expression is affected by a singularity at early times. This singularity has been discussed in many papers such as (*Loyka*, 1999; *Loyka & Kouki*, 2001); *Rachidi et al.*, (2003) provided a careful treatment of such a singularity approximating the transient ground resistance at early times with its asymptotic value, that for the diagonal terms is given by

$$\xi'_{g,ii}(t=0) = \lim_{\omega \rightarrow \infty} j\omega \frac{Z'_{g,ii}}{j\omega} = \frac{1}{2\pi h_i} \sqrt{\frac{\mu_o}{\epsilon_o \epsilon_{rg}}} \quad (1.21)$$

and for the off-diagonal terms is given by

$$\xi'_{g,ij}(t=0) = \lim_{\omega \rightarrow \infty} j\omega \frac{Z'_{g,ij}}{j\omega} = \frac{1}{2\pi \hat{h}_{ij}} \sqrt{\frac{\mu_o}{\epsilon_o \epsilon_{rg}}} \quad (1.22)$$

Diagonal Elements

Let us consider the Sunde expression for the diagonal terms of the ground impedance matrix

$$Z'_{g,ii} = \frac{j\omega\mu_o}{\pi} \int_0^{\infty} \frac{e^{-2h_i x}}{\sqrt{x^2 + \gamma_g^2} + x} dx \quad (1.23)$$

The inverse Fourier transform of (1.23) is not available in the literature. One of the most accurate approximations of (1.23) has been derived by Sunde itself (*Sunde*, 1968)

$$Z'_{g,ii} = \frac{j\omega\mu_o}{2\pi} \ln \frac{1 + \gamma_g h_i}{\gamma_g h_i} \quad (1.24)$$

As shown in (*Rachidi et al.*, 1999), this approximation is accurate for a wide frequency range and for typical ground electrical parameters.

The early time response of (1.24) can be evaluated by using the following formula (see relevant Appendix for its derivation)

$$\xi'_{g,ii}(t) = \frac{\mu_o}{2\pi} \sum_{n=1}^m (-1)^{n+1} \frac{1}{nb_i^n} \frac{\sqrt{\pi}}{\Gamma\left(\frac{n}{2}\right)} \cdot \left(\frac{t}{a}\right)^{\frac{n}{2}-\frac{1}{2}} \exp\left(-\frac{at}{2}\right) \cdot I_{\frac{n}{2}-\frac{1}{2}}\left(\frac{at}{2}\right) \quad (1.25)$$

where

$\Gamma(n/2)$ is the Euler Gamma function of the real argument $n/2$;

$I_{n/2-1/2}(at/2)$ is the modified Bessel function of the first kind, of the order $(n/2 - 1/2)$ and of the real argument $at/2$.

As shown in Appendix, the series (1.25) with $m \rightarrow \infty$ is the inverse Laplace transform of (12) in the half plane of convergence defined by

$$|h_i \gamma_g| > 1. \quad (1.26)$$

By increasing m , the formula converges up to greater times, and depending whether m is an even or odd number, it deviates towards lower or higher values respectively.

The first term of (1.25) corresponds to the inverse Fourier transform of the fast-transient approximation derived in (Semlyen, 1981) by Semlyen and discussed by Araneo & Celozzi (2001). This is in agreement with the fact that increasing m in (1.25) leads to a better approximation of the late time response of the transient ground resistance.

Figure 1-22 shows a comparison between the derived expression (1.25) with $m = 26$ and $m = 150$, the Timotin formula (1.17), the Rachidi *et al.* formula and the numerical inverse Fourier transform of the Sunde logarithmic expression evaluated with (1.24) and (1.16), for a 10-m high, single conductor line above a conducting ground ($\sigma_g = 0.001$ S/m and $\epsilon_{rg} = 10$). The conductor diameter is 1 cm. It can be seen that the proposed formula and the inverse Fourier transform of the Sunde logarithmic expression are in excellent agreement until the series expansion diverges due to the finite number of terms assumed in the evaluation of (13).

As shown in Figure 1-22, combining (1.25), with $m = 26$, and (1.17) makes it possible to approximate the transient ground resistance for any value of time. In this regard, for high accuracy results, the use of at least $m = 26$ in (1.25) is recommended.

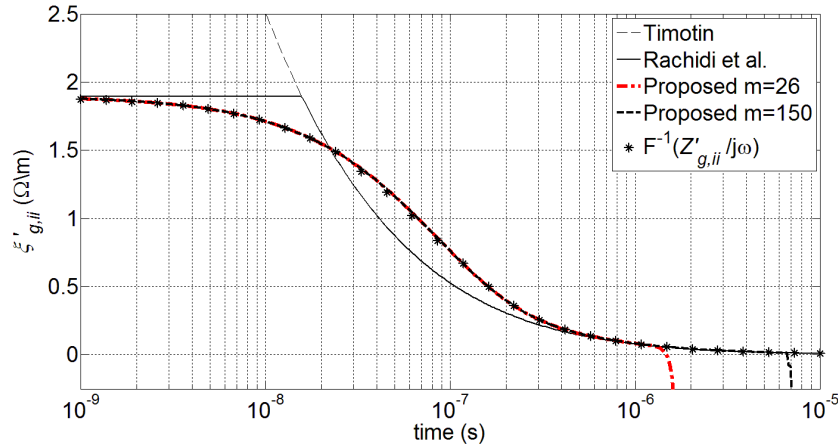


Figure 1-22 – Comparison between the proposed expression (1.25) with $m = 26$ and $m = 150$, the Timotin formula (1.17), the Rachidi et al. formula and the numerical inverse Fourier transform of $Z'_{g,ii}/j\omega$ for a 10 m high, single conductor line above a conducting ground $\sigma_g = 0.001$ S/m and $\epsilon_{rg} = 10$.

Off-Diagonal Elements

In (Rachidi et al., 1999), the authors extended Sunde logarithmic expression for the off-diagonal elements of the ground impedance matrix

$$Z'_{g,ij} = \frac{j\omega\mu_0}{4\pi} \left[\ln \frac{1 + \gamma_g \hat{h}_{ij}}{\gamma_g \hat{h}_{ij}} + \ln \frac{1 + \gamma_g \hat{h}_{ij}^*}{\gamma_g \hat{h}_{ij}^*} \right] \quad (1.27)$$

where \hat{h}_{ij} is defined by (1.19) and \hat{h}_{ij}^* is its complex conjugate.

Following the same procedure adopted for the diagonal elements, (see relevant Appendix) the early time response of (1.27) can be evaluated by the following formula:

$$\xi'_{g,ij}(t) = \frac{\mu_0}{2\pi} \sum_{n=1}^m (-1)^{n+1} \frac{1}{n} \frac{1}{|\hat{b}_{ij}|^n} \cos(n\delta_{ij}) \frac{\sqrt{\pi}}{\Gamma\left(\frac{n}{2}\right)} \cdot \left(\frac{t}{a}\right)^{\frac{n}{2}-\frac{1}{2}} \exp\left(-\frac{at}{2}\right) \cdot I_{\frac{n}{2}-\frac{1}{2}}\left(\frac{at}{2}\right) \quad (1.28)$$

where

$$\hat{b}_{ij} = \sqrt{\mu_0 \epsilon_0 \epsilon_{rg}} \hat{h}_{ij} \quad (1.29)$$

and \hat{b}_{ij}^* is its complex conjugate, and

$$\delta_{ij} = \text{Arg}(\hat{b}_{ij}). \quad (1.30)$$

In Figure 1-23, a comparison between (1.28) with $m = 26$ and the numerical inverse Fourier transform of the logarithmic expression (1.27) is presented as a function of time. The Orzan formula and the formula by Rachidi *et al.* for the case of a multiconductor line are also shown. The figure refers to a double conductor line above a ground with conductivity $\sigma_g = 0.001$ S/m and relative permittivity $\epsilon_{rg} = 10$. The two conductors are located at 10 m and 12 m above ground respectively and they are separated by a distance of 1 m. As for the case of the diagonal elements, the proposed analytical formula and the numerical inverse Fourier transform of (1.27) provide the same results until the series diverges. The divergence due to use of (1.28) with finite m can be overcome by the same analytical approach proposed for the diagonal elements, namely the use of the Orzan formula for the late time response of the transient ground resistance.

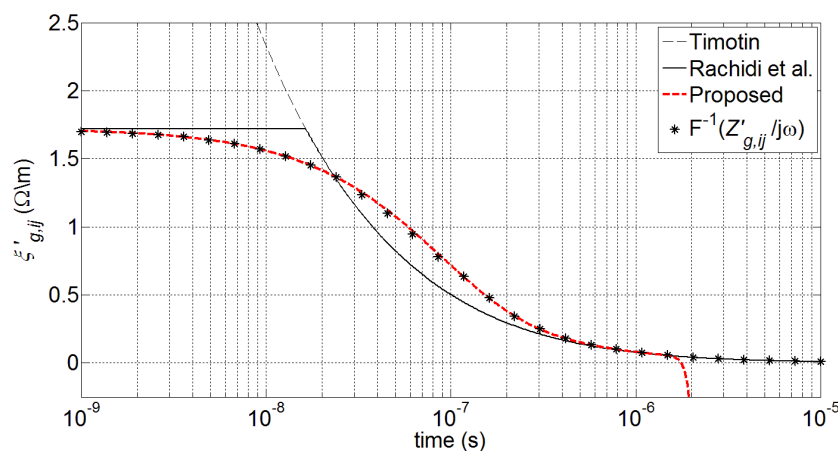


Figure 1-23 – Comparison between the proposed expression (1.28) with $m = 26$, the Orzan formula (1.18), the Rachidi *et al.* formula and the numerical inverse Fourier transform of $Z'_{g,ii}/j\omega$ for a 10-m and 12-m high, double conductor line, above a conducting ground $\sigma_g = 0.001$ S/m and $\epsilon_{rg} = 10$, $r_{ij} = 1$ m.

Also for very poor conducting ground, the proposed analytical approach is in very good agreement with exact numerical solutions, at any value of time. For $\sigma_g = 10^{-4}$ S/m the use of at least 56 terms in the formulae is recommended.

As shown in the presented comparisons, the proposed analytical formula reproduces more accurately the transient ground resistance matrix elements than the formula of Rachidi *et al.* does.

Petrache et al. (2005) showed that the Sunde logarithmic expression is an excellent approximation of the general solution of the ground impedance of a buried cable. Therefore, the proposed approach can be adopted also for the evaluation of transients in buried cables directly in the time domain avoiding the computational costs associated with numerical inverse Fourier transform.

In order to show the advantages of the proposed formulation, this section shows a comparison between the overvoltages induced on a lossy line taking into account the losses in the surge

propagation using the Rachidi *et al.* formula, with those calculated using the proposed approach. To do that, let us consider two geometrical configurations illustrated in Figure 1-24. Configuration (a) is a single-conductor line while configuration (b) is a three phase line where the external conductors are 1 m distant from the central one. Each wire is situated at a height of 10 m above ground and has a diameter of 1 cm.

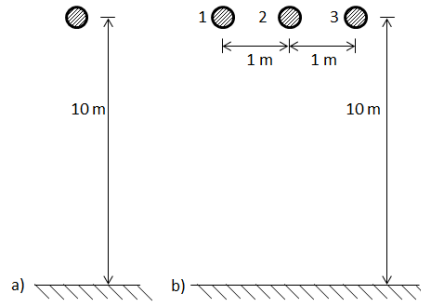


Figure 1-24 – Considered line configurations: a) Single-conductor line.
b) Three-conductor line.

The ground conductivity is assumed to be $\sigma_g = 10^{-3}$ S/m, if not otherwise specified, and its relative permittivity is set to $\epsilon_{rg} = 10$. The channel-base current is typical of subsequent return strokes (Berger *et al.*, 1975) with a peak value of 12 kA and a maximum time-derivative of 40 kA/ μ s, represented using the sum of two Heidler functions (Nucci *et al.*, 1993). The stroke location has been assumed to be at 50 m from the line center and equidistant to the line terminations. The return stroke velocity is assumed to be $1.5 \cdot 10^8$ m/s and the adopted return stroke model is the transmission line one (TL). The incident EM field is calculated with the analytical formulae described in (Napolitano, 2011) and by using the Cooray - Rubinstein formula (Cooray, 1992; Rubinstein, 1996). The coupling equations according to the model by Agrawal *et al.* for the case of lossy line are

$$\begin{aligned} \frac{\partial}{\partial x} [v_i^s(x, t)] + [L'_{ij}] \frac{\partial}{\partial t} [i_j(x, t)] + \\ + \int_0^t [\xi'_{g,ij}(t - \tau)] \frac{\partial}{\partial \tau} [i_j(x, \tau)] d\tau = [E_x^e(x, h_i, t)] \end{aligned} \quad (1.31)$$

$$\frac{\partial}{\partial x} [i_i(x, t)] + [C'_{ij}] \frac{\partial}{\partial t} [v_j^s(x, t)] = 0 \quad (1.32)$$

where:

- $[E_x^e(x, h_i, t)]$ is the vector of the horizontal component of the incident electric field;

- $[L'_{ij}]$ and $[C'_{ij}]$ are the matrices of the line per-unit-length inductances and capacitances respectively;
- $[i_i(x,t)]$ is the vector of the currents;
- $[v_i^s(x,t)]$ is the scattered voltage vector;
- $[\xi'_{g,ij}(t)]$ is the transient ground resistance matrix.

The total voltages $[v_i(x,t)]$ are given by

$$[v_i(x,t)] = [v_i^s(x,t)] - \left[\int_0^{h_i} E_z^e(x,z,t) dz \right] \quad (1.33)$$

where $E_z^e(x,z,t)$ is the vertical component of the incident electric field.

The line terminations are connected to the characteristic impedance of the line. The following considerations are valid also in case of line terminations open or far from the observation point.

Before comparing the proposed formula with the one by Rachidi *et al.*, let us first show in Figure 1-25 the comparison between the induced voltage at the termination of a 5-km long line for the following two cases: transient ground resistance calculated numerically solving (1.13) and (1.16) and by the proposed formula (analytical). The comparison is reported for both power line configurations. As it can be seen from the figure, numerical and analytical formulations are in excellent agreement.

It is worth noting that the implementation of the proposed formula is obtained without significant increase in time computation even adopting a very large number of terms of the series (the calculation of the exciting lightning electromagnetic field and the convolution integral in equation (1.31) represent, for the problem of interest, the bulk of the computation time).

In Figure 1-26, a comparison between the induced voltages at the termination of a 5-km long, single conductor line (configuration a) evaluated with the Rachidi *et al.* formula and the proposed one is shown. The results associated with the case of an ideal (lossless) line are also presented. The attenuation effect of the transient ground resistance evaluated with the proposed formula is somewhat stronger compared to that obtained using the Rachidi *et al.* one. Specifically, the negative peak of the overvoltage predicted by the proposed formula is 11% lower than the one obtained using Rachidi *et al.* formula. In addition, the maximum value of the time derivative of the induced voltage evaluated making use of the proposed approach is 22% lower than with the use

of Rachidi *et al.* formula, and the rise time is 4% larger. In Figure 1-27, the same comparison is shown for a three-phase line (configuration b in Figure 1-24). While the induced voltage on an ideal line is not affected by the presence of the other conductors (Napolitano *et al.*, 2015), the effect of the mutual transient ground resistance matrix elements is to increase the attenuation effect on the overvoltage. For the assumed configuration, the increasing of the number of conductors leads to a more significant difference between the two formulae in terms of time derivative and peak value of the overvoltage.

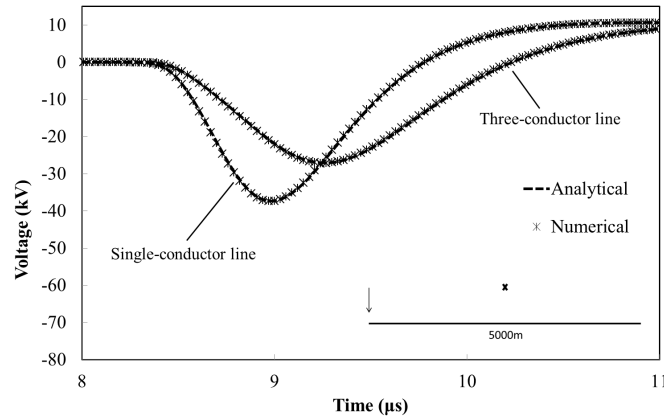


Figure 1-25 – Induced voltage at the end of the line. Comparison between the proposed formula (analytical) and the numerical evaluation of the transient ground resistance. 5-km long line, $\sigma_g = 10^{-3}$ S/m, $\epsilon_{rg} = 10$.

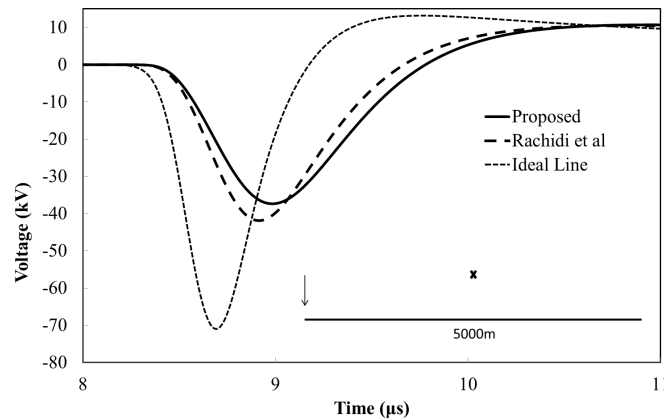


Figure 1-26 – Induced voltage at the end of the line. Comparison between the proposed formula and the Rachidi *et al.* one. The results associated with a lossless (ideal) line are also shown for comparison. Single-conductor, 5-km long line, $\sigma_g = 10^{-3}$ S/m, $\epsilon_{rg} = 10$.

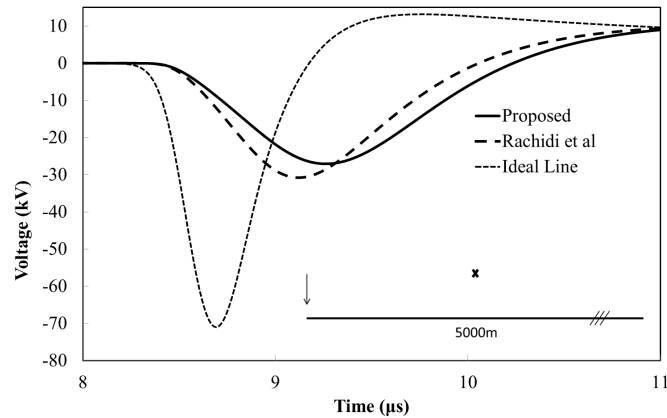


Figure 1-27 – Induced voltage at the end of the line. Comparison between the proposed formula and the Rachidi *et al.* one. The results associated with a lossless (ideal) line are also shown for comparison. Three-phase, 5-km long line, $\sigma_g = 10^{-3}$ S/m, $\epsilon_{rg} = 10$.

The main factors that influence the difference between the proposed formulation and the Rachidi *et al.* one are the following:

- Ground conductivity and relative permittivity

In Figure 1-28, a comparison between the induced voltage at the termination of a 5-km long single-conductor line evaluated with the Rachidi *et al.* formula and the proposed algorithm is shown for the case of a ground conductivity $\sigma_g = 10^{-4}$ S/m. In this case, the voltage peak calculated with the new approach is 16% lower, the rise-time is 24% larger and the maximum time derivative is 37% lower. The lower the ground conductivity, the higher will be the difference between the two formulations. Opposite consideration can be drawn for the relative ground permittivity; an increase of the ground permittivity leads to more significant differences between the two formulations.

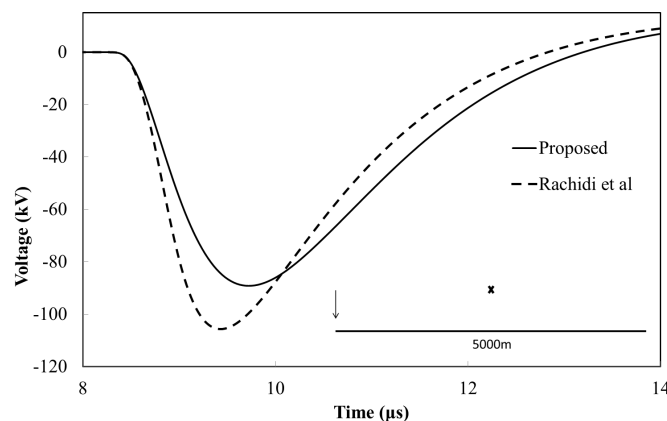


Figure 1-28 – Induced voltage at the end of the line. Comparison between the proposed formula and the Rachidi *et al.* one. Single-conductor, 5-km long line, $\sigma_g = 10^{-4}$ S/m, $\epsilon_{rg} = 10$.

– *Current derivative*

In Figure 1-29, the same case of Figure 1-25 (shown in black) is compared with the case in which the overvoltages are evaluated assuming three different channel-base current waveforms, having same current peak amplitude of 12 kA and three different maximum time derivative, specifically 12 and 120 kA/ μ s instead of 40 kA/ μ s. The currents are named A1, A2 and A3, respectively. Current A2, that is the one adopted in the calculation previously shown, is assumed as representative of a subsequent return stroke. The Heidler functions parameters reported in (Guerrieri *et al.*, 1996) are adopted. For given values of the ground parameters, as the steepness of the electromagnetic source increases, the differences between the two formulation increase. A summary of the previous considerations is reported in Table 1-2. The values are reported in relative value respect to the Rachidi *et al.* formula. As Table 1-2 shows, significant differences in peak and maximum steepness can be found also for a ground conductivity of 2 mS/m when dealing with fast electromagnetic sources. In view of this, the adoption of the proposed approach is advisable when the ground conductivity is less or equal to 2 mS/m.

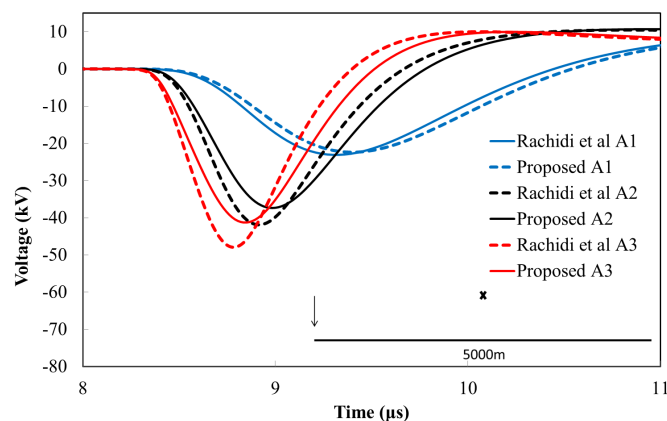


Figure 1-29 – Induced voltage at the end of the line. Comparison between the proposed formula and the Rachidi *et al.* one for the three different return stroke current A1, A2 and A3. Single-conductor, 5-km long line, $\sigma_g = 10^{-3}$ S/m, $\epsilon_{rg} = 10$.

TABLE 1-2 – INDUCED VOLTAGES – DIFFERENCES BETWEEN THE TWO APPROACHES

| σ_g (mS/m) | Current | Peak | Raise-Time | $(dV/dt)_{\max}$ |
|-------------------|-----------|------|------------|------------------|
| 2 | A1 | -1% | 3% | -6% |
| | A2 | -7% | 4% | -14% |
| | A3 | -9% | 5% | -17% |
| 1 | A1 | -3% | 8% | -12% |
| | A2 | -11% | 4% | -22% |
| | A3 | -14% | 9% | -25% |
| | A2 3phase | -12% | 17% | -30% |
| 0.1 | A1 | -9% | 14% | -26% |
| | A2 | -16% | 24% | -37% |
| | A3 | -19% | 26% | -39% |

– *Length of the line*

An increase of the length of the line would generally lead to more significant differences between overvoltages calculated using the two different formulae.

Other factors such as the height of the line, the stroke location and the number of conductors have, in general, a minor influence on the difference between the two discussed formulae.

Let us finally discuss the impact of using different approaches to calculate the transient ground resistance on induced voltages considering also a line including a conductor with multiple ground terminations. In this respect, let us make reference to configuration b of Figure 1-24 with the presence of a fourth conductor located under the central phase, at 8.37 m above ground, with multiple groundings every 200 m with resistance equal to 50 Ω . The line is 4 km long with open terminations and the stroke location is 50 m far from the line. The base channel current waveform is the one suggested in (*Cigré Working Group 33.01*, 1991) to represent a typical negative first-stroke with current peak $I_p = 31$ kA, equivalent front time $t_F = 3$ μ s, maximum steepness $S_m = 26$ kA/ μ s and time to half value $t_h = 75$ μ s. The ground conductivity is $\sigma_g = 10^{-4}$ S/m. In Figure 1-30, the overvoltage on the central conductor calculated at the line termination is reported for the two different methods. The first negative peak is about 15% lower in case the proposed formula is adopted; the differences between the two waveforms increase with time due to the subsequent traveling wave reflections. Such differences are expected to be more significant if lower t_F or higher S_m are adopted in the lightning base channel current representation.

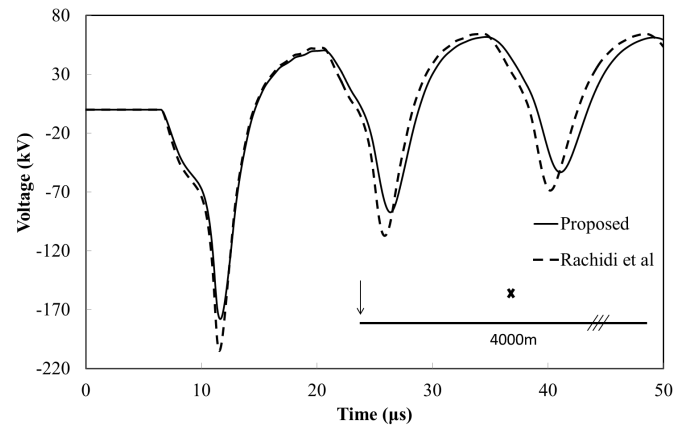


Figure 1-30 – Induced voltage at the end of the line. Comparison between the proposed formula and the Rachidi *et al.* Three-conductor, 4-km long line, with neutral grounded every 200 m. $\sigma_g = 10^{-4}$ S/m, $\epsilon_{rg} = 10$.

Conclusion

A new analytical approach for the evaluation of the transient ground resistance matrix of an overhead multiconductor line above a lossy ground has been proposed. The approach adopts an early-time analytical formula derived from the inverse Laplace transform of the Sunde logarithmic expression of the ground impedance matrix and the late time inverse transforms of Carson formula proposed by Timotin and Orzan. It has been proven that the proposed formula is not affected by any singularity at the early times, contrary to the previously proposed low frequency expressions such as the one by Timotin and its derivations. The proposed approach has been used for the evaluation of lightning-induced transients along a multi-conductor line. In order to show the advantages of the proposed formulation with respect to others recently proposed aimed at fixing the low frequency singularity, a comparison between the overvoltages induced on a lossy line according to the approach used by Rachidi *et al.*, with those calculated using the proposed approach has been carried out. It was shown that for fast electromagnetic sources, and/or poor ground conductivities, the proposed expression provides more accurate results compared to the approach used by Rachidi *et al.*

1.3.2. Inverse Laplace Transform of Sunde's Logarithmic Formula – The Integral Expression

In this section the sum of the series proposed in (Tossani *et al.*, 2015b) is achieved and to this purpose a new formula for the assessment of the transient ground resistance matrix of a multiconductor overhead line is proposed. This new formula is the integral of the difference

between a modified Struve function and a modified Bessel function, of order -1 and 1 respectively, over a finite interval.

The expression proposed by Sunde for the diagonal elements of the ground impedance matrix is (Sunde, 1968)

$$Z'_{g,ii}(s) = \frac{s\mu_0}{2\pi} \ln \frac{1 + \gamma_g h_i}{\gamma_g h_i} \quad (1.34)$$

where h_i is the height of the i -th conductor and γ_g is the wave propagation constant above a finitely conducting ground characterized by its conductivity σ_g and its relative permittivity ϵ_{rg} , defined as

$$\gamma_g = \sqrt{s\mu_0(\sigma_g + s\epsilon_0\epsilon_{rg})} \quad (1.35)$$

The diagonal elements of the transient ground resistance matrix are defined as the inverse Laplace transform of (1.34) divided by s , and are given by (Tossani et al., 2015b)

$$\xi'_{g,ii}(t) = \frac{\mu_0\sqrt{\pi}}{2\pi} e^{-\frac{at}{2}} \sum_{n=1}^{\infty} (-1)^{n+1} \frac{1}{nb_i^n} \left(\frac{t}{a}\right)^{\frac{n-1}{2}} \frac{I_{\frac{n-1}{2}}\left(\frac{at}{2}\right)}{\Gamma\left(\frac{n}{2}\right)} \quad (1.36)$$

where $a = \sigma_g / \epsilon_0\epsilon_{rg}$, $b_i = h_i\sqrt{\mu_0\epsilon_0\epsilon_{rg}}$.

According to (Gustav Doetsch, 1974) theorem 30.1, the series (1.36) is the inverse Laplace transform of (1.34) in the half plane of convergence defined by $|h_i\gamma_g| > 1$ and it converges absolutely for any real time $t \geq 0$.

Using the recurrence formula for the Gamma function one gets

$$\Gamma\left(\frac{k+1}{2}\right)(k+1) = 2 \cdot \Gamma\left(\frac{k+3}{2}\right) \quad (1.37)$$

which substituted in (1.36) yields to

$$\xi'_{g,ii}(t) = \frac{\mu_0}{2\pi} e^{-\frac{at}{2}} \frac{\sqrt{\pi}}{2b_i} \sum_{k=0}^{\infty} (-1)^k \left(\frac{t}{ab_i^2}\right)^{\frac{k}{2}} \frac{I_k\left(\frac{at}{2}\right)}{\Gamma\left(\frac{k+3}{2}\right)} \quad (1.38)$$

The series (1.38) can be split in two parts as follows:

$$\xi'_{g,ii}(t) = \frac{\mu_0}{2\pi} e^{-\frac{at}{2}} \frac{\sqrt{\pi}}{2b_i} (S_1 - S_2) \quad (1.39)$$

where

$$S_1 = \sum_{k=0}^{\infty} \left(\frac{t}{ab^2} \right)^k \frac{I_k \left(\frac{at}{2} \right)}{\Gamma \left(k + \frac{3}{2} \right)} \quad (1.40)$$

and

$$S_2 = \sum_{k=0}^{\infty} \left(\frac{t}{ab^2} \right)^{k+1/2} \frac{I_{k+1/2} \left(\frac{at}{2} \right)}{\Gamma(k+2)} \quad (1.41)$$

Let us now substitute the integral definition of the modified Bessel function of real order (see *Abramowitz & Stegun*, 1964) equation 9.6.18) in both (1.40) and (1.41). For the first series we obtain

$$S_1 = \frac{1}{\sqrt{\pi}} \int_0^{\pi} e^{\frac{at}{2} \cos x} \sum_{k=0}^{\infty} \frac{\left(\frac{t}{2b} \sin x \right)^{2k}}{\Gamma \left(k + \frac{3}{2} \right) \Gamma \left(k + \frac{1}{2} \right)} dx \quad (1.42)$$

while for the second one

$$S_2 = \frac{1}{\sqrt{\pi}} \int_0^{\pi} e^{\frac{at}{2} \cos x} \sum_{k=0}^{\infty} \frac{\left(\frac{t}{2b} \sin x \right)^{2k+1}}{k! \Gamma(k+2)} dx \quad (1.43)$$

By using the series definition of the modified Struve function \mathbf{L}_{-1} and that of the modified Bessel function I_1 in (1.42) and (1.43) respectively (see *Abramowitz & Stegun*, 1964) equations 9.6.10 and 12.2.1), one obtains the following expression for the diagonal elements of the transient ground resistance matrix

$$\xi'_{g,ii}(t) = \frac{\mu_0}{4\pi b_i} \int_0^{\pi} \left[\mathbf{L}_{-1} \left(\frac{t}{b} \sin x \right) - I_1 \left(\frac{t}{b} \sin x \right) \right] e^{\frac{at}{2}(\cos x - 1)} dx \quad (1.44)$$

The off-diagonal elements of the transient ground resistance matrix are given by (*Tossani et al.*, 2015b)

$$\xi'_{g,ij}(t) = \frac{\mu_0 \sqrt{\pi}}{2\pi} e^{-\frac{at}{2}} \sum_{n=1}^m (-1)^{n+1} \frac{\cos(n\delta_{ij})}{n |\hat{b}_{ij}|^n} \left(\frac{t}{a}\right)^{\frac{n-1}{2}} \frac{I_{\frac{n-1}{2}}\left(\frac{at}{2}\right)}{\Gamma\left(\frac{n}{2}\right)} \quad (1.45)$$

where, being the height of the conductors h_i and h_j and their mutual distance r_{ij} , we have

$$\hat{b}_{ij} = \sqrt{\mu_0 \varepsilon_0 \varepsilon_{rg}} \left(\frac{h_i + h_j}{2} + j \frac{r_{ij}}{2} \right) \text{ and } \delta_{ij} = \text{Arg}(\hat{b}_{ij}).$$

Following the same procedure adopted for the diagonal elements we can express (1.45) as

$$\xi'_{g,ij}(t) = \text{Re} \left\{ \frac{\mu_0}{4\pi} \frac{e^{j\delta_{ij}}}{|\hat{b}_{ij}|} \int_0^\pi \left[\mathbf{L}_{-1} \left(\frac{te^{j\delta_{ij}}}{|\hat{b}_{ij}|} \sin x \right) - I_1 \left(\frac{te^{j\delta_{ij}}}{|\hat{b}_{ij}|} \sin x \right) \right] e^{\frac{at}{2}(\cos x - 1)} dx \right\} \quad (1.46)$$

Considering that δ_{ij} is, in general, small for realistic configurations of distributions and transmission lines, to avoid unessential complexities (i.e. the presence of complex arguments in the integrand), the following approximation is proposed

$$\xi'_{g,ij}(t) \approx \frac{\mu_0}{4\pi} \frac{\cos \delta_{ij}}{|\hat{b}_{ij}|} \int_0^\pi \left[\mathbf{L}_{-1} \left(\frac{t}{|\hat{b}_{ij}|} \sin x \right) - I_1 \left(\frac{t}{|\hat{b}_{ij}|} \sin x \right) \right] e^{\frac{at}{2}(\cos x - 1)} dx \quad (1.47)$$

Let us now discuss the behavior of the integrand in (1.44) and (1.47). Many accurate approximations for the evaluation of the modified Struve function are available such as (Luke, 1975; Newman, 1984; Allan J. Macleod, 1993). However, the evaluation of $\mathbf{L}_{-1} - I_1$ by separate computation of the Bessel and Struve functions leads to severe cancellation problems. In (Allan J. Macleod, 1993) the evaluation of $\mathbf{L}_{-1} - I_1$ is carried out by using Chebyshev expansions and the coefficients are derived to an accuracy of 20D. The same author proposes in (Allan J. Macleod, 1996) an algorithm for evaluating a Chebyshev series, using the Clenshaw method with Reinsch modification, as analyzed in (Oliver, 1977). We here make use of the coefficients given in (Allan J. Macleod, 1993) and the algorithm in (Allan J. Macleod, 1996) to calculate our integrand by using the following relation

$$\mathbf{L}_{-1} = \frac{2}{\pi} + \mathbf{L}_1. \quad (1.48)$$

As the argument of the exponential varies from 0 to $-at$, it is clear that the function being integrated is bounded by $\mathbf{L}_{-1} - I_1$. Considering that for large arguments stands the following relevant expansion (*Allan J. Macleod, 1993*)

$$I_1 - \mathbf{L}_1 \sim \frac{2}{\pi} \left[1 - \frac{1}{x^2} - \frac{3}{x^4} - \frac{45}{x^6} - \dots \right] \quad (1.49)$$

one can conclude that the integrals (1.44) and (1.47) tend to zero fairly quickly as time increases. It is worth noting that by the substitution $x' = \cos x$ in (1.44) and (1.47), the integral can be easily approximated by means of a Chebyshev-Gauss quadrature (see (*Abramowitz & Stegun, 1964*), 25.4.38) making the evaluation of the transient ground resistance straightforward.

In Figure 1-31, a comparison between (1.47) and the numerical inverse Fourier transform of Sunde logarithmic expression is presented as a function of time. The sum of the first 26 terms of (1.45) is also shown. The figure refers to a 10-m and 12-m high conductors distant 1 m to each other, above a conducting ground with $\sigma_g = 0.001$ S/m and $\varepsilon_{rg} = 10$. The integration has been carried out adopting a simple Chebyshev-Gauss quadrature formula:

$$\int_{-1}^1 \frac{f(x)}{\sqrt{1-x^2}} dx = \frac{\pi}{n} \sum_{i=1}^n f \left(\cos \frac{(2i-1)\pi}{2n} \right) \quad (1.50)$$

where

$$f(x) = \left[\mathbf{L}_{-1} \left(\frac{t}{|\hat{b}_{ij}|} \sqrt{1-x^2} \right) - I_1 \left(\frac{t}{|\hat{b}_{ij}|} \sqrt{1-x^2} \right) \right] e^{\frac{at}{2}(x-1)} \quad (1.51)$$

and the assumed number of nodes n is 64. By using 64 nodes, the evaluation of the integral is in good agreement with the more accurate quadgk integration method (Matlab routine) for various ground conductivity values and conductors height. The computational time is comparable to the one required for the implementation of the Bessel series, as proposed in (*Tossani et al., 2015b*). It is worth noting that the method proposed in (*Tossani et al., 2015b*) requires to increase the number of terms considered in order to obtain accurate results for very low conductivity values, a complication that is no longer required with this new formula.

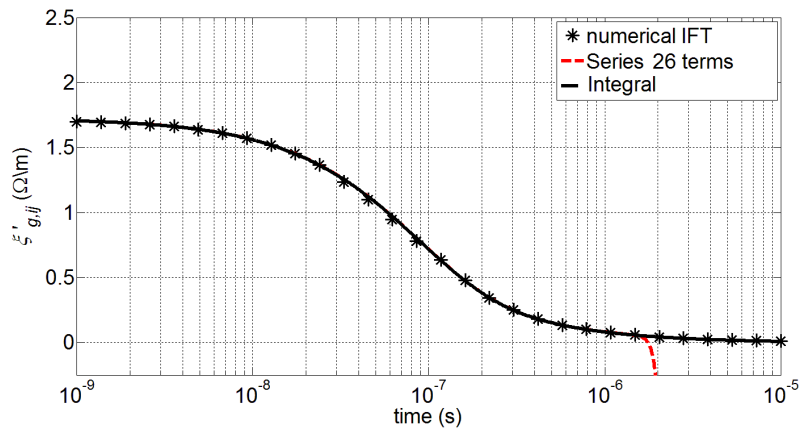


Figure 1-31 – Comparison between the proposed expression (1.47), equation (1.45) with 26 terms and the numerical inverse Fourier transform of $Z'_{g,ij}/j\omega$ for a 10-m and 12-m high, double conductor line, above a conducting ground $\sigma_g = 0.001$ S/m and $\epsilon_{rg} = 10$. $r_{ij} = 1$ m.

As confirmed by Figure 1-31, the proposed expression (1.47) is in excellent agreement with both the numerical evaluation of the inverse Fourier transform of Sunde logarithmic expression and series (1.45). In case the sum of the heights of the two conductors is comparable with their mutual distance, equation (1.46) should be used instead of (1.47). Equation (1.47) can be considered accurate if the following condition applies:

$$\frac{r_{ij}}{h_i + h_j} < 0.1. \quad (1.52)$$

In Figure 1-32 the same comparison of Figure 1-31 is reported but for two 5-m high conductors at a mutual distance of 2.5 m. From Figure 1-32 it can be seen that (1.47) is a good approximation even in the ratio in (1.52) is equal to 0.25.

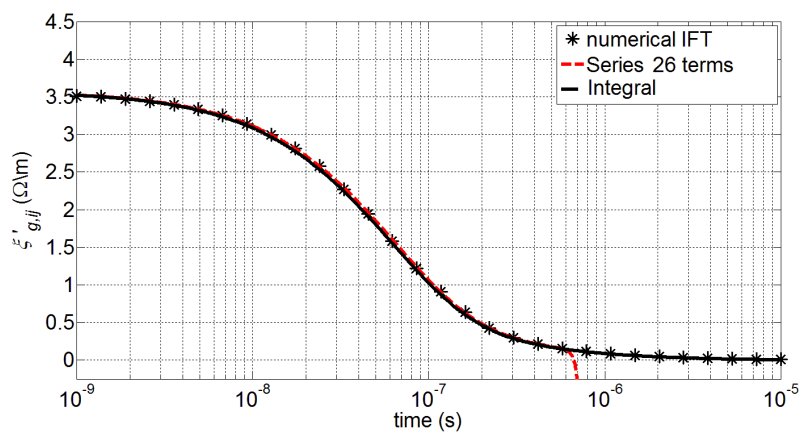


Figure 1-32 – Comparison between the proposed expression (1.47), equation (1.45) with 26 terms and the numerical inverse Fourier transform of $Z'_{g,ij}/j\omega$ for a 5-m high double conductor line, above a conducting ground $\sigma_g = 0.001$ S/m and $\epsilon_{rg} = 10$. $r_{ij} = 2.5$ m.

Conclusion

A new integral expression for the evaluation of the transient ground resistance matrix has been proposed. This expression is the inverse Laplace transform of the Sunde logarithmic equation for the ground impedance, which has been shown to be very accurate even for fast electromagnetic sources and low ground conductivities. The new expression consists in the integral of the difference between a modified Struve function and a modified Bessel function, of order -1 and 1 respectively, over a finite interval. The evaluation of such an integral does not present any complexity as many approaches for the accurate representation of the difference between these two modified Struve and Bessel function are available in the literature. For the fast evaluation of the integral, a simple procedure based on the Chebyshev-Gauss quadrature formulas has been adopted, making the transient ground resistance matrix evaluation very straightforward. The issues in the representation of the transition between early time and late time response of the line arising when one adopts the expressions available in the literature for the evaluation of the transient ground resistance matrix elements are no longer present if the proposed formula is used.

1.3.3. Inverse Laplace Transform of Sunde's Integrals

This section presents the inverse Laplace transform of the most general expression for the ground impedance matrix of overhead multiconductor lines under TL approximation: Sunde's integral formula. As already mentioned this formula is an extension of that Carson that takes also into account the effect of displacement currents in the ground return. All the details regarding the mathematical derivation of this inverse Laplace transform are reported in the relevant appendix. Furthermore, in the appendix, this derivation is extended to the case of buried cables.

The inverse Laplace transform of Sunde's integral formula for the diagonal elements of the ground impedance matrix is given by

$$\begin{aligned}
 L^{-1} \left\{ \frac{Z'_{g,ii}(s)}{s} \right\} &= \frac{\mu_0}{\pi} L^{-1} \left\{ \int_0^{\infty} \frac{\exp(-2h_i x)}{\sqrt{x^2 + \gamma_g^2} + x} dx \right\} = \\
 &= \frac{\mu_0}{\pi} \frac{e^{-\frac{at}{2}}}{2b_i} \left[\sqrt{1 + \frac{t^2}{4b_i^2}} + \int_0^t \frac{ak}{2} \sqrt{1 + \frac{k^2}{4b_i^2}} \frac{I_1 \left(\frac{a}{2} \sqrt{t^2 - k^2} \right)}{\sqrt{t^2 - k^2}} dk \right] - \frac{\mu_0}{\pi} \frac{1}{4b_i^2 a} (1 - e^{-at}) \quad (1.53)
 \end{aligned}$$

where $a = \sigma_g / \epsilon_0 \epsilon_{rg}$, $b_i = h_i \sqrt{\mu_0 \epsilon_0 \epsilon_{rg}}$.

The expression for the off-diagonal elements is the following

$$\begin{aligned}
 L^{-1} \left\{ \frac{Z'_{g,ij}(s)}{s} \right\} &= \frac{\mu_0}{\pi} L^{-1} \left\{ \int_0^\infty \frac{e^{-(h_i+h_j)x}}{\sqrt{x^2 + \gamma_g^2} + x} \cos(r_{ij}x) dx \right\} = \\
 &= \frac{\mu_0}{\pi} \text{Re} \left\{ \frac{e^{-\frac{at}{2}}}{2\hat{b}_{ij}} \left[\sqrt{1 + \frac{t^2}{4\hat{b}_{ij}^2}} + \int_0^t \frac{ak}{2} \sqrt{1 + \frac{k^2}{4\hat{b}_{ij}^2}} \frac{I_1\left(\frac{a}{2}\sqrt{t^2 - k^2}\right)}{\sqrt{t^2 - k^2}} dk \right] \right\} + \\
 &\quad - \frac{\mu_0}{\pi} \frac{(h_1 + h_2)^2 - r_{ij}^2}{[(h_1 + h_2)^2 + r_{ij}^2]^2} \frac{1}{\mu_0 \epsilon_g \cdot a} (1 - e^{-at})
 \end{aligned} \tag{1.54}$$

where, being the height of the conductors h_i and h_j and their mutual distance r_{ij} ,

$$\hat{b}_{ij} = \sqrt{\mu_0 \epsilon_0 \epsilon_{rg}} \left(\frac{h_i + h_j}{2} + j \frac{r_{ij}}{2} \right) \text{ and } \delta_{ij} = \text{Arg}(\hat{b}_{ij}).$$

The comparison between these new analytical expressions and the others discussed so far in this thesis is reported in Figure 1-33 and Figure 1-34. Both equations (1.53) and (1.54) are in perfect agreement with the numerical inversion of Sunde’s formula.

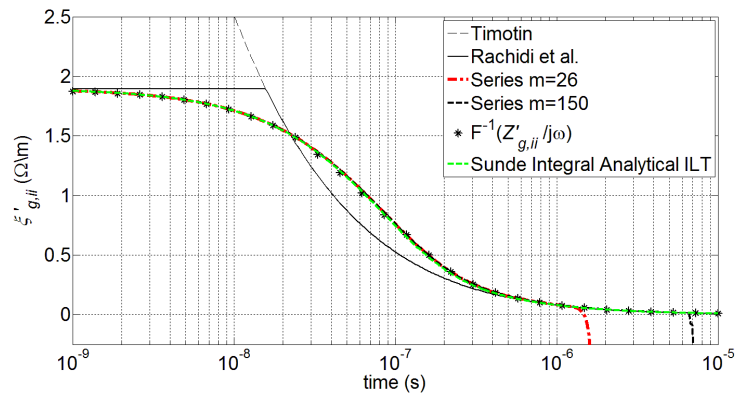


Figure 1-33 – Comparison between the proposed expression (1.53), equation (1.36) with 26 terms and the numerical inverse Fourier transform of $Z'_{g,ij}/j\omega$ for a 10-m high, single conductor line, above a conducting ground $\sigma_g = 0.001$ S/m and $\epsilon_{rg} = 10$.

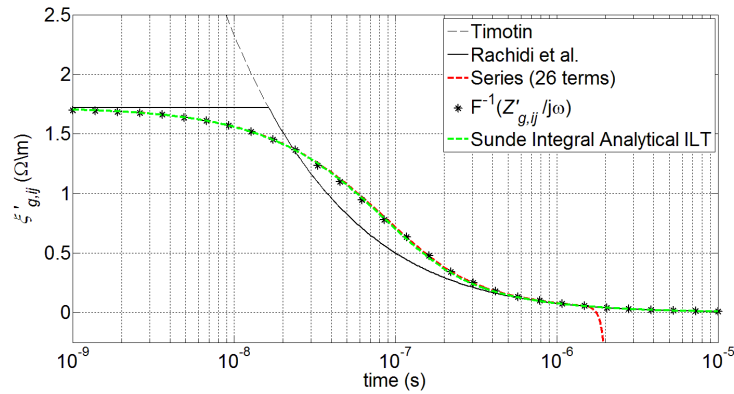


Figure 1-34 – Comparison between the proposed expression (1.54), equation (1.45) with 26 terms and the numerical inverse Fourier transform of $Z'_{g,ij}/j\omega$ for a 10-m and 12-m high, double conductor line, above a conducting ground $\sigma_g = 0.001$ S/m and $\epsilon_{rg} = 10$. $r_{ij} = 1$ m.

The analytical derivation of (1.53) and (1.54) can be extended to the case of buried cables. The self and mutual ground impedance of buried cables can be calculated according to Pollaczek's expressions (Pollaczek, 1926). In the original form proposed by Pollaczek the displacement currents in the ground are neglected. Lately, in (Sunde, 1968) the case in which also displacement currents are taken into account has been investigated. For the underground configuration shown in Figure 1-35, the ground impedance matrix elements are:

$$Z_{ii}(s) = \frac{s\mu_0}{2\pi} \left[\mathbf{K}_0(\gamma_g r_i) - \mathbf{K}_0(\gamma_g \sqrt{r_i^2 + 4h_i^2}) + \right. \\ \left. + 2 \int_0^\infty \frac{\exp(-2h_i \sqrt{x^2 + \gamma_g^2})}{\sqrt{x^2 + \gamma_g^2} + x} \cos(r_i x) dx \right] \quad (\text{A2.55})$$

$$Z_{ij}(s) = \frac{s\mu_0}{2\pi} \left[\mathbf{K}_0(\gamma_g d_{ij}) - \mathbf{K}_0(\gamma_g D_{ij}) + \right. \\ \left. + 2 \int_0^\infty \frac{\exp(-2h_{ij} \sqrt{x^2 + \gamma_g^2})}{\sqrt{x^2 + \gamma_g^2} + x} \cos(r_{ij} x) dx \right] \quad (\text{A2.56})$$

where \mathbf{K}_0 is the modified Bessel function of the second kind and order 0, r_i is the radius of the i -th conductor and

$$\begin{aligned}
 \gamma_g &= \sqrt{s\mu_0(\sigma_g + s\epsilon_0\epsilon_{rg})} \\
 h_{ij} &= h_i + h_j \\
 d_{ij} &= \sqrt{r_{ij}^2 + (h_i - h_j)^2} \\
 D_{ij} &= \sqrt{r_{ij}^2 + (h_i + h_j)^2}
 \end{aligned}
 \tag{A2.57}$$

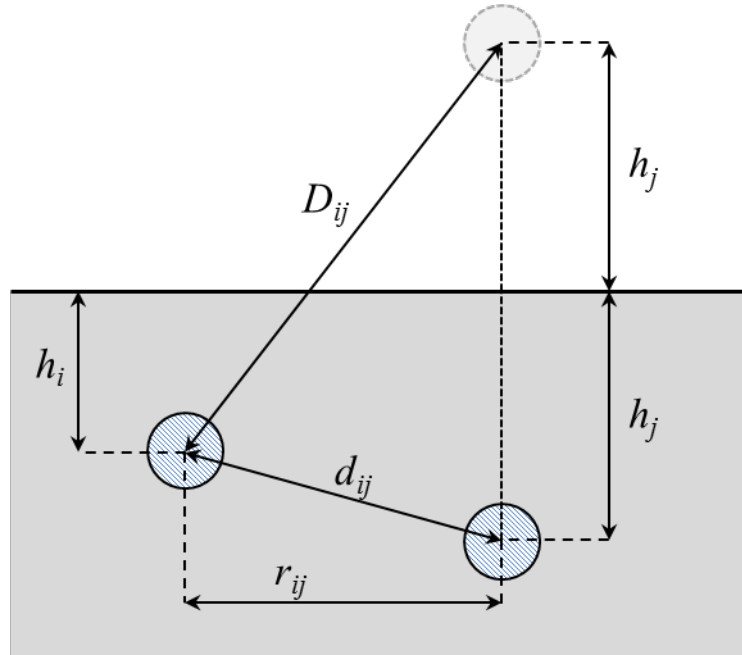


Figure 1-35 – Geometrical configuration of an underground multiconductor line

The inverse Laplace transform for the mutual elements is reported hereafter; the diagonal elements are a particular case of (A2.59) and (A2.61). For a detailed derivation see the relevant appendix.

Defining the Pollaczek-Sunde integral as

$$J_{ij}(s) = \frac{s\mu_0}{\pi} \int_0^{\infty} \frac{\exp\left(-2h_{ij}\sqrt{x^2 + \gamma_g^2}\right)}{\sqrt{x^2 + \gamma_g^2} + x} \cos(r_{ij}x) dx
 \tag{A2.58}$$

its inverse Laplace transform reads

$$\begin{aligned}
L^{-1}\left[\frac{J_{ij}(s)}{s}\right] &= L^{-1}\left[\frac{\mu_0}{\pi}\int_0^\infty\frac{\exp(-2h_{ij}\sqrt{x^2+\gamma_g^2})}{\sqrt{x^2+\gamma_g^2}+x}\cos(r_{ij}x)dx\right]= \\
&= \frac{\mu_0}{\pi}\frac{e^{-\frac{at}{2}}}{2b_{ij}}\theta\left(t-2h_{ij}\sqrt{\mu_0\varepsilon_g}\right)\operatorname{Re}\left\{\left[\sqrt{1+y^2(t)}-y(t)\right]\left[\frac{y(t)}{\sqrt{1+y^2(t)}}+j\frac{r_{ij}}{2h_{ij}}\right]^{-1}\right. \\
&\quad \left.+\int_{2h_{ij}\sqrt{\mu_0\varepsilon_g}}^t\left(\sqrt{1+y^2(k)}-y(k)\right)\left[\frac{y(k)}{\sqrt{1+y^2(k)}}+j\frac{r_{ij}}{2h_{ij}}\right]^{-1}\frac{ak}{2}\frac{I_1\left(\frac{a}{2}\sqrt{t^2-k^2}\right)}{\sqrt{t^2-k^2}}dk\right\}
\end{aligned} \tag{A2.59}$$

where

$$y(k)=\frac{-jkr_{ij}+2\sqrt{h_{ij}^2k^2-b_{ij}^2(4h_{ij}^2+r_{ij}^2)}}{\sqrt{\mu_0\varepsilon_g}(4h_{ij}^2+r_{ij}^2)} \tag{A2.60}$$

and $b_{ij}=\sqrt{\mu_0\varepsilon_0\varepsilon_{rg}}(h_i+h_j)$

The inverse Laplace transform of the difference between the two Bessel functions is given by:

$$\begin{aligned}
&\frac{\mu_0}{2\pi}L^{-1}\left[\mathbf{K}_0(\gamma_g d_{ij})-\mathbf{K}_0(\gamma_g D_{ij})\right]= \\
&\frac{\mu_0}{2\pi}e^{-\frac{at}{2}}\theta\left(t-d_{ij}\sqrt{\mu_0\varepsilon_g}\right)\left[\frac{1}{\sqrt{t^2-d_{ij}^2\mu_0\varepsilon_g}}+\int_{d_{ij}\sqrt{\mu_0\varepsilon_g}}^t\frac{\frac{ak}{2}I_1\left(\frac{a}{2}\sqrt{t^2-k^2}\right)}{\sqrt{t^2-k^2}}\frac{1}{\sqrt{k^2-d_{ij}^2\mu_0\varepsilon_g}}dk\right]+ \\
&-\frac{\mu_0}{2\pi}e^{-\frac{at}{2}}\theta\left(t-D_{ij}\sqrt{\mu_0\varepsilon_g}\right)\left[\frac{1}{\sqrt{t^2-D_{ij}^2\mu_0\varepsilon_g}}+\int_{D_{ij}\sqrt{\mu_0\varepsilon_g}}^t\frac{\frac{ak}{2}I_1\left(\frac{a}{2}\sqrt{t^2-k^2}\right)}{\sqrt{t^2-k^2}}\frac{1}{\sqrt{k^2-D_{ij}^2\mu_0\varepsilon_g}}dk\right]
\end{aligned} \tag{A2.61}$$

1.4. The Response of Multi-Conductor Lines to Lightning- Originated Electromagnetic Pulse

The response of a multiconductor overhead line to an external incident electromagnetic field such as the one originated by a nearby lightning return stroke has been treated by several authors (*Rusck, 1958a; Chowdhuri, 1969, 1990; Cinieri & Fumi, 1979; Eriksson et al., 1982; Yokoyama et al., 1983; Yokoyama, 1984; Yokoyama et al., 1986; Liew & Mar, 1986; Yokoyama et al., 1989; Cinieri & Muzi, 1996; Rachidi et al., 1997; Andreotti et al., 1998*). In case of lines with no grounded conductors (shield wires, neutrals), this effect has been considered as insignificant (*Cinieri & Fumi, 1979; Chowdhuri, 1990; Cinieri & Muzi, 1996*) or null (*Rusck, 1958a; Yokoyama, 1984; Liew & Mar, 1986*), (*Andreotti et al., 1998*), while in other studies, it has been found that the magnitude of the induced voltages on a multiconductor line is higher (*Chowdhuri, 1969*), or could be higher (*Chowdhuri, 1990*) than that on a single-conductor line of the same height above ground. The paper by *Rachidi et al. (1997)* has helped to clarify some of the mentioned disagreements, which in most cases were due to the use of a particular coupling model (*Chowdhuri, 1969, 1990*) which has been demonstrated not to be adequate (*Nucci et al., 1995*). The aim of this section is to further clarify some issues which were not fully covered in (*Rachidi et al., 1997*) and to add some more general considerations on the subject making reference to the coupling models proposed in the literature. In particular, the shielding capabilities of the line assumed by *Rachidi et al.* in which each wire is terminated on a resistance equal to its surge impedance calculated in absence of the other conductors is worth of further discussion, that the present section is aimed at providing.

The second point that the present section is aimed at addressing is the effect of the ground losses on the surge propagation along a multiconductor line illuminated by an external field. Such an issue has been treated by several authors e.g. (*Rachidi et al., 1996; Kannu & Thomas, 2005; Rachidi et al., 1999*) by representing the ground losses as an additional longitudinal term in the coupling equations (the so-called ground impedance in the frequency domain, or its time-domain counterpart the transient ground resistance). One conclusion of these studies is that the finite ground conductivity decreases the magnitude of the induced voltage at the line terminations for a stroke location equidistant from them. Further, in (*Kannu & Thomas, 2005*) the authors have correctly observed that the transient ground resistance effect is to slightly increase the induced voltage at the mid-point of the line for the same type of stroke location. In this section, some further elements on the above are provided, by extending the analysis to a matched multiconductor line.

Voltages Induced on a Three-Phase Line by an External Incident Electromagnetic Field

Let us consider the same two configurations of (Chowdhuri, 1990) and (Rachidi *et al.*, 1997), which are shown in Figure 1-36. In the first one (vertical configuration), the three conductors are disposed along the same vertical axis at different heights above ground (Figure 1-36.a); in the second (horizontal configuration), the conductors are located at the same height above the ground surface (Figure 1-36.b). The presence of one and two ground (or shielding) wires for configurations (a) and (b), respectively, is also taken into account. The radius of each conductor is 9.14 mm for phase conductors and 3.96 mm for the ground wires. The length of the line is assumed to be 1 km, if not otherwise specified. The lightning return-stroke location is assumed to be at 50 m from the center of the line and equidistant to the line terminations.

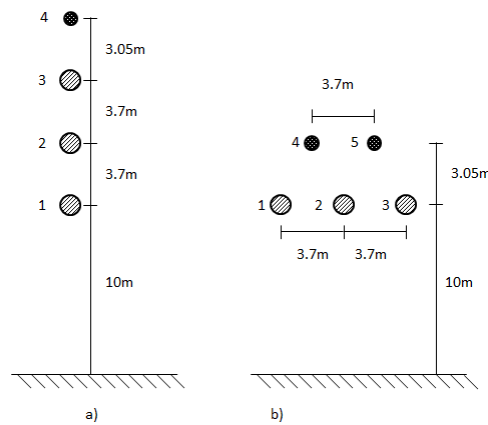


Figure 1-36 – Considered power line configurations. (a) Vertical, (b) horizontal. Conductors numbered 1, 2 and 3 refer to phase conductors, 4 and 5 to ground wires.

The channel-base current is typical of subsequent return strokes (Berger *et al.*, 1975) with a peak value of 12 kA and a maximum time-derivative of 40kA/μs, represented by using the sum of two Heidler's functions (Nucci *et al.*, 1993). The return stroke velocity is assumed to be $1.3 \cdot 10^8$ m/s and the adopted return stroke model is the modified transmission line model with exponential decay (MTLE) (Nucci *et al.*, 1988; Rachidi & Nucci, 1990) with a decay constant $\lambda = 2$ km. The incident electromagnetic field is evaluated assuming an ideal ground (perfectly conducting), if not otherwise specified.

The induced voltages can be evaluated using the Agrawal *et al.* model (Agrawal *et al.*, 1980), which are recall here for convenience:

$$\frac{\partial}{\partial x} [v_i^s(x, t)] + [L'_{ij}] \frac{\partial}{\partial t} [i_j(x, t)] = [E_x^e(x, h_i, t)] \quad (1.62)$$

$$\frac{\partial}{\partial x} [i_i(x,t)] + [C'_{ij}] \frac{\partial}{\partial t} [v_i^s(x,t)] = 0 \quad (1.63)$$

where

- $[E_x^e(x, h_i, t)]$ is the vector of the horizontal component of the incident electric field (calculated in absence of the line conductors) along the x axis at the conductor's height h_i where the sub-index i denotes the particular wire;
- $[L'_{ij}]$ and $[C'_{ij}]$ are the matrices of the line per-unit-length inductances and capacitances respectively;
- $[i_i(x,t)]$ is the line current vector;
- $[v_i^s(x,t)]$ is the scattered voltage vector, from which the total voltage vector $[v_i(x,t)]$ can be evaluated as

$$[v_i(x,t)] = [v_i^s(x,t)] - \left[\int_0^{h_i} E_z^e(x, z, t) dz \right] \quad (1.64)$$

where

- $E_z^e(x, z, t)$ is the vertical component of the incident electric field (calculated in absence of the line conductors).

Let us assume that the line is terminated on pure resistive terminations represented by the matrices $[R_{0,ij}]$ and $[R_{L,ij}]$. The boundary conditions are given by

$$[v_i^s(0,t)] = -[R_{0,ij}][i_i(0,t)] + \left[\int_0^{h_i} E_z^e(0, z, t) dz \right] \quad (1.65)$$

$$[v_i^s(L,t)] = [R_{L,ij}][i_i(L,t)] + \left[\int_0^{h_i} E_z^e(L, z, t) dz \right] \quad (1.66)$$

A common practice in lightning induced overvoltage calculations is to match the line ends with the line surge impedance in order to avoid reflections. Diversely from the case of non-illuminated lines, a matched impedance at the line ends does not prevent the presence of 'bumps', that are not to be ascribed to reflections, but to the effect of the so-called 'risers' (Nucci *et al.*, 1993).

Figure 1-37 shows the voltages induced at the terminations of the three line conductors for the vertical configuration disregarding the presence of the ground wire. Each wire is terminated on a resistance equal to its characteristic impedance determined in absence of the other conductors (henceforth called surge diagonal matrix terminations). Hence, the line is not matched and some reflections arise in agreement with what previously found in (Rachidi *et al.*, 1997; Kannu & Thomas, 2005).

The same case is shown in Figure 1-38 but, this time, for a matched line, namely using a full matrix termination impedance as detailed in what follows.

For the considered case of a lossless, homogeneous multiconductor line, the characteristic impedance matrix $[Z_C'_{ij}]$ can be simply expressed as the multiplication of the per-unit-length inductance matrix and the surge propagation speed. Therefore, for the case of Figure 1-38, the termination matrices of resistances are given by

$$[R_{0,ij}] = [R_{L,ij}] = [Z_C'_{ij}] = c_0[L'_{ij}] \quad (1.67)$$

where c_0 is the speed of light.

For the case of Figure 1-37, all off-diagonal terms of the termination resistance matrices are set to zero, while the diagonal term ii correspond to the characteristic impedance of the i -th conductor, evaluated in absence of other conductors (corresponding to the so-called surge diagonal matrix terminations).

The difference between the results of Figure 1-37 and Figure 1-38 is due to the effect of the off-diagonal terms of the surge impedance matrix, disregarded in the induced voltage calculation shown in Figure 1-37. As a matter of fact, the same partial differential equation problem defined by (1.62) and (1.63) leads to different solutions depending on the boundary conditions.

Figure 1-39 shows the voltages induced on the three conductors of configuration (b) (in absence of the shield wires) when the off-diagonal terms of the matrix terminations are set to zero. In Figure 1-40, the results are shown, instead, for the case of matched terminations. Now, for such a case, as well as for the case of an infinitely-long line, the boundary conditions relevant to the terminations do not introduce any dependence among the conductors voltages. It is interesting to observe that the same applies for the case of an open line for which the currents in equations (1.65) and (1.66) are both equal to zero and therefore no dependencies among the conductors voltages are introduced.

Note that the results presented in Figure 1-37 and Figure 1-39 correspond to the same configuration assumed in (Rachidi *et al.*, 1997) with surge diagonal matrix terminations.

In Figure 1-41 and Figure 1-42, the currents relative to the cases of Figure 1-39 and Figure 1-40 are shown, respectively. Considering that the distance between the line conductors is much smaller than the distance to the lightning strike location, the resulting differences between the induced voltages will be negligible, hence, before they could be affected by the boundary conditions, the induced voltages on the three conductors are equal, while the currents in each conductor differ from one another due to mutual coupling.

Case of an Infinitely Long Line

The voltages induced by an external EM field along an infinitely-long lossless line without discontinuities are not affected by the presence of other conductors (Rusck, 1958a; Rachidi *et al.*, 1997; Yokoyama, 1984), while the currents do. This is shown by the two sets of three D'Alembert inhomogeneous equations (1.68) and (1.69), which can be derived from the Agrawal *et al.* coupling equations (1.62) and (1.63) (the equivalent circuit for a single conductor line is shown in Figure 1-43)

$$\frac{\partial^2 [v_i^s(x,t)]}{\partial x^2} - \frac{1}{c_0^2} \frac{\partial^2 [v_i^s(x,t)]}{\partial t^2} = \frac{\partial}{\partial x} [E_x^e(x, h_i, t)] \quad (1.68)$$

$$\frac{\partial^2 [i_i(x,t)]}{\partial x^2} - \frac{1}{c_0^2} \frac{\partial^2 [i_i(x,t)]}{\partial t^2} = -[C'_{ij}] \frac{\partial}{\partial t} [E_x^e(x, h_i, t)] \quad (1.69)$$

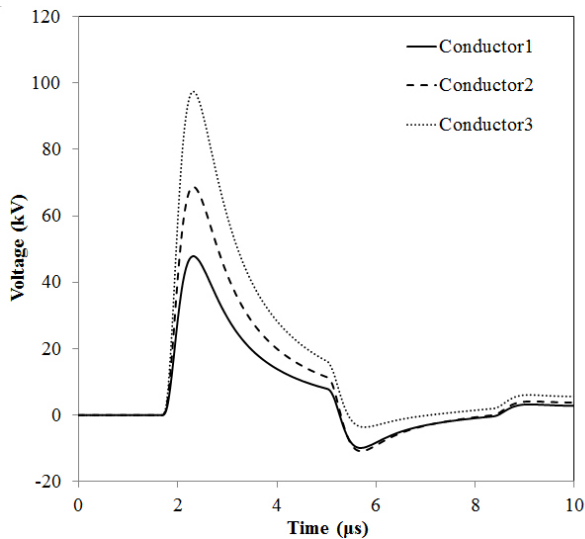


Figure 1-37 - Voltages induced at the three-conductor line ends of configuration (a) for surge diagonal matrix terminations (disregarding the presence of ground wire).

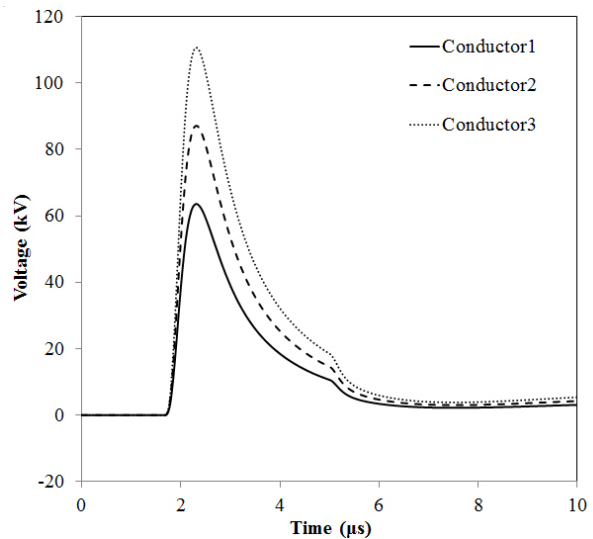


Figure 1-38 - Voltages induced at the three-conductor line ends of configuration (a) for matched terminations (disregarding the presence of ground wire).

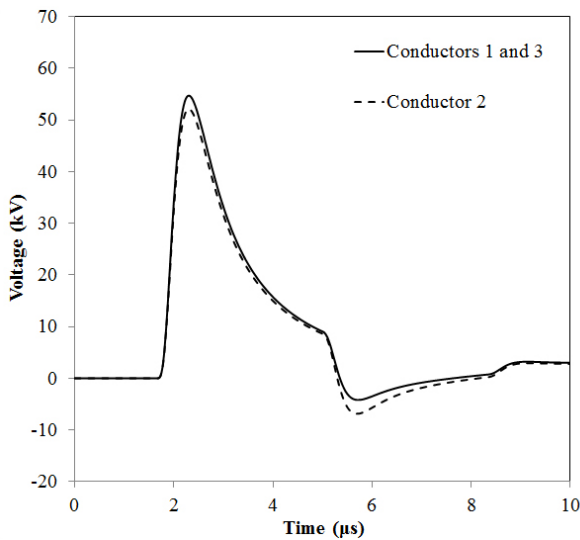


Figure 1-39 - Voltages induced at the three-conductor line ends of configuration (b) for surge diagonal matrix terminations (disregarding the presence of ground wire).

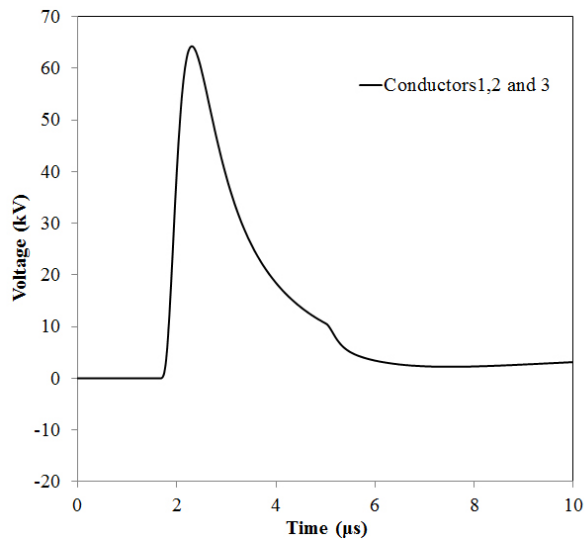


Figure 1-40 - Voltages induced at the three-conductor line ends of configuration (b) for matched terminations (disregarding the presence of ground wire).

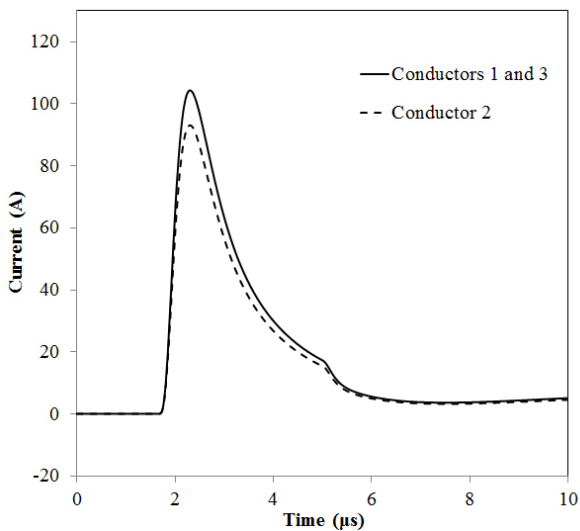


Figure 1-41 - Currents flowing at the termination of the three-conductor line of configuration (b) for surge diagonal matrix terminations (disregarding the presence of ground wire).

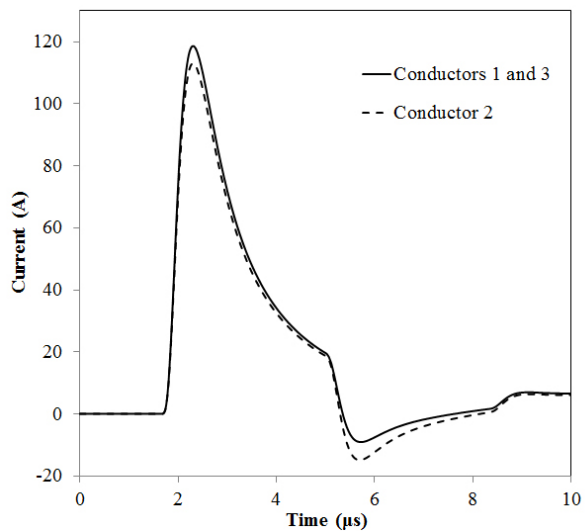


Figure 1-42 - Currents flowing at the termination of the three-conductor line of configuration (b) for matched terminations (disregarding the presence of ground wire).

For the case of the horizontal configuration, equations in (1.68) share the same forcing functions, while (1.69) can be written for each conductor as

$$\frac{\partial^2 i_i(x,t)}{\partial x^2} - \frac{1}{c_0^2} \frac{\partial^2 i_i(x,t)}{\partial t^2} = -\frac{\partial E_{x,i}^e(x,h,t)}{\partial t} \sum_{j=1}^n C'_{ij} \quad (1.70)$$

For the assumed geometry, the capacitance matrix is:

$$[C'_{ij}] = \begin{bmatrix} 7.66 & -1.54 & -0.71 \\ -1.54 & 7.96 & -1.54 \\ -0.71 & -1.54 & 7.66 \end{bmatrix} \text{ pF/m} \quad (1.71)$$

Equations (1.70) and (1.71) clearly show that the forcing function in the D'Alembert equation for the middle conductor is smaller than those corresponding to the external conductors.

It is interesting now to consider the coupling model by *Rachidi* (1993) where only the incident magnetic field components appear explicitly as forcing functions in the equations

$$\frac{\partial}{\partial x} [v_i(x,t)] + [L'_{ij}] \frac{\partial}{\partial t} [i_i^s(x,t)] = 0 \quad (1.72)$$

$$\frac{\partial}{\partial x} [i_i^s(x,t)] + [C'_{ij}] \frac{\partial}{\partial t} [v_i(x,t)] = -[L'_{ij}]^{-1} \left[\int_0^{h_i} \frac{\partial B_x^e(x,z,t)}{\partial y} dz \right] \quad (1.73)$$

where

– $[i_i^s(x,t)]$ is the scattered current vector, related to $[i_i(x,t)]$, the total current vector, by the following expression

$$[i_i(x,t)] = [i_i^s(x,t)] + [L'_{ij}]^{-1} \left[\int_0^{h_i} B_y^e(x,z,t) dz \right] \quad (1.74)$$

– $B_x^e(x,z,t)$ and $B_y^e(x,z,t)$ are the horizontal components of the incident magnetic field.

The equivalent circuit of *Rachidi* model (Figure 1-44) contains only currents sources. Nevertheless, we will show that the predicted voltage on each conductor is again not affected by the presence of the others, while the currents flowing in the line conductors do.

As for the case of the *Agrawal* model, the two coupled equations of *Rachidi* model (1.72) and (1.73) can be combined to derive uncoupled inhomogeneous D'Alembert equations:

$$\frac{\partial^2 [v_i(x,t)]}{\partial x^2} - \frac{1}{c_0^2} \frac{\partial^2 [v_i(x,t)]}{\partial t^2} = \left[\int_0^h \frac{\partial^2 B_x^e(x,z,t)}{\partial y \partial t} dz \right] \tag{1.75}$$

$$\frac{\partial^2 [i_i^s(x,t)]}{\partial x^2} - \frac{1}{c_0^2} \frac{\partial^2 [i_i^s(x,t)]}{\partial t^2} = -[L'_{ij}]^{-1} \left[\int_0^h \frac{\partial^2 B_x^e(x,z,t)}{\partial y \partial x} dz \right]. \tag{1.76}$$

Assuming the same incident magnetic field for each conductor, the induced overvoltages given by equation (1.75) are equal while, according to (1.76), the currents will generally be different from one conductor to another which is by the way in perfect agreement with the fact that the two coupling models – Agrawal and Rachidi – are equivalent (Nucci & Rachidi, 1995). Needless to add that the same development can be repeated adopting the Taylor et al. (1965b) model leading to the same conclusion.

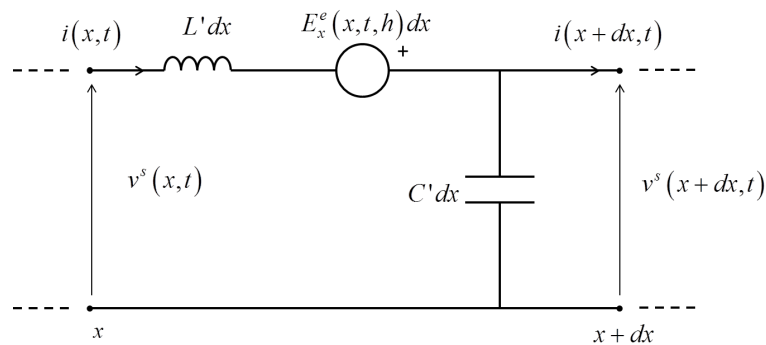


Figure 1-43 – Equivalent differential circuit of Agrawal et al. coupling model for the case of a lossless line

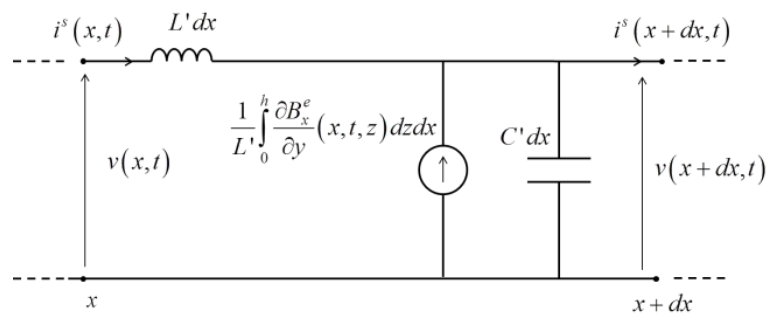


Figure 1-44 – Equivalent differential circuit of Rachidi coupling model for the case of a lossless line

Case of a Finite Length Line

Let us consider, without losing generality, the vertical configuration (Figure 1-36.a) in absence of the shield wire. The distributions of the voltage peak amplitudes along the line for the case of matched terminations (solid lines) and surge diagonal matrix terminations (dashed line) are shown in Figure 1-45. For the considered case, the profile of the overvoltage peak amplitudes in the internal part of the line is the same, independently from the type of the terminations. The peak distribution plots of Figure 1-45 show some minor sags nearby the line ends for the case of matched terminations too, which, however, have to be ascribed to the effect of the so-called ‘risers’.

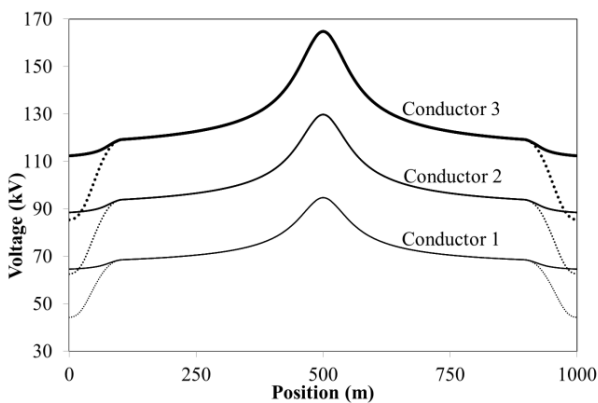


Figure 1-45 – Voltage peak amplitudes along the line of each conductor, for the case of perfectly matched terminations (solid lines) and surge diagonal matrix terminations (dotted lines). Vertical configuration.

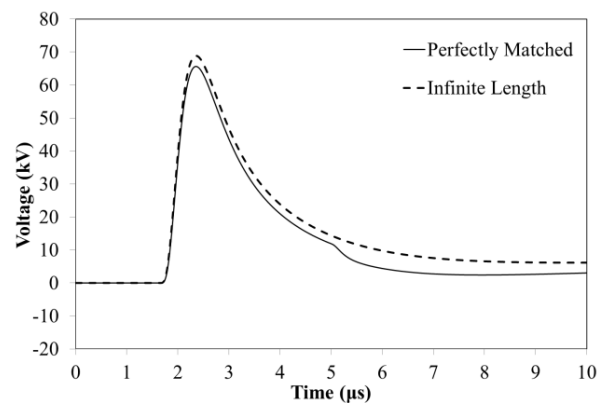


Figure 1-46 – Induced voltages at x=0 m (500m far from the point of the line facing the stroke location); comparison between an infinite line and a matched one. Horizontal configuration

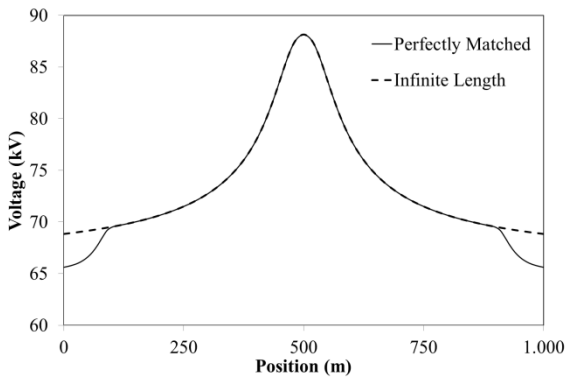


Figure 1-47 – Induced voltage peak amplitude along the line; comparison between an infinite line and a matched one. Horizontal configuration.

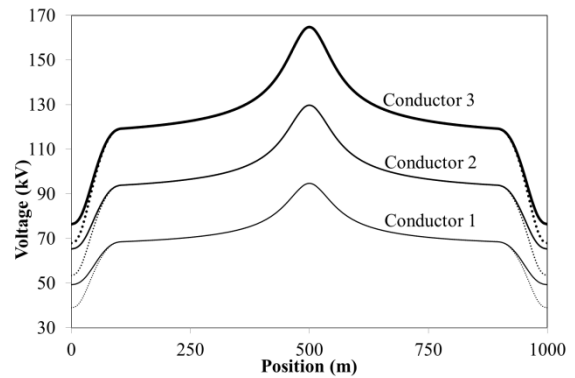


Figure 1-48 – Distribution of the voltage peak amplitudes along the line of each conductor for the case of matched terminations (solid lines) and surge diagonal matrix terminations (dotted lines) with the presence of a shield wire grounded at the line terminations. Vertical configuration.

To better illustrate this effect, Figure 1-46 presents a comparison, for the case of a horizontally-configured line, between the overvoltage measured at $x = 0\text{m}$ (500m away from the position of the line ‘facing’ the strike location) of a matched line and an infinitely long one (the considered length is 5 km so that, in the observed time window, there is no influence of the portions beyond 5 km on the presented overvoltages). In Figure 1-47 the same comparison is presented, this time concerning the voltage peak amplitudes along the line, again for a horizontally-configured line. As expected, the ‘risers’ effect results in some further sag of the amplitude distribution plots in the immediate vicinity of the terminations.

For the assumed stroke location, the effect of the presence of the other conductors for the case of surge diagonal matrix terminations or, more in general, non-matched terminations appears only at the neighborhood of the line ends. This result is of interest for lightning performance assessment of distribution lines (*Borghetti et al., 2007*), in particular when the lightning performance has to be evaluated at a specific pole (*Borghetti et al., 2009*), as for some stroke locations there is no effect due to the presence of other conductors in the central portion of the line. Of course, the situation is different for a lightning return stroke located in the vicinity of one of the line ends.

In Figure 1-48, the same case of Figure 1-45 is shown, but this time assuming the presence of a grounded wire. Since the upper wire is assumed to be grounded only at the line ends, the profile of the overvoltage peak amplitudes in the inner part of the line is the same of Figure 1-45. This is an expected result since the reflected voltages/effect of risers at the line ends will reach these central positions at a time longer than the zero-to-peak time of the induced voltages. To obtain a significant shielding effect, multiple grounding along the line are required (*Borghetti et al., 2007; Paolone et al., 2004; Munhoz Rojas, 2009; Piantini & Janiszewski, 2009; Silveira et al., 2011*).

Surge Propagation Losses

Accounting for the presence of a lossy ground characterized by its conductivity σ_g and its relative permittivity ϵ_{rg} , the Agrawal *et al.* coupling equations in time domain read (*Rachidi et al., 1999*)

$$\frac{\partial}{\partial x}[v_i^s(x,t)] + [L'_{ij}] \frac{\partial}{\partial t}[i_i(x,t)] + \int_0^t [\xi_g'_{ij}(t-\tau)] \frac{\partial}{\partial \tau}[i_i(x,\tau)] d\tau = [E_x^e(x, h_i, t)] \quad (1.77)$$

$$\frac{\partial}{\partial x}[i_i(x,t)] + [C'_{ij}] \frac{\partial}{\partial t}[v_i^s(x,t)] = 0 \quad (1.78)$$

in which $[\xi_g'_{ij}(t)]$ is the transient ground resistance matrix. In this analysis, the wire impedance, the ground admittance and the line conductance have been disregarded (an approximation valid for typical overhead lines a few meters above the ground (Rachidi *et al.*, 1996)).

Following the same procedure adopted for the case of a lossless line, (1.77) and (1.78) can be combined to obtain

$$\frac{\partial^2 [v_i^s(x,t)]}{\partial x^2} - \frac{1}{c_0^2} \frac{\partial^2 [v_i^s(x,t)]}{\partial t^2} = \frac{\partial}{\partial x} \left([E_x^e(x, h_i, t)] - [v_g'_{ij}(x,t)] \right) \quad (1.79)$$

$$\frac{\partial^2 [i_i(x,t)]}{\partial x^2} - \frac{1}{c_0^2} \frac{\partial^2 [i_i(x,t)]}{\partial t^2} = -[C'_{ij}] \frac{\partial}{\partial t} \left([E_x^e(x, h_i, t)] - [v_g'_{ij}(x,t)] \right) \quad (1.80)$$

where

$$[v_g'_{ij}(x,t)] = \int_0^t [\xi_g'_{ij}(t-\tau)] \frac{\partial}{\partial \tau} [i_i(x,\tau)] d\tau \quad (1.81)$$

The corresponding equivalent circuit is shown in Figure 1-49.

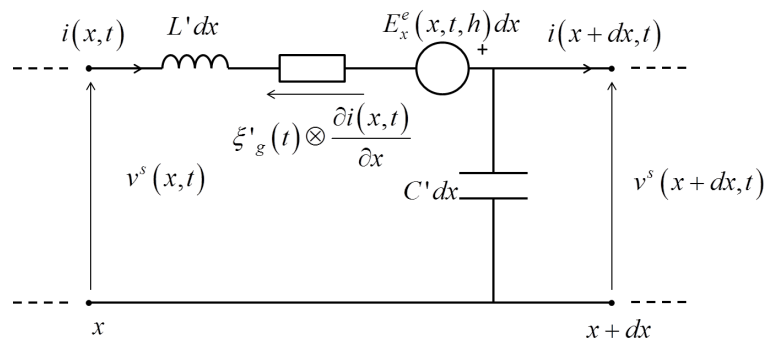


Figure 1-49 – Equivalent differential circuit of Agrawal *et al.* coupling model for the case of a lossy line (the symbol \otimes denotes the convolution product).

The above equations show that the presence of the transient ground resistance matrix introduces in the right side of (1.79) a term $v'_{g,i}(x,t)$, which is a function of the currents flowing into the line conductors and in the ground return. Therefore, even if the line is infinitely long or matched, the voltage induced by an external electromagnetic field in a lossy line is affected by the presence of the other conductors of the line.

A comparison between the overvoltage induced on an ideal (lossless) single-conductor line, a lossy single-conductor line, an ideal (lossless) 3-phase line, and a lossy 3-phase line is shown in Figure 1-50, for a horizontal configuration and a symmetrical stroke location. The observation points are: a) at the line termination, b) 500 m away from the mid-point of the line, c) in the middle of the line. The ground conductivity is assumed to be $\sigma_g=0.001$ S/m and its relative permittivity is set to $\epsilon_{rg}=10$; the incident horizontal electromagnetic field is evaluated with the Cooray-Rubinstein formula.

The return stroke model and the channel-base current are the same described in Section II. The line is 2 km long, and it is matched taking into account the frequency dependence of the characteristic impedance. For the case of a homogeneous lossy ground, the characteristic impedance of the line is frequency dependent, so the matrix of the termination becomes:

$$\left[Z'_c{}'_{ij}(\omega) \right] = \left[Z'_{ij} \right] \left(\sqrt{\left[Y'_{ij} \right] \left[Z'_{ij} \right]} \right)^{-1} \quad (1.82)$$

in which $\left[Z'_g{}'_{ij}(\omega) \right]$ is the ground impedance matrix

$$\left[Z'_{ij} \right] = \text{Re} \left[Z'_g{}'_{ij}(\omega) \right] + j \left(\omega \left[L'_{ij} \right] + \text{Im} \left[Z'_g{}'_{ij}(\omega) \right] \right) \quad (1.83)$$

and

$$\left[Y'_{ij} \right] = j\omega \left[C'_{ij} \right]. \quad (1.84)$$

For the case of frequency dependent terminations, the product of the termination matrix and the current vector in equations (1.65) and (1.66) turns into a convolution product, which has to be solved numerically.

As can be seen from Figure 1-50, the induced voltages for the case of a three-phase ideal line are the same as those along a single-phase ideal line, in agreement with the analysis presented in the previous section. On the other hand, the induced voltage at the termination of a lossy single conductor line has lower peak amplitude and a longer rise-time compared to the case of

an ideal line. Such an effect is even more significant for the case of a three-phase lossy line. Contrary to what occurs at the line terminations, at the middle point (Fig 15.c) the effect of the transient ground resistance matrix in the coupling model is to slightly increase the peak of the induced voltage amplitude compared to the ideal case, in agreement with the conclusions reported by Kannu and Thomas for a non-matched line (*Kannu & Thomas, 2005*).

Note that all the simulation results presented in Figure 1-50 have been obtained using the same incident field. As a result, the observed increase in Figure 1-50.c for the case of lossy lines can only be ascribed to the effect of the transient ground resistance, which in the Agrawal *et al.* model (Figure 1-49) is represented by the term (1.81), whose effect is to alter the scattered voltage with respect to the ideal case, as shown by (1.79). The observed above-mentioned effect is stronger as the number of conductors grows.

Let us now analyze the different effect that the transient ground resistance has on the total voltage in different positions along the line. Figure 1-51 refers to the same cases of Figure 1-50, but this time the incident and scattered voltages are shown individually. The total voltage is given by the sum of the scattered voltage and the incident one; while the incident voltage remains practically unchanged when the ground is lossy (*Cooray, 2008*), the scattered voltage is clearly affected by the line losses. The effect of the transient ground resistance on the scattered voltage depends on the position along the line. At the point in front of the stroke location the effect is to weaken the reaction of the line to the external LEMP; therefore, a decrease of the scattered voltage magnitude results in an increase of the total voltage as scattered and incident voltages have different polarity. At the line terminations (for the considered configuration), a reduction of the scattered voltage peak results in the observed decrease of the total voltage peak as both scattered and incident voltages have the same polarity. Figures 1-50 and 1-51 further show that the transient ground resistance effect on the induced voltage varies as a function of the time. Initially, the line losses effect is to decrease the voltage peak and to increase its rise-time; as the time goes by the effect of losses is to increase the voltage with respect to the ideal case.

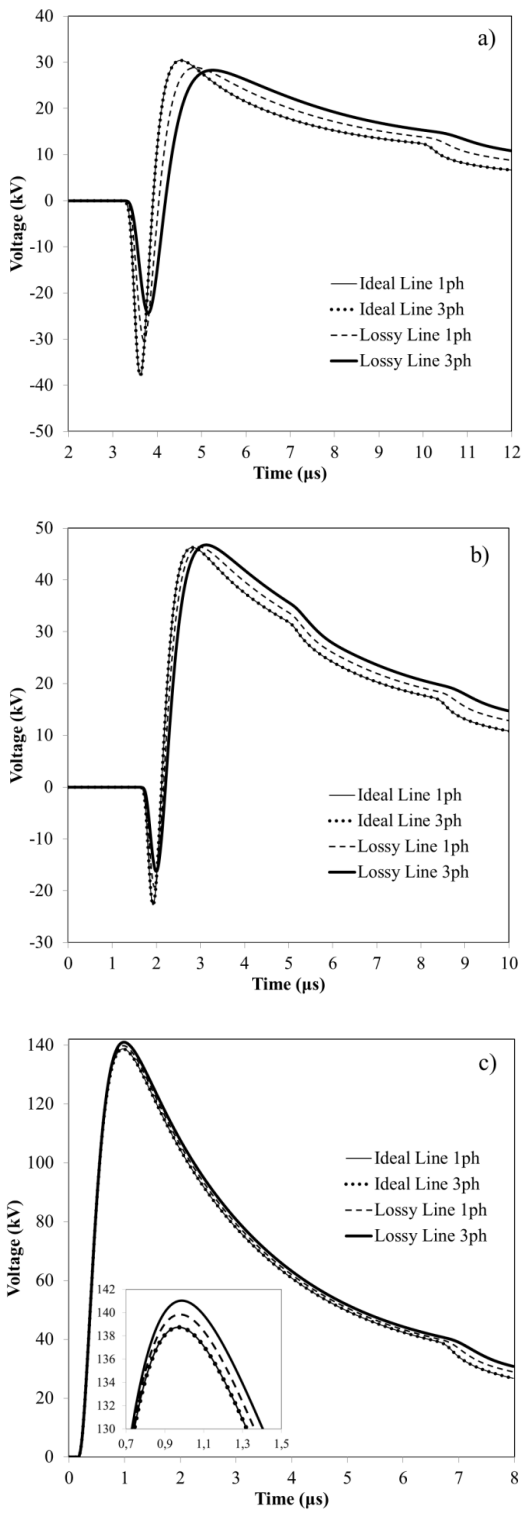


Figure 1-50 – Total voltages. Comparison between an ideal line (single phase and 3-phase), a lossy single-conductor line and a lossy 3-phase line; $\sigma_g=0.001$ S/m, $\epsilon_{rg}=10$. Horizontal configuration, 2 km long line matched at both ends. The incident horizontal EM field is evaluated using the CR formula for all the considered cases (lossy and ideal).

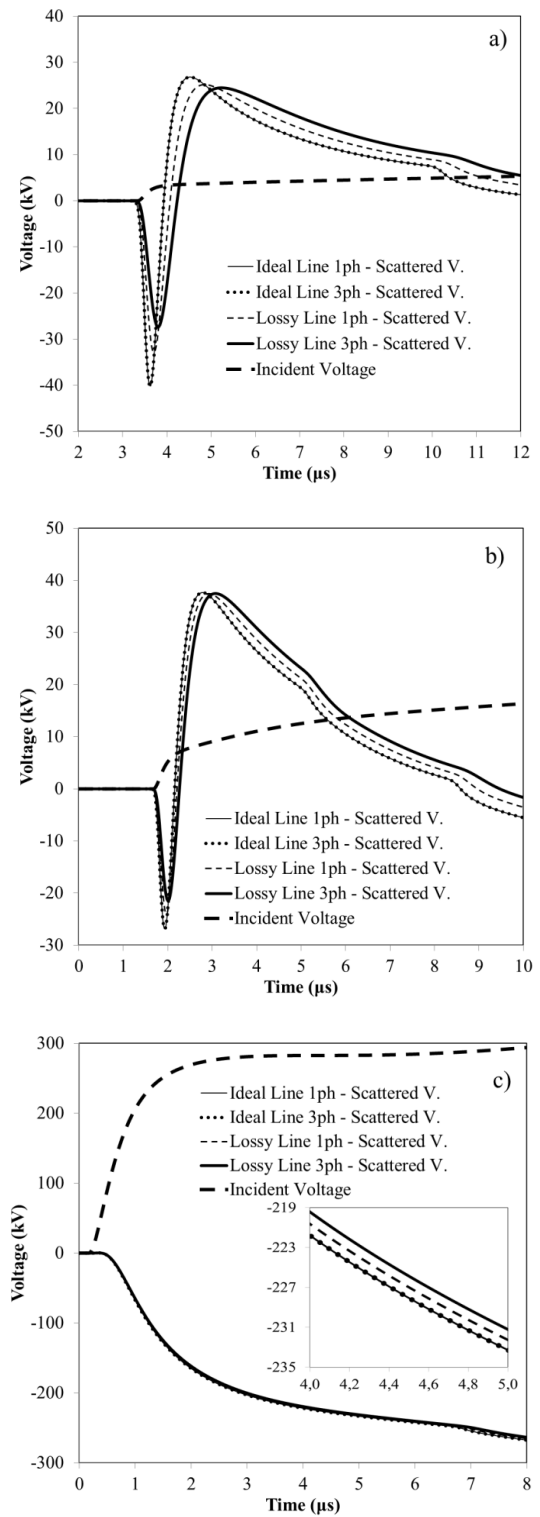


Figure 1-51 – Scattered and incident voltages. Comparison between an ideal line (single phase and 3-phase), a lossy single-conductor line and a lossy 3-phase line; $\sigma_g=0.001$ S/m, $\epsilon_{rg}=10$. Horizontal configuration, 2 km long line matched at both ends. The incident horizontal EM field is evaluated using the CR formula for all the considered cases (lossy and ideal).

In the case of a lossy-line the induced overvoltages along a horizontally-configured line are the same in all the wires, as in the case of an ideal-line; however, the multiconductor line response is different from the single-conductor one. This result is in agreement with those presented in (*Kannu & Thomas, 2005*).

Conclusion

The differences between the behavior of matched and non-matched lines concerning the effect of the various line conductors as well as the effect of the ground losses have been addressed making use of coupling models based on the transmission line theory. The cases for which the induced voltage on one conductor is not affected by the presence of other conductors are those of an infinitely long lossless line, of a lossless matched line and of a lossless open line. For the second case, a reduction of the amplitude of the induced voltages with respect to the case of an infinitely long line is observed, but only nearby the line terminations, and this is not due to the presence of the other conductors but to the so-called ‘risers’, which describe the effect of the missing portion of the illuminated line beyond the line terminations. The response of a matched lossless multiconductor line differs from that of a single-conductor line at the same height only in the line currents. The effect of the nearby line conductors on the induced voltages is, indeed, noticeable when the ground losses are taken into account in the surge propagation.

Note, finally, that the conclusions of this section remain valid for multiconductor lines illuminated by any arbitrary incident electromagnetic fields.

2. Statistical Evaluation of the Lightning Performance of Distribution Networks

2.1. The Lightning Performance of Overhead Distribution Lines

The statistical procedure for the evaluation of the lightning performance of distribution lines adopted in this thesis is based in the application of the Monte Carlo method and on the calculation of the induced voltages by using the LIOV code. In each of the following sessions the procedure is adapted and improved starting from the standard case of a straight line.

In this section a 10 m high, single conductor line is considered. The Monte Carlo procedure is described in the following steps.

- A large number of lightning events is randomly generated. Each event is characterized by three parameters I_p , t_f , and the distance y from the line. The first two values characterize the lightning current waveform and are assumed to follow the log-normal probability distributions adopted by Cigré for negative downward first strokes (*Cigré Working Group 33.01, 1991*). The parameters of the statistical distribution are shown in Table 2-1; a correlation coefficient between I_p and t_f equal to 0.47 is assumed. The distance y from the line center is assumed to be uniformly distributed between the line and a certain distance y_{max} of 1 km beyond which it is supposed that none of the lightning events could cause a flash on the line. The events are discriminated between direct and indirect ones according to the electro-geometric (EGM) model (*IEEE Std 1410-2010, 2011*).
- Each of the indirect events is simulated by using the LIOV code and the maximum induced voltage value on the line is evaluated by approximating the return stroke base channel current as a linear ramp increasing for a duration t_f , followed by a flat top of amplitude I_p . The return stroke velocity is assumed equal to half the speed of light in vacuum.

| Parameter | Median | | Standard deviation (of the natural logarithm of the population) | |
|-------------------------|----------------------------|-------------------------|--|-------------------------|
| | $(I_p \leq 20 \text{ kA})$ | $(I_p > 20 \text{ kA})$ | $(I_p \leq 20 \text{ kA})$ | $(I_p > 20 \text{ kA})$ |
| I_p (kA) | 61 kA | 33.3 kA | 1.33 | 0.605 |
| t_f (μs) | 3.83 μs | | 0.533 | |

TABLE 2-1 PARAMETERS OF LOG-NORMAL DISTRIBUTION FOR NEGATIVE DOWNWARD FIRST STROKES

- At each event, the length of the line is dynamically adapted so that no effect of the termination (reflections if open, risers if matched) could affect the overvoltage peak value at the mid-point of the line. In particular, defining T_{max} as the time at which the maximum of the overvoltage occurs, and $2x$ as the length of the line, the following condition must be satisfied

$$T_{max} < \frac{\sqrt{x^2 + y^2} + x - y}{c} \rightarrow x > \frac{cT_{max}(cT_{max} + 2y)}{2(cT_{max} + y)} \tag{2.1}$$

As in this procedure T_{max} have to be estimated a priori, a precautionary value must be assumed in order to properly evaluate the overvoltage peak also in case of events characterized by very large t_f values. Further details will be provided later in the discussion.

- the number of annual insulation flashovers per 100 km of distribution line is obtained as

$$F_p = 200 \frac{n}{n_{tot}} N_g \cdot y_{max} \tag{2.2}$$

- where n is the number of events generating induced voltages larger than the insulation level – here assumed being equal to the line critical flashover voltage (CFO), multiplied by a factor equal to 1.5, as in the IEEE Standard – and N_g is the annual ground flash density. In all the calculation performed in this thesis $N_g = 1 \text{ flash/km}^2/\text{yr}$ is assumed.

The value y_{max} to be assumed for the procedure can be estimated as follows. First, one can approximate the maximum value of the overvoltage that may be induced by the highest I_p of the currents distribution by using the simplified formula by Rusck (1958a, 1977) for the case

of ideal ground and one by *Darveniza* (2007) for the case of a lossy ground. Second, the minimum y_{max} required for the simulation is selected as the distance at which the voltage induced by the lightning with the highest peak current I_p does not exceed 1.5 CFO of the line.

The Rusck formula is given by the following expression

$$V_p = Z_0 \frac{I_p \cdot h}{y_{max}} \left(1 + \frac{v}{\sqrt{2}c_0} \frac{1}{\sqrt{1 - 0.5(v/c_0)^2}} \right) \tag{2.3}$$

where $Z_0 = 30 \Omega$, h is the line height, v is the return stroke speed and c_0 is the speed of light in vacuum. The *Darveniza's* correction for lossy ground can be obtained by substituting $h = h + 0.15\sqrt{1/\sigma_g}$ in (2.3). In Figure 2-1, the plot of y_{max} as a function of the maximum value of the induced voltage on the line is shown. The dashed curves are relevant to the case of a 340 kA current, while the solid ones to the 99% percentile of a distribution of 200 000 events (134 kA). The curves are plotted for different values of the ground conductivity, namely $\sigma_g = \infty$, $\sigma_g = 10 \text{ mS/m}$ and $\sigma_g = 1 \text{ mS/m}$.

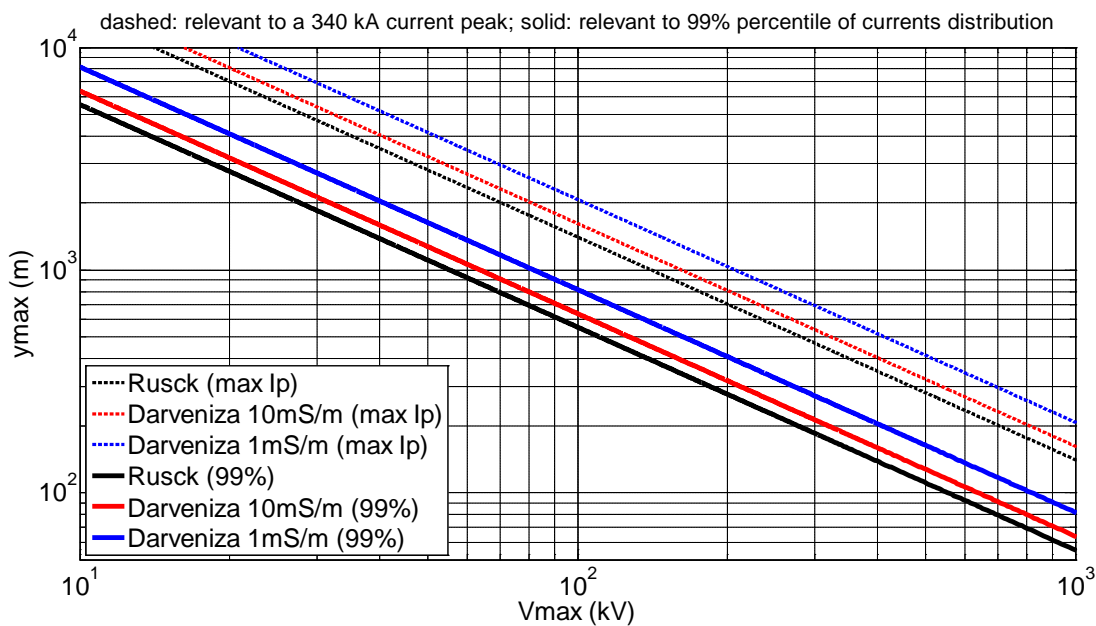


Figure 2-1 – Choice of the minimum y_{max} value for the Monte Carlo procedure as a function of max voltage amplitude

In Figure 2-2 the lightning performance of an infinite line calculated by means of the procedure described so far is shown. The number of events is 200 000 for the cases of infinite and 10 mS/m ground conductivity and 20 000 for the case of 1 mS/m. The number of events required to have an efficient estimation of the number of flashovers per year every 100 km of

line is lower for the case of higher ground conductivity (*Borghetti et al., 2007*). The curves in Figure 2-2 are obtained by combining the results obtained with $y_{max} = 1$ km for the lowest values of CFO and with $y_{max} = 0.5$ km for the highest ones. More precisely, the resulting curve is equal to the one calculated with $y_{max} = 1$ km until it intersects the one obtained with $y_{max} = 0.5$ km, as specified as follows

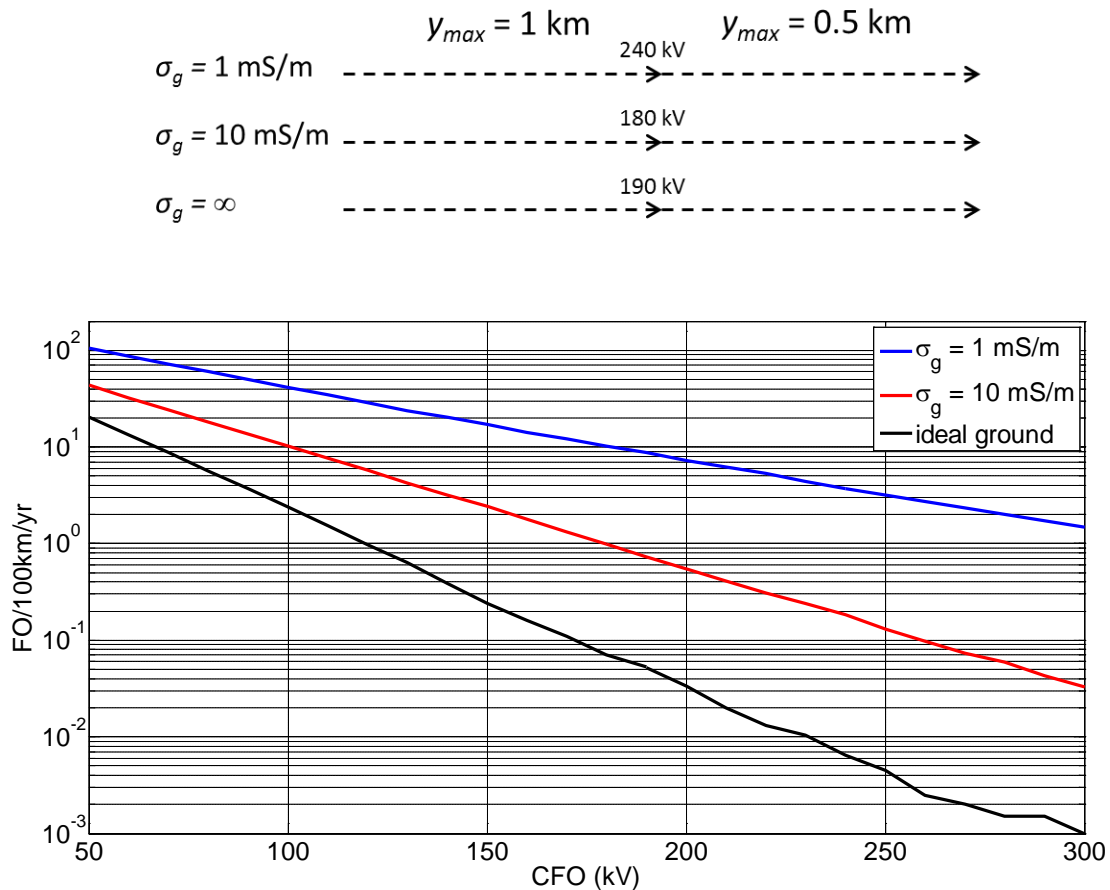


Figure 2-2 – Indirect lightning performance of an infinite line

In Figure 2-3 the plot of the induced voltage time to peak as a function of the raise time t_f of the lightning base channel current is shown for different values of the ground conductivity and different maximum distance of the stroke locations adopted in the Monte-Carlo procedure. A very strong correlation can be observed for the case of the lossless line for both cases of $y_{max} = 1$ km and $y_{max} = 500$ m. A reduction of the correlation can be observed as the ground conductivity decreases. The correlation between the two observed parameters is highly dependent on the maximum distance from the line; the induced voltage time to peak of the events closest to the line are more correlated to the current raise time respect to the farther ones.

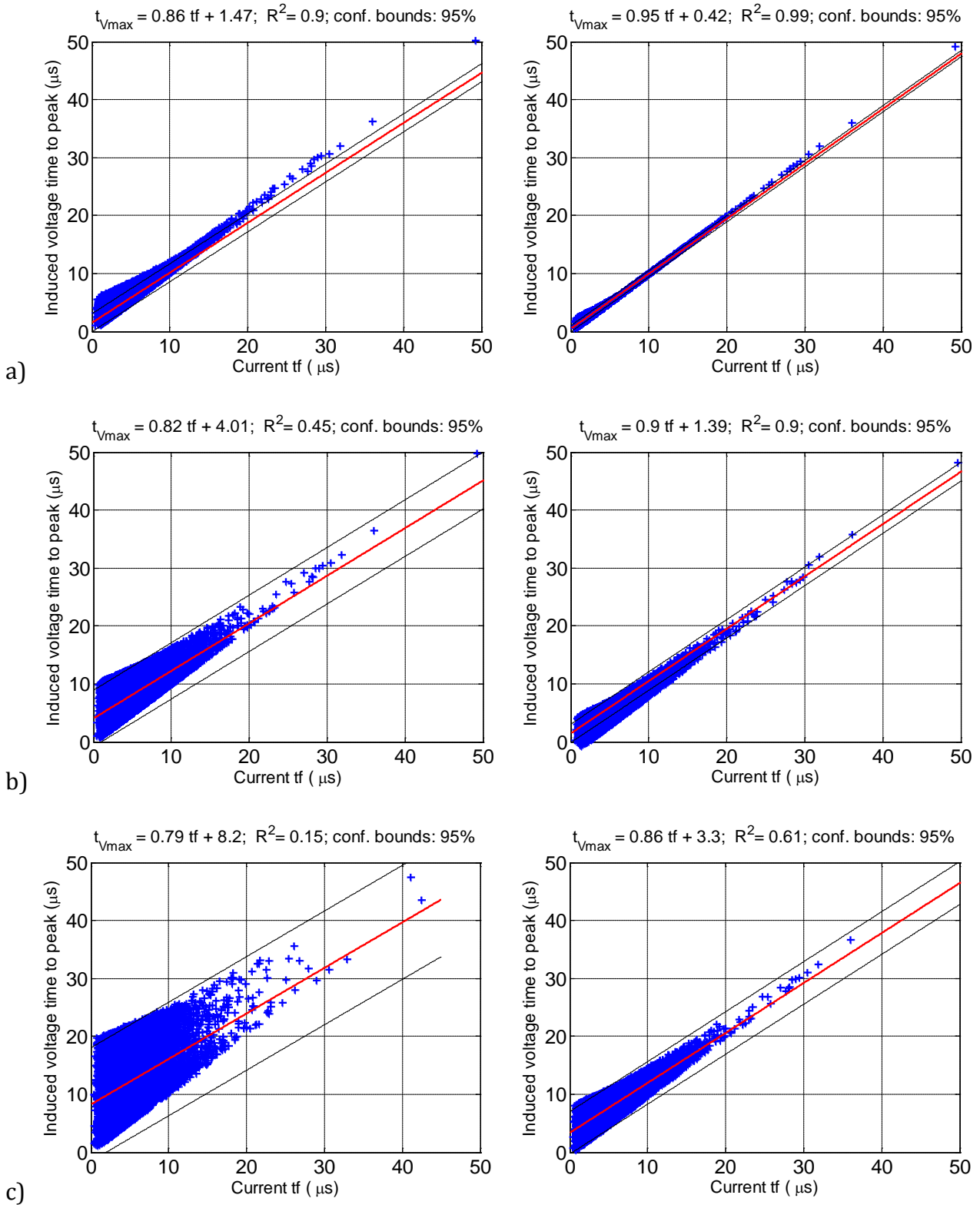


Figure 2-3 – Induced voltage time to peak as a function of the raise time t_r of the lightning base channel current. a) lossless ground, b) $\sigma_g = 10 \text{ mS/m}$, c) $\sigma_g = 1 \text{ mS/m}$. Max distance from the line ymax is 1 km for figs. on the left and 500 m for those on the right.

2.2. The Influence of Direct Strikes on the Lightning Performance of Overhead Distribution Lines

The flashover rate of overhead distribution lines due to lightning is affected, in principle, by both direct and indirect strikes. Since direct lightning flashes, even those characterized by strokes of rather low current amplitude, are expected to produce overvoltages greater than the insulation levels of overhead distribution lines, most studies on the lightning performance of distribution lines focus on the effects of the overvoltages induced by indirect strikes only. The accurate evaluation of the indirect lightning performance of distribution lines, i.e. the flashover rate due to lightning strikes hitting the ground nearby the line, requires the use of elaborate models of the coupling between the lightning electromagnetic pulse (LEMP) and the overhead line, especially when realistic line configurations are analyzed (*IEEE Std 1410-2010*, 2011). Recent papers addressed the issue of the lightning performance of distribution lines appraisal taking into account both direct and indirect lightning events (*Mikropoulos & Tsovilis*, 2013; *Chen & Zhu*, 2014). In some cases indeed, the taking into account of both direct and indirect events appears of interest, especially when the distribution systems configuration makes it worth the analysis of suitable protection means also for the case of direct strikes.

This section addresses the problem of evaluating the lightning performance of specific points of medium voltage distribution networks, in order to ascertain the possibility of leaving some distribution transformers not equipped with surge arresters (SA). Such a possibility is of interest for the utilities that have to undertake a major upgrade of surge arresters e.g., as a consequence of the change of the grounding method from grounded neutral to resonant one (*Napolitano et al.*, 2014), (*Borghetti et al.*, 2014). The analysis is accomplished taking into account both indirect and direct events.

The lightning performance of an electric power line can be expressed by means of a curve providing the number of events per year as a function of the insulation level of the line; the number of events is given per unit length of line if straight line configuration are analyzed (*IEEE Std 1410-2010*, 2011), or for the whole system if real topologies are considered (*Borghetti et al.*, 2007, 2009).

If the rate of flashovers along the whole line is of interest, independently from the their locations, the effect of the direct strikes can be accounted for by simply adding the rate of direct strikes to the indirect lightning performance, as each direct strike to the line is supposed to cause a flashover. In this section, as it is the lightning performance of specific

points of a distribution network that is of interest, in principle the above consideration does no longer apply, and therefore the response of the line to direct strikes is also evaluated by means of a computer model. Monte Carlo procedure starts from the random generation of a large number of lightning events with waveshape parameters as proposed by the Cigré probability distributions (*Cigré Working Group 33.01*, 1991), followed by the evaluation of the response on the line to each event. The events are discriminated between direct and indirect ones according to the electro-geometric model suggested in (*Borghetti et al.*, 2007). The response of the line to indirect strikes is simulated by means the LIOV-EMTP-rv code. The response to the direct strikes is calculated by means of the EMTP-rv thanks to surge current sources, in order to take into account the effect of the current injected by the direct strike and by means of the LIOV code in order to account for the electromagnetic field generated by the direct strike.

Let us consider a single straight line. The line is composed by three overhead conductors of diameter equal to 1 cm and assumed horizontally placed at 9.3 m above ground. The distance between subsequent poles is 35 m. The pole configuration is illustrated in Figure 2-4.

Figure 2-5 shows the considered line topology. The overall length of the line is 3.5 km and the lightning strike is assumed to hit the central phase.

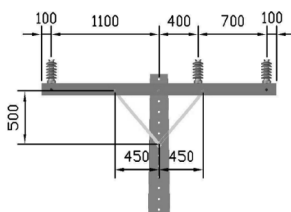


Figure 2-4 – Pole configuration.

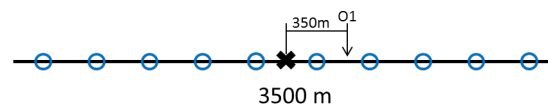


Figure 2-5 – Line topology: O1: observation point; blue circles: surge arresters locations; cross: middle point of the line.

At each pole of the line the flashovers are simulated with EMTP-rv by means of ideal switches between the line conductors and the grounding resistance. The flashover switches close according to the disruptive effect criterion (*Darveniza & Vlastos*, 1988). In particular, a flashover occurs if the integral D becomes greater than a constant value DE . D is given by the following expression

$$D = \int_{t_0}^t [|v(t)| - V_0]^k dt \quad (2.4)$$

where $v(t)$ is the voltage at the pole insulator, V_0 is the minimum voltage to be exceeded before any breakdown process can start, k is a dimensionless factor, and t_0 is the time at which $|v(t)|$ becomes greater than V_0 . The parameters of the disruptive effect criterion are reported in table 2-2 and are chosen according to the values proposed in (De Conti et al., 2010) from the results of laboratory tests performed on a 15 kV pin-type ceramic insulator alone and in series with a 40 cm of wood. A set of three surge arrester is installed every 10 spans. The voltage-current characteristic of the adopted 15-kV class surge arresters is shown in Figure 2-6. The poles not equipped by surge arresters are assumed to provide a grounding resistance equal to 400 Ω . The surge arresters are assumed to be grounded with a resistance equal to 10 Ω and the effect of soil ionization at the grounded poles is accounted by using Weck’s approximation (Cigré Working Group 33.01, 1991). The poles are assumed to be made of concrete.

TABLE 2-2 – PARAMETERS ASSUMED FOR THE DE MODEL

| Disruptive Effect model parameters | | | |
|------------------------------------|------------|-----|-------------------|
| CFO (kV) | V_0 (kV) | k | DE (kV μ s) |
| 100 | 90 | 1 | 60.9 |
| 165 | 132 | 1 | 255 |

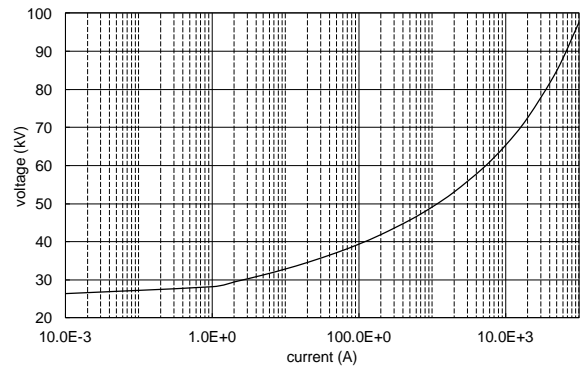


Figure 2-6 – Voltage-current characteristic of the adopted SA.

A channel-base current with a peak value of 31 kA and a maximum time-derivative of 26 kA/ μ s, assumed as typical of a first negative return stroke, is simulated by using the Cigré current functions (Cigré Working Group 33.01, 1991); the channel impedance is assumed equal to 1 k Ω . The LEMP is calculated assuming that the lightning return stroke current propagates along a straight vertical path according to the transmission line (TL) model. The stroke location in the LEMP calculation is assumed to be 10 m far from the line, in order to avoid numerical singularities. The soil conductivity, equal to 0.001 S/m, is taken into account in the electromagnetic field calculation by means of the Cooray-Rubinstein formula (Cooray, 1992; Rubinstein, 1996). The effect of the soil conductivity is neglected in the surge propagation along the line.

Figure 4 shows overvoltages calculated at the stricken point of the line due to a direct event, under the assumptions of absence of SA and flashovers. The solid thin line represents the direct overvoltage when the effect of the LEMP is neglected. This thesis is focused on the study of negative flashes only; therefore, the polarity of the overvoltage is negative. The thin dashed line in Figure 2-7 represents the effect of the LEMP 10 m far the line, whose polarity is opposite to the direct overvoltage. The LEMP effect on the direct overvoltage, therefore, appears to slightly decrease the voltage amplitude at the stricken point. Farther from the observation point, the peak of the induced voltage is expected to reduce quickly. At 350 m from the stricken point, the effect of the LEMP is no more appreciable if the line is not equipped with SA and flashovers are neglected.

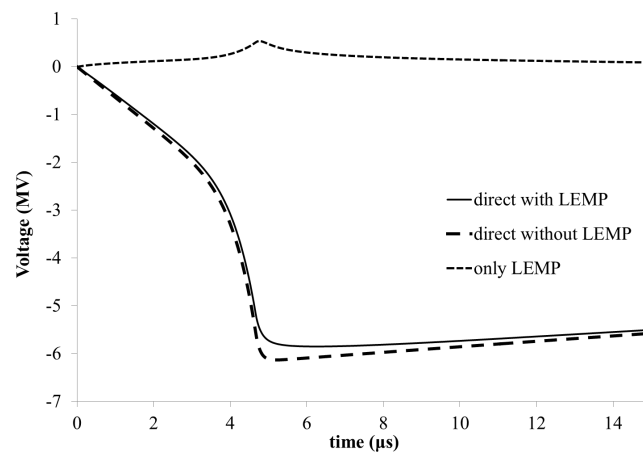
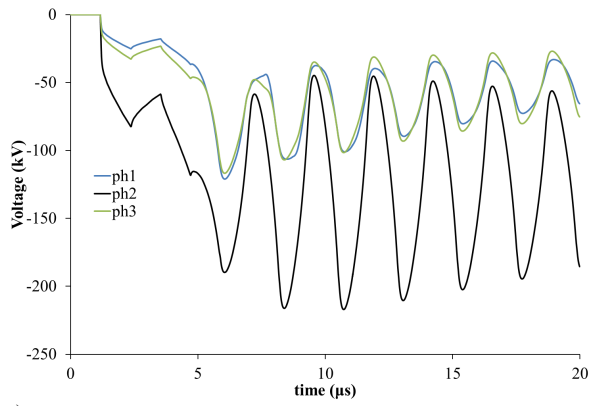
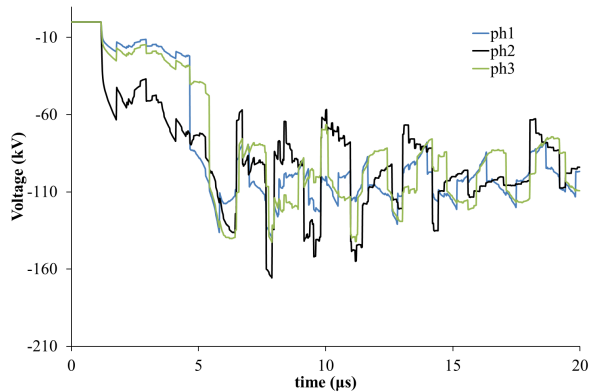


Figure 2-7 – Direct overvoltage and LEMP effect on the stricken point in absence of SA and flashovers.

Figure 2-8 shows the overvoltage at a point 350 m far from the direct strike (point O1 in Figure 2-5) obtained by disregarding the effects of the LEMP. Figure 2-8.a flashovers are disregarded, while in Figure 2-8.b they are taken into account. The effect of the flashovers along the line is to decrease the peak of the overvoltage at point O1. In Figure 2-9 the same calculation is repeated taking into account the LEMP. The comparison between the two figures shows that the influence of the LEMP on the line response to a direct strike is more evident in presence of flashovers.

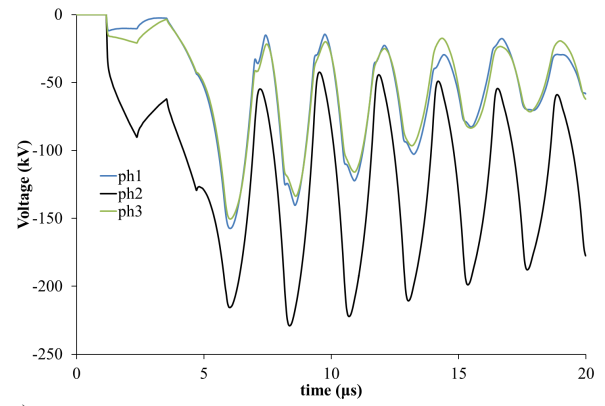


a)

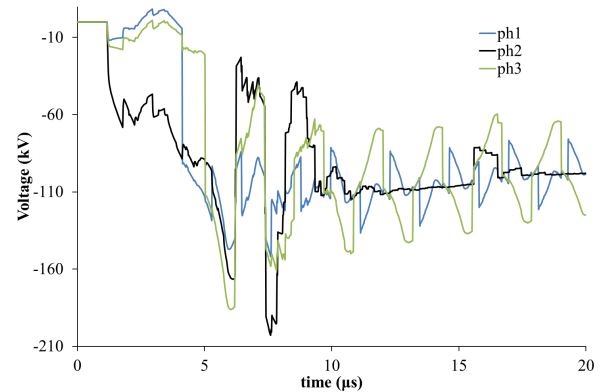


b)

Figure 2-8 – Overvoltage at observation point O1, in absence of LEMP: a) disregarding flashover occurrence, b) considering flashover occurrence.



a)



b)

Figure 2-9 – Overvoltage at observation point O1, with LEMP effect: a) disregarding flashover occurrence, b) considering flashover occurrence.

Monte Carlo Simulations

A large number n_{tot} of lightning events is randomly generated. Each event is characterized by four parameters: lightning current amplitude I_p , time to peak t_f and stroke location with coordinates x and y . The events are assumed to follow the Cigré log-normal probability distributions (Anderson & Eriksson, 1980), (Cigré Working Group 33.01, 1991) for negative first strokes, with a correlation coefficient between t_f and I_p equal to 0.47. The lightning current waveshape is assumed to have a linear front with a flat top.

The expected annual numbers of events F_p that causes overvoltages with amplitude larger than a given value V is:

$$F_p = \frac{n_i + n_d}{n_{tot}} A N_g \tag{2.5}$$

where n_i is the number of the considered indirect events generating induced voltages larger than V , n_p is the number of the considered direct events generating induced voltages higher

than that value, n_{tot} is the number randomly generated events, A is the striking area and N_g is the annual ground flash density. In this section $N_g = 1 \text{ flash/km}^2/\text{yr}$ has been assumed.

Figure 2-10 shows the top view of a 3.5 km long line and the stroke locations generated by the Monte Carlo method. n_{tot} is 20000, 2368 of which are direct strikes to line conductors. The events are generated uniformly over a 1.75 km² area, whose borders are 500 m far from the line. Due to the symmetry of the geometry, the overall striking area A is equal to 3.5 km². The line ends are assumed to be open. The occurrence of flashovers is simulated according to the criterion illustrated in the previous section.

The lighting performance of the central point of the line under the assumption of distance between consecutive SA equal to 350 m is reported in Figure 2-11, as the annual number of the direct and indirect events having amplitude higher than the value in abscissa. The estimation of the lighting performance against direct overvoltages has been repeated without and with the LEMP effect, with the outcome of a worst performance in the latter case.

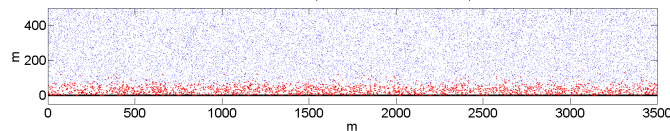


Figure 2-10 – Location of Monte Carlo events (blue: indirect events, red: direct events).

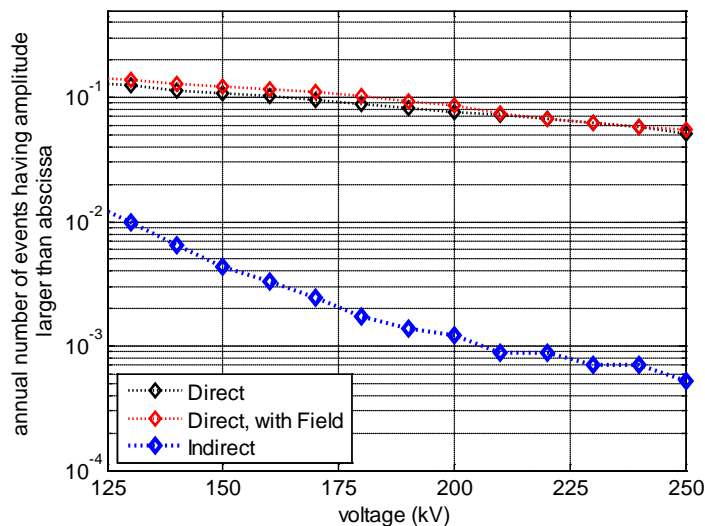


Figure 2-11 – Annual number of overvoltages in the central point of the line having amplitude higher than the value in abscissa, due to indirect events and direct events calculated with and without LEMP, distance between consecutive SA 350 m.

The inverse of the annual number of events having amplitude larger than the withstand voltage of the generic component connected to the line conductor gives the mean time between failures (MTBF). The MTBF values for the unprotected central point for different

distances between SA and a single value of withstand voltage equal to 150 kV are reported in Table 2-3. In Table 2-3 the effect of the direct events is evaluated without the LEMP. The MTBF due to direct strokes evaluated with the LEMP effect is 52.9 years with $d = 70$ m, 18.7 years with $d = 140$ m, 13.1 years with $d = 210$ m, 10.0 years with $d = 280$ m, 8.13 years with $d = 350$ m.

Table 2-4 reports the annual number of flashovers per year in at least one of the three phases per 100 km of line, with and without LEMP for different SA configurations. In Table 2-5, an analogous comparison is reported with the events causing a fault in at least two different phases.

TABLE 2-3 – MTBF (IN YEARS) AT MIDPOINT OF THE LINE FOR DIFFERENT DISTANCES BETWEEN CONSECUTIVE SURGE ARRESTERS, WITHSTAND VOLTAGE OF 150 kV

| | without SA | with SA | | | | |
|-------------------|------------|----------|-----------|-----------|-----------|-----------|
| | | $d=70$ m | $d=140$ m | $d=210$ m | $d=280$ m | $d=350$ m |
| direct + indirect | 1.4 | 53.4 | 21.3 | 14.8 | 11.4 | 8.8 |
| direct only | 2.4 | 53.4 | 21.3 | 14.9 | 11.6 | 9.1 |
| indirect only | 3.2 | inf | inf | 1430 | 520 | 229 |

TABLE 2-4 – FLASHOVER RATE DUE TO DIRECT EVENTS FOR DIFFERENT DISTANCES BETWEEN CONSECUTIVE SURGE ARRESTERS

| | without SA | with SA | | | | |
|--------------|------------|----------|-----------|-----------|-----------|-----------|
| | | $d=70$ m | $d=140$ m | $d=210$ m | $d=280$ m | $d=350$ m |
| without LEMP | 11.8 | 10.0 | 11.1 | 11.4 | 11.6 | 11.7 |
| with LEMP | 11.8 | 9.0 | 10.5 | 11.3 | 11.5 | 11.6 |

TABLE 2-5 – FLASHOVER RATE ON DIFFERENT PHASES DUE TO DIRECT EVENTS FOR DIFFERENT DISTANCES BETWEEN CONSECUTIVE SURGE ARRESTERS

| | without SA | with SA | | | | |
|--------------|------------|----------|-----------|-----------|-----------|-----------|
| | | $d=70$ m | $d=140$ m | $d=210$ m | $d=280$ m | $d=350$ m |
| without LEMP | 11.8 | 4.3 | 8.1 | 9.4 | 10.2 | 10.8 |
| with LEMP | 11.8 | 3.9 | 7.8 | 9.4 | 10.4 | 10.8 |

Statistical Analysis Of The Overvoltages And Flashovers Due To The Direct Strikes

In what follows, some statistical results are shown relevant to a population of 2000 lightning current waveshapes, with a linear front and a flat top, generated by using the Monte Carlo method with peak amplitude and front time following the Cigré probability

distributions. Each event is supposed to randomly hit one of the three conductors at the pole located in the mid-point of the line. The lightning channel impedance is assumed to be very large respect to that of the stricken poles. The following figures show the probability that the overvoltage peak exceeds 150 kV, assumed to be representative of the withstand voltage of a device connected to a point of the line not equipped by SA, for both cases of LEMP disregarded and accounted. The probability is evaluated as the ratio of the events giving overvoltage peak amplitude exceeds 150 kV, and it is illustrated for each pole and each phase. The voltages are referred to the ground, which potential rises due to the grounding resistance. Two cases with different distances between the arresters are shown: 70 m and 350 m. As the comparison between Figure 2-12 and Figure 2-13 shows, the probability of exceeding a given withstand voltage along the line is different if the LEMP is taken into account or not in the overvoltage calculation. In particular, the effect of the LEMP is to weaken the lightning performance of far points of the line from the stricken pole and to improve the one of the closer points. The performance of phase number one and three are the most influenced by the LEMP, while that of phase two appears to be the less affected. After three or four SA, the exceeding of the assumed withstand voltage of 150 kV is not observed. Figure 2-14 and Figure 2-15 refer to distance between SA equal to 350 m.

The flashover probability along the line in case the LEMP is disregarded is shown in Figure 2-16 and Figure 2-18, the case it is taken into account is shown in Figure 2-17 and Figure 2-19. The probability is reported, for each pole and each phase, as the ratio of direct events for which the *DE* is exceeded.

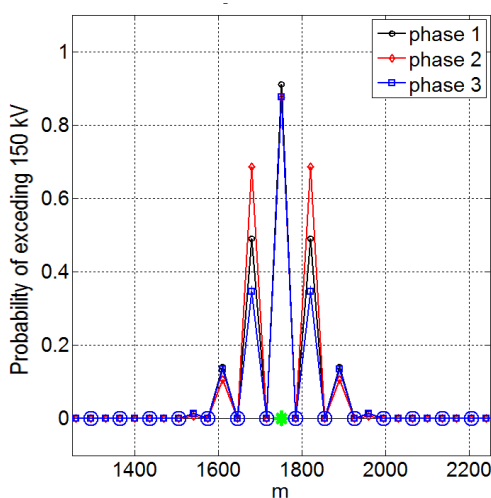


Figure 2-12 – Probability of overvoltages greater than 150 kV along the line due to direct strike at 1750 m, LEMP neglected and SA every 70 m.

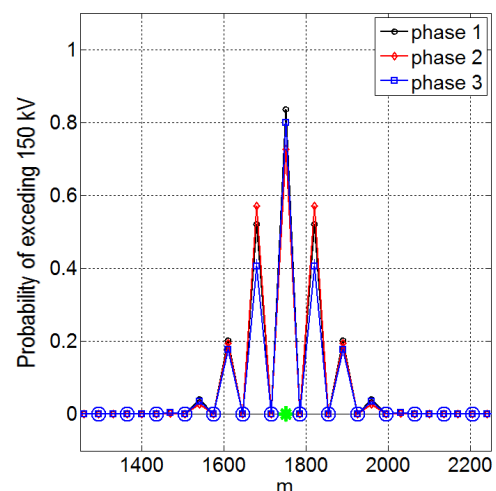


Figure 2-13 – Probability of overvoltages greater than 150 kV along the line due to direct strike at 1750 m, LEMP accounted and SA every 70 m.

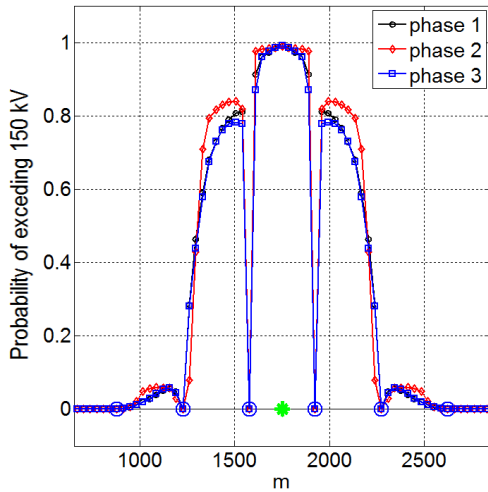


Figure 2-14 – Probability of overvoltages greater than 150 kV along the line due to direct strike at 1750 m, LEMP neglected and SA every 350 m.

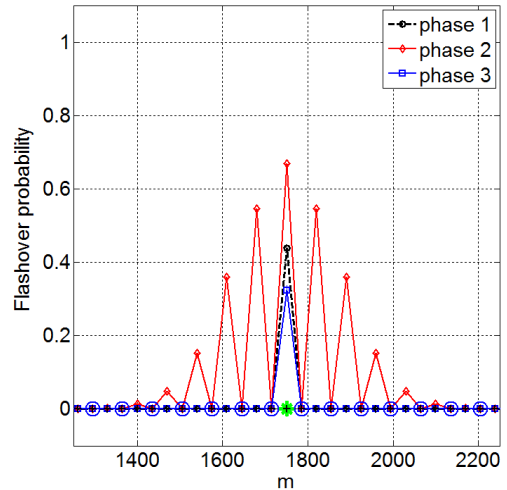


Figure 2-17 – Probability of flashovers along the line due to a direct strike at 1750 m, LEMP accounted and SA every 70 m.

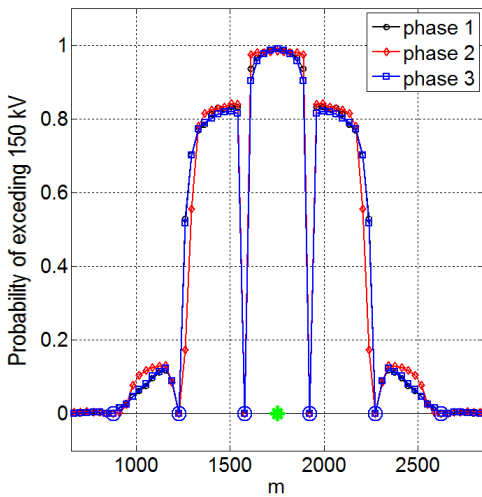


Figure 2-15 – Probability of overvoltages greater than 150 kV along the line due to direct strike at 1750 m, LEMP accounted and SA every 350 m.

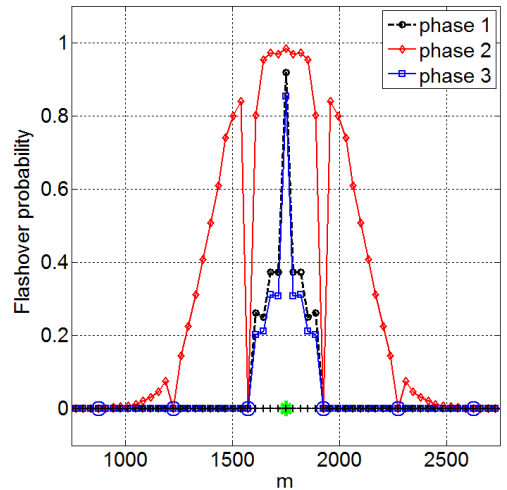


Figure 2-18 – Probability of flashovers along the line due to a direct strike at 1750 m, LEMP neglected and SA every 350 m.

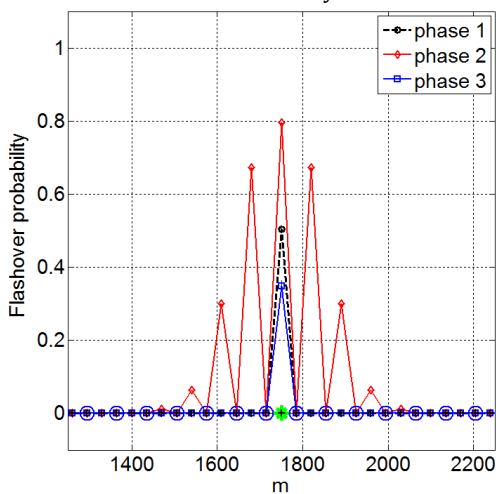


Figure 2-16 – Probability of flashovers along the line due to a direct strike at 1750 m, LEMP neglected and SA every 70 m.

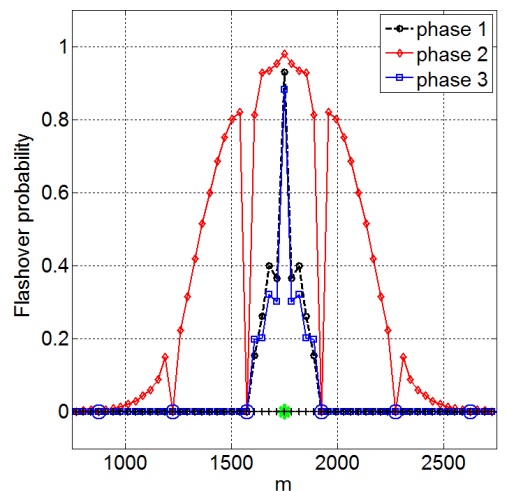


Figure 2-19 – Probability of flashovers along the line due to a direct strike at 1750 m, LEMP accounted and SA every 350 m.

Conclusion

This section has presented a procedure to evaluate the lightning performance of a distribution line, due to both direct and indirect strokes. The response of the line to direct strokes requires to be suitably evaluated for the lightning performance of specific points of the line. Simulation results obtained by means of a Monte Carlo procedure applied to a typical configuration of distribution line show that the occurrence of flashovers at the pole insulators is very low if the number of surge arresters along the path from the observed point to the stricken one is greater than four. For portions of the line far enough from the stricken point the contribution of the LEMP to the overvoltage appears to be not negligible. These results are useful for the evaluation of the lightning performance if the intrinsically complex configuration of a real distribution network is of interest or if specific points of the network are observed, e.g. when the upgrade of the protection has to be undertaken.

2.3. The Effect of the Channel Base Current Waveform on the Lightning Performance of Overhead Distribution Lines

This section deals with the calculation of the expected annual number of flashovers in an overhead line due to both direct and indirect strikes (lightning performance).

As known, lightning originated voltages along the lines exhibit peaks, front time and more in general wave shapes that are influenced by the waveform of the relevant lightning current. Different functions have been proposed in order to represent the typical lightning current waveform. The most commonly used are: the one adopted by (*Cigré Working Group 33.01*, 1991) and the one proposed by *Heidler* (1985). Other functions that can be found in the literature are the classical double exponential (*Bruce & Golde*, 1941), others derived from it e.g., (*Jones*, 1977), the combination of multiple *Heidler* functions e.g. (*Nucci & Rachidi*, 1989) and more recent ones, e.g. (*Javor & Rancic*, 2011). Functions for multi-peaked waveforms have been also proposed in (*De Conti & Visacro*, 2007; *Javor*, 2012).

For the calculation of the induced voltages along overhead lines due to indirect strikes, several analytical equations have been derived thanks to simplified representations of the channel base current waveforms, i.e. the step waveform (used by *Rusck* to derive his classical formula (*Rusck*, 1958b)) and the linearly rising current, linear ramp with flat top (trapezoidal) or with drooping tail, as in e.g., (*Høidalen*, 2003; *Andreotti et al.*, 2013; *Paulino et al.*, 2015). The use of these analytical equations limits the analysis to the case of single lines.

For the case of studies relevant to distribution networks with surge arresters (SAs) and other non-linear components, the adoption of numerical models of the coupling between the lightning electromagnetic pulse (LEMP) and line conductors (e.g., the *Agrawal et al.* (1980) model) is preferred. However, even if the numerical approach is adopted, for the statistical assessment of the lightning performance of distribution lines by using Monte Carlo simulations e.g., (*Borghetti et al.*, 2007, 2009), a simplified representation of the current waveform is usually adopted in order to reduce the computational time.

It is known that the waveform of the voltages due to direct strikes in absence of corona phenomena and/or flashovers does reproduce the one of the originating current, as the voltage waveform is given by the current one times the surge impedance of the line, while for the case of voltages induced by indirect strikes the similarity between lightning current and voltage waveforms is less straightforward (*Nucci & Rachidi*, 2014). As a matter of fact Figure

2-20 reports the induced voltages in a single conductor overhead line calculated by using different lightning current functions (namely trapezoidal, Heidler and Cigré) with the same peak amplitude I_p of 31.1 kA and equivalent front times $t_f = t_{30} / 0.6$ variable from 1 μs to 8 μs (t_{30} is the interval from 30 to 90 percent amplitude intercepts on the wavefront). The Heidler and Cigré waveforms have wavetail time to half value $t_h = 75 \mu\text{s}$. For the Cigré waveform the calculations are repeated for maximum front steepness $S_m = 26 \text{ kA}/\mu\text{s}$ and for S_m values that change as a function of t_f .

Table 2-6 shows the differences of the maximum voltages calculated by using the Heidler and Cigré waveforms with respect to the corresponding values calculated by adopting the trapezoidal waveform. These differences may be more evident in the presence of non-linear power components connected to the line, which is worth investigating.

Hence, the main aim of this section is the analysis of the influence of different lightning current functions on the lightning performance of distribution lines, calculated by using the Monte Carlo method described in (*Borghetti et al., 2007*), (*Borghetti et al., 2009*), taking into account also the presence of surge arresters and an accurate representation of the insulators flashovers. This analysis is useful in order to evaluate the effects of a simplified representation of the current waveform on the final results.

Since both Heidler and Cigré functions are characterized by more than two parameters (whilst the trapezoidal one is completely defined by I_p and t_f), an additional purpose of this section is to present the extension of the Monte Carlo approach presented in (*Borghetti et al., 2007*) that allows the adoption of these current functions.

| | t_f | | | | | |
|-------------------------|-----------|-------------|-------------|-------------|-------------|-----------|
| | 1 μ s | 2.4 μ s | 3.8 μ s | 5.2 μ s | 6.6 μ s | 8 μ s |
| Heidler | -2.1% | -5.3% | -7.1% | -8.0% | -8.7% | -9.3% |
| Cigré fixed S_m | -0.22% | -1.2% | -0.17% | 1.8% | 3.9% | 6.10% |
| Cigré variable S_m | -0.73% | -0.95% | -0.94% | -0.79% | -0.63% | -0.47% |

TABLE 2-6 - PERCENTAGE DIFFERENCES BETWEEN THE MAXIMUM VOLTAGES CALCULATED BY USING THE HEIDLER AND CIGRÉ WAVEFORMS WITH RESPECT TO THE MAXIMUM VOLTAGES CALCULATED BY USING THE TRAPEZOIDAL WAVEFORM.

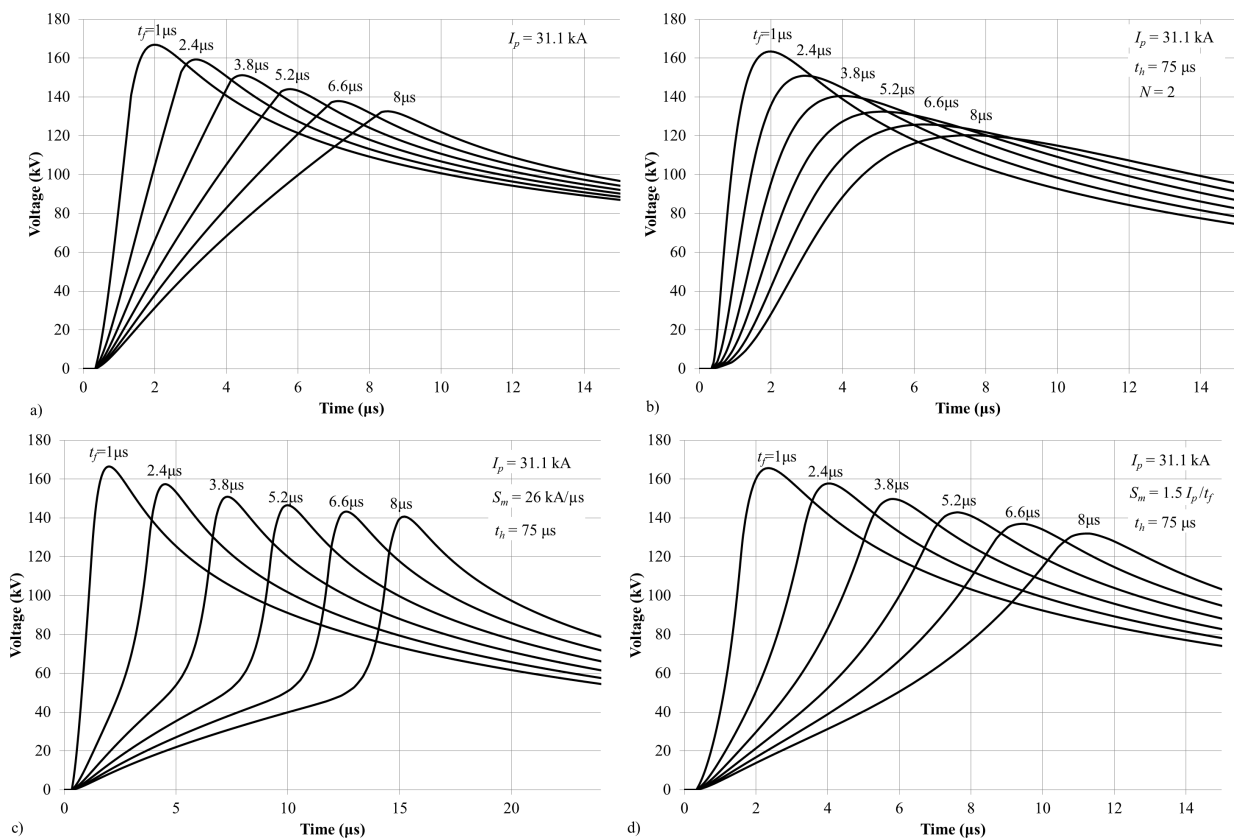


Figure 2-20 – Induced voltages calculated at the midpoint of a 10 km-long 10 m-high overhead single-conductor ideal line over an ideal soil due to a strike at a distance of 100 m in front of the midpoint of the line. Different channel base current waveforms: a) trapezoidal; b) Heidler with parameter $N = 2$; c) Cigré with fixed S_m ; d) Cigré with variable S_m .

In this section the analysis is limited to the assessment of the lightning performance of a single overhead line.

A large number n_{tot} of lightning events is randomly generated. Each event is characterized by the parameters that describe the current waveform at the channel base and the coordinates of the stroke location. Only negative first strokes are taken into account; the effects of the presence of positive flashes and of subsequent strokes in negative flashes on the line lightning performance are assumed negligible. The stroke locations are assumed to be uniformly distributed within striking area A , having a size large enough to contain the entire line and all the lightning events that could cause voltages larger than the minimum voltage value of interest for the analysis.

Each lightning event is classified as either a direct strike to a line conductor or as an indirect strike by using a lightning incidence model. For all the calculations of this thesis, the electro-geometric model suggested in (*IEEE Std 1410-2010*, 2011) is adopted.

For each pole of the line the overvoltages due to both indirect and direct strikes are calculated using the LIOV-EMTP-RV code.

For the entire line, the expected annual numbers of events F_p that cause overvoltages with amplitude larger than a given value V is:

$$F_p = \frac{n_i + n_d}{n_{tot}} A N_g \quad (2.6)$$

where n_i and n_d are the number of indirect events and direct events, respectively, that generate overvoltages larger than V and N_g is the annual ground flash density.

The estimation of the mean time between failures (MTBF) expected at specific poles of the line, generally of interest for the protection of the transformer connected to that specific pole, is calculated as the inverse of the F_p value given by (2.6) with n_i and n_d evaluated by comparing the overvoltage at the pole with the withstand voltage of the connected transformer.

Calculation of the overvoltages due to indirect lightning events

In this section the LEMP is calculated by using the analytical formulation presented by *Napolitano* (2011) with the assumption that the lightning return stroke current propagates along a straight vertical channel according to the transmission line (TL) model. This analytical formulation allows for the representation of a generic waveshape of the lightning current at

the channel base. The assumed value for the return-stroke propagation speed is $1.5 \cdot 10^8$ m/s (0.5 of the speed of light).

The lossy ground effect on the LEMP are accounted by means of the Cooray-Rubinstein formula (Cooray, 1992; Rubinstein, 1996; Cooray, 2002). The bus steady state voltage at the utility frequency is taken into account by using the procedure described in (Napolitano et al., 2014).

Calculation of the overvoltages due to direct lightning events

Each randomly-generated strike classified as a direct event is represented by a current source connected to the pole closest to its location coordinates. The surge impedance of the lightning channel is assumed much larger than that of the line and, therefore, neglected.

Direct strikes to distribution overhead lines are always expected to cause flashovers at line insulators, unless very close SAs are installed (IEEE Std 1410-2010, 2011), even in presence of ground wires (Nakada et al., 2003; Miyazaki & Okabe, 2009). The overvoltages at buses not equipped by SAs are greatly influenced by the occurrence of flashovers at the line insulators and by the number of SAs along the path from the stricken point to the observed buses.

In both the simulations relevant to direct and indirect strikes, at each pole of the line the flashovers are simulated with EMTP-rv by means of ideal switches between the line conductors and the grounding resistance. The flashover switches close according to the disruptive effect (DE) criterion (Darveniza & Vlastos, 1988). In particular, a flashover occurs if the integral D becomes greater than a constant value DE . Integral D is given by the following expression

$$D = \int_{t_0}^t [|v(t)| - V_0]^k dt \quad (2.7)$$

where $v(t)$ is the voltage at the pole insulator, V_0 is the minimum voltage to be exceeded before any breakdown process can start, k is a dimensionless factor, and t_0 is the time at which $|v(t)|$ becomes greater than V_0 .

The poles not equipped by surge arresters are assumed to provide a grounding resistance equal to 400Ω . The surge arresters are represented by their specific non-linear voltage current characteristic and are assumed to be grounded with a resistance $R_0 = 10 \Omega$. The effect of soil ionization at the grounded poles is accounted by using the Weck's approximation (Cigré Working Group 33.01, 1991):

$$R_i = \frac{R_0}{\sqrt{1 + I/I_g}} \quad (2.8)$$

with the limiting current

$$I_g = \frac{1}{2\pi} \left(\frac{E_0 \rho_0}{R_0^2} \right) \quad (2.9)$$

where soil breakdown gradient E_0 is equal to 400 kV/m.

Multivariate Distribution Of Lightning Current Parameters

Typical lightning channel base current waveforms are defined by the following parameters: peak I_p , front time t_f , maximum front steepness S_m and wavetail time to half value t_h . The correlation between these parameters has been recently reviewed by Rakov et al. in (*CIGRE WG C4.407*, 2013). In particular, in direct current measurements relatively strong correlation is observed between the current rate-of-rise characteristics and current peak.

The application of the Monte Carlo method requires the knowledge of the multivariate distribution of the lightning current parameters. Let us assume that every parameter follows the log-normal probability distribution.

Let x_1, \dots, x_n be n jointly Gaussian random variable (in this case they are the four natural logarithms of I_p , t_f , S_m and t_h). The multivariate normal distribution is said to be non-degenerate when the symmetric covariance matrix \mathbf{K} is positive definite. In this case the probability density function is

$$f(x_1, \dots, x_n) = \frac{1}{\sqrt{(2\pi)^n |\mathbf{K}|}} \exp\left(-\frac{1}{2}(\mathbf{x} - \boldsymbol{\mu})^T \mathbf{K}^{-1}(\mathbf{x} - \boldsymbol{\mu})\right) \quad (2.10)$$

where \mathbf{x} is a real n -dimensional column vector, $\boldsymbol{\mu}$ is the corresponding mean vector and $|\mathbf{K}|$ is the determinant of \mathbf{K} .

The ij -th off-diagonal element of \mathbf{K} is given by correlation coefficient ρ_{ij} between x_i and x_j multiplied by the product of their two corresponding standard deviations (i.e., σ_{x_i} and σ_{x_j}), whilst the ii -th diagonal element is equal to variance $\sigma_{x_i}^2$ of random variable x_i .

Let be $\mathbf{Q} = \mathbf{K}^{-1}$, the conditional variance of x_n is

$$\left(\sigma_{x_n}^*\right)^2 = \text{Var}\left(x_n \mid x_1, \dots, x_{n-1}\right) = \frac{1}{Q_{nn}} \quad (2.11)$$

and the conditional mean of x_n is

$$\mu_{x_n}^* = \text{E}\left(x_n \mid x_1, \dots, x_{n-1}\right) = \mu_n - \frac{1}{Q_{nn}} \sum_{j=1}^{n-1} Q_{nj} \left(x_j - \mu_j\right) \quad (2.12)$$

where Q_{nj} is the nj -th element of matrix \mathbf{Q} .

The Monte Carlo random generation of a quadruple of lightning current parameters values is obtained by applying the following steps, where $Z_k, Z_{k+1}, Z_{k+2}, Z_{k+3}$ are four standard normal variates.

Step 1) for the calculation of an I_p value:

$$1.1) I_p = \exp\left(\mu_{\ln I_p} + \sigma_{\ln I_p} \cdot Z_k\right);$$

Step 2) for the calculation of a t_f value:

$$2.1) \sigma_{\ln t_f}^*, \sigma_{\ln S_m}^*, \sigma_{\ln t_h}^* \text{ are calculated by using (2.11);}$$

$$2.2) \mu_{\ln t_f}^* \text{ is calculated by using (2.12);}$$

$$2.3) t_f = \exp\left(\mu_{\ln t_f}^* + \sigma_{\ln t_f}^* \cdot Z_{k+1}\right);$$

Step 3) for the calculation of a S_m value:

$$3.1) \mu_{\ln S_m}^* \text{ is calculated by using (2.12);}$$

$$3.2) S_m = \exp\left(\mu_{\ln S_m}^* + \sigma_{\ln S_m}^* \cdot Z_{k+2}\right);$$

Step 4) for the calculation of a t_h value:

$$4.1) \mu_{\ln t_h}^* \text{ is calculated by using (2.12);}$$

$$4.2) t_h = \exp\left(\mu_{\ln t_h}^* + \sigma_{\ln t_h}^* \cdot Z_{k+3}\right).$$

A complete set of the data required for the Monte Carlo generation procedure is provided by *Berger & Garbagnati* (1984) and is reported in Table 2-7 and Table 2-8. For each parameter y ,

Table 2-7 provides median value \bar{y} ($\mu_{\ln y} = \ln \bar{y}$) and $\sigma_{\ln y}$. Table 2-8 provides correlation coefficients $\rho_{\ln y_1 \ln y_2}$ between parameters y_1 and y_2 .

The parameters of the distribution relevant to the front duration T_{cr} is given instead of the ones relevant to t_f . Since (Cigré Working Group 33.01, 1991) provides both the parameters of T_{cr} (the same as Table 2-7) and of t_f ($\bar{t}_f = 3.8 \mu\text{s}$, $\sigma_{\ln t_f} = 0.55$) obtained from almost the same set of experimental measurements used in (Berger & Garbagnati, 1984), the implemented Monte Carlo procedure generates the values of T_{cr} according to step 2). The values relevant to t_f are obtained by multiplying each value of T_{cr} by the ratio between \bar{t}_f and \bar{T}_{cr} provided by (Cigré Working Group 33.01, 1991).

TABLE 2-7 - STATISTICAL PARAMETERS OF THE LOG-NORMAL DISTRIBUTIONS FOR NEGATIVE DOWNWARD FIRST STROKES (Berger & Garbagnati, 1984)

| Parameter | Median value | Standard deviation of the parameter logarithm (base 10) |
|-----------|----------------------|--|
| I_p | 30 kA | 0.26 |
| T_{cr} | 5.5 μs | 0.31 |
| S_m | 12 kA/ μs | 0.26 |
| t_h | 75 μs | 0.26 |

TABLE 2-8 - CORRELATION COEFFICIENTS BETWEEN PARAMETERS (Berger & Garbagnati, 1984)

| Parameter | I_p | T_{cr} | S_m | t_h |
|-----------|-------|----------|-------|-------|
| T_{cr} | 0.37 | 1 | | |
| S_m | 0.36 | -0.21 | 1 | |
| t_h | 0.56 | 0.33 | 0.1 | 1 |

For a given quadruple of values for I_p , t_f , S_m and t_h , the procedures implemented in order to obtain the corresponding values of the parameters of the Cigré function and of the Heidler function are shown in the following two Subsections.

Cigré function

The current waveform is (Cigré Working Group 33.01, 1991):

$$\begin{aligned}
 i(t) &= At + Bt^n, \quad t \leq t_n \\
 i(t) &= I_1 e^{-(t-t_n)/t_1} - I_2 e^{-(t-t_n)/t_2}, \quad t > t_n
 \end{aligned}
 \tag{2.13}$$

where

$$\begin{aligned}
 S_N &= S_m t_f / I_p \\
 n &= 1 + 2(S_N - 1)(2 + 1/S_N) \\
 t_n &= 0.6 t_f \left[3S_N^2 / (1 + S_N^2) \right] \\
 A &= \frac{1}{n-1} \left(0.9 \frac{I_p}{t_n} n - S_m \right) \\
 B &= \frac{1}{t_n^n (n-1)} (S_m t_n - 0.9 I_p) \\
 t_1 &= (t_h - t_n) / \ln 2 \\
 t_2 &= 0.1 I_p / S_m \\
 I_1 &= \frac{t_1 t_2}{t_1 - t_2} \left(S_m + 0.9 \frac{I_p}{t_2} \right) \\
 I_2 &= \frac{t_1 t_2}{t_1 - t_2} \left(S_m + 0.9 \frac{I_p}{t_1} \right)
 \end{aligned} \tag{2.14}$$

This formulation presents some numerical issues if $n < 1$ or $n > 55$. In case a Monte Carlo event presents a value of n out of these bounds, the value of S_m is adjusted as

$$\begin{aligned}
 S_m &= 1.01 I_p / t_f & \text{if } n < 1 \\
 S_m &= 12 I_p / t_f & \text{if } n > 55
 \end{aligned} \tag{2.15}$$

As this procedure can lead to small errors on the resulting current peak, the current is normalized to the desired peak value.

Table 2-9 compares the expected median value of the parameters with those obtained by 20,000 current waveforms calculated by using the Cigré function. The small deviations in the Cigré model are due to the corrections previously mentioned.

TABLE 2-9 - MEDIAN VALUES OF THE PARAMETERS OBTAINED FROM (2.13) AND FROM THE GA COMPARED TO THE EXPECTED VALUES GIVEN IN (Berger & Garbagnati, 1984).

| | I_p (kA) | t_f (μs) | S_m (kA/μs) | t_h (μs) |
|----------|------------|------------|---------------|------------|
| Expected | 30.0 | 3.80 | 12.0 | 75.0 |
| Cigré | 30.0 | 3.89 | 13.1 | 74.7 |
| Heidler | 30.0 | 3.81 | 12.0 | 75.4 |

Heidler function

The Heidler function is (Heidler, 1985)

$$i(t) = \frac{I_0}{\eta} \frac{(t/\tau_1)^N}{1+(t/\tau_1)^N} \exp(-t/\tau_2) \quad (2.16)$$

$$\eta = \exp\left[\left(-\frac{\tau_1}{\tau_2}\right)\left(\frac{\tau_2 N}{\tau_1}\right)^{1/N}\right]$$

It is completely defined by four parameters, i.e. I_0 , τ_1 , τ_2 and N , which cannot be obtained from the values I_p^* , t_f^* , S_m^* and t_h^* by analytical equations. Therefore, as in e.g. (Chandrasekaran & Punekar, 2014; Bermudez et al., 2002), a procedure based on the use of the Matlab genetic algorithm (GA) has been developed.

The objective of the algorithm is to determine a set of values I_0 , τ_1 , τ_2 and N such as to minimize the following fitness function

$$f = c_1 \left| \frac{I_{pc} - I_p^*}{I_p^*} \right| + c_2 \left| \frac{t_{fc} - t_f^*}{t_f^*} \right| + c_3 \left| \frac{t_{hc} - t_h^*}{t_h^*} \right| \quad (2.17)$$

where I_{pc} , t_{fc} and t_{hc} are the peak value, the equivalent front time and the time to half value of the current calculated at every iteration of the algorithm. Parameters c_1 , c_2 and c_3 are the weights ascribed to the relative errors of the three parameters I_p^* , t_f^* , and t_h^* , respectively. The algorithm is stopped if the relative errors on the three parameters satisfy all the three following conditions

$$\left| \frac{I_{pc} - I_p^*}{I_p^*} \right| < 0.5\% ; \quad \left| \frac{t_{fc} - t_f^*}{t_f^*} \right| < 0.5\% ; \quad \left| \frac{t_{hc} - t_h^*}{t_h^*} \right| < 1\% \quad (2.18)$$

The possible values of N are limited to the integer values 2, 3 or 4. At first the values of c_1 , c_2 and c_3 are equal to each other. The initial population size and the maximum number of generations are set to 50 and 100, respectively, and they are subsequently enlarged in case any of the conditions of (2.18) is not satisfied. If after some tens of attempts, conditions (2.18) are still not satisfied, then the time to half value is penalized by means of a reduction of c_3 with respect to c_1 and c_2 . At the end of this procedure, only for 10 out of 20,000 events the constraint on t_h is not satisfied, while the constraints relevant to peak and equivalent front time are always fulfilled.

Table 2-9 compares the expected median value of the parameters with those obtained by 20,000 current waveforms calculated by using Heidler function (2.16) with the parameter given by the GA. The mean errors resulting on 20,000 Heidler waveforms are: 0.004% for I_p , 0.17% for t_f and 0.21% for t_h). Although the S_m is not taken directly into account by the GA, also the relevant median value is in close agreement with the expected one.

The next figures represent the plot of the induced voltage time to peak as a function of the raise time t_f of the lightning base channel current for different types of return stroke currents. The ground conductivity is $\sigma_g = 10^{-3}$ S/m. The Cigré and Heidler function present a higher mean rise time with respect to the case of a trapezoidal current waveform, but a higher correlation between induced voltage time to peak and equivalent rise time t_f .

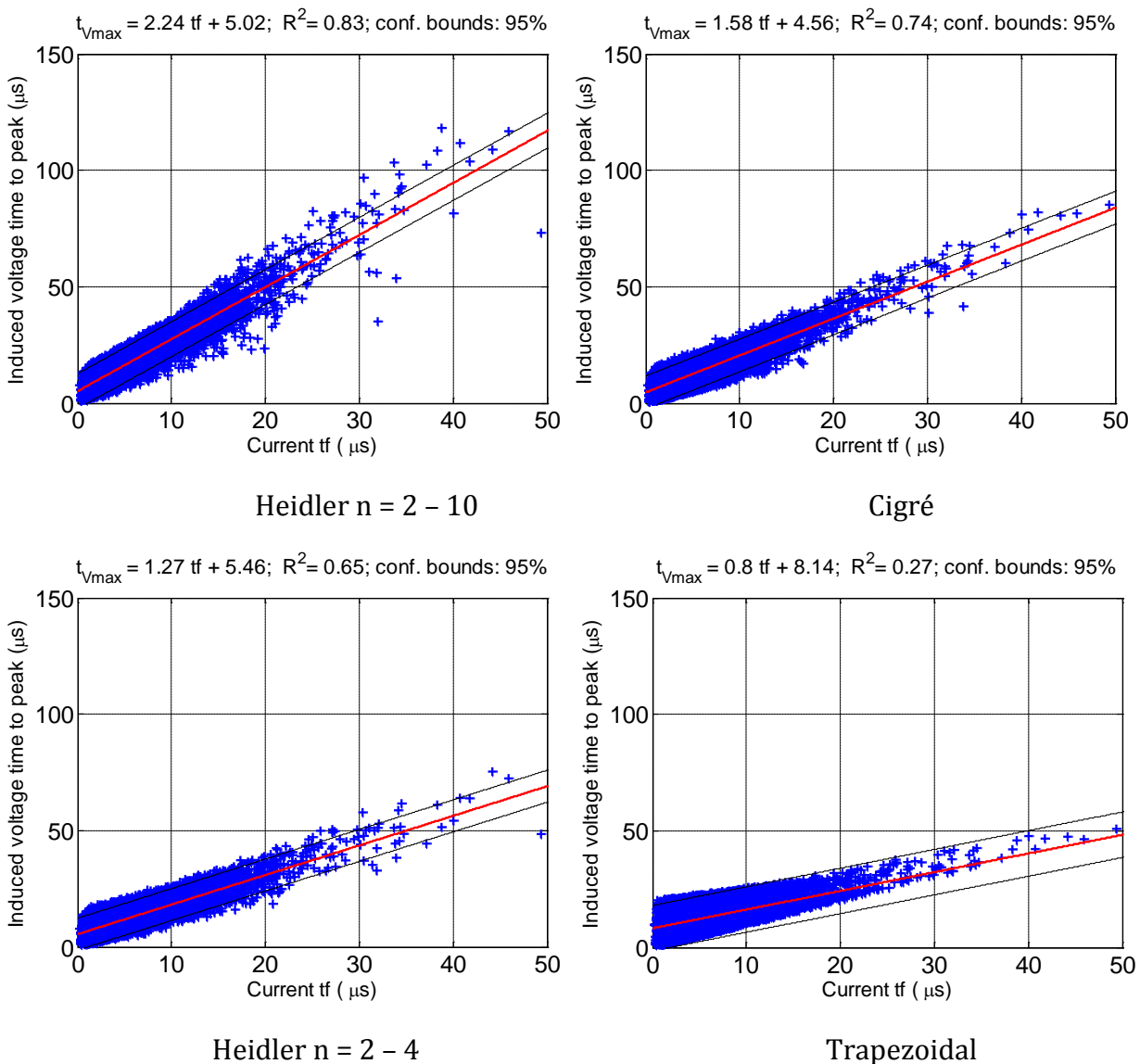


Figure 2-21 – Induced voltage time to peak as a function of the raise time t_f of the lightning base channel current.

Perspective lightning performance of the distribution line

As already mentioned, a three phase overhead line is considered, straight in shape. The conductors are assumed horizontally placed at 9.3 m above ground, with diameter equal to 1 cm. The distances between the lateral conductors and the central one are 1.5 m and 0.7 m. In all the calculations of this section the assumed soil conductivity is $\sigma_g = 10^{-3}$ S/m.

Striking area A is chosen as a 1-km band from the line. Number of lightning events n is 20,000. Direct events n_d are 1,208. Indirect events n_{id} are 18,792.

Figure 2-22 shows the annual number of overvoltages of the line with length equal to 2 km for the three different current waveshapes adopted caused by indirect events only. Such a result is here denoted as the perspective lightning performance of the distribution line, as the calculations are run in absence of surge arresters and by neglecting the insulators flashovers along the line. The steady state voltage at the utility frequency is not taken into account. Figure 2-22 shows that the choice of different current waveshapes has a limited impact on the estimation of the perspective lightning performance. It is worth mentioning that the lowest curve is obtained by using the Heidler function.

In order to verify that this conclusion is not affected by the limited length of the line the same calculations are repeated for the case of a very long line (i.e., for each event the length is adjusted to be large enough to avoid the influence of the so called 'risers' (Nucci & Rachidi, 2014) at the line terminations on the overvoltage peak) and the resulting curves shown in Figure 2-23. The results are indeed still similar, namely the choice of different current waveshapes has a limited impact on the estimation of the perspective lightning performance. The calculation relevant to the Cigré function has been also repeated assuming the median value of S_m equal to 26 kA/ μ s (instead of 12 kA/ μ s) as suggested in (Cigré Working Group 33.01, 1991). The results are very similar to the curve corresponding to the Cigré function already shown in Figure 2-23.

Without surge arresters and flashovers, as expected, all direct events result in overvoltages greater than the maximum value in abscissa (i.e., 0.24 events/yr for the case of the 2-km long line and 12.08 events/100km/yr for the very long line).

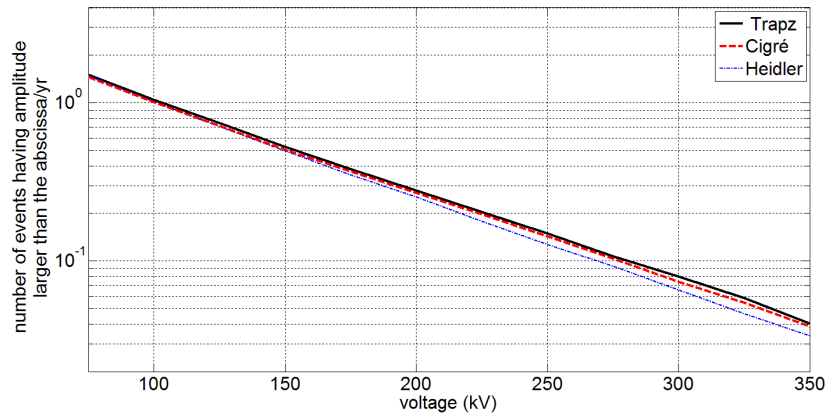


Figure 2-22 – Comparison of the perspective indirect lighting performances calculated by using three different current waveshapes. Length of the line equal to 2 km.

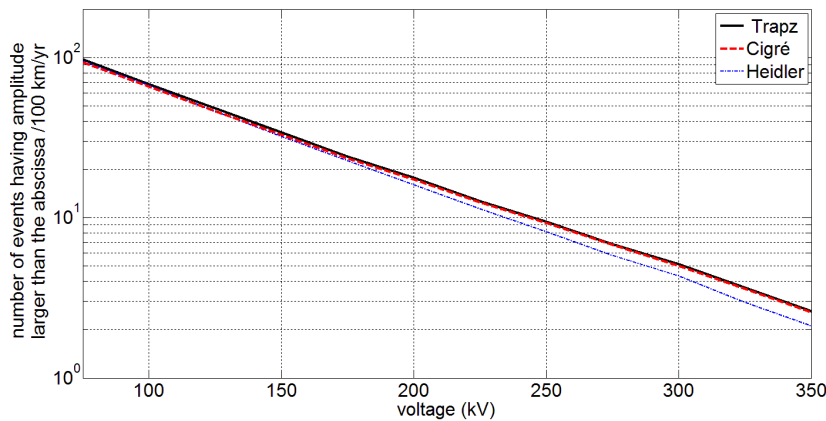


Figure 2-23 – Comparison of the perspective indirect lighting performances calculated by using three different current waveshapes. Very long line.

Lightning performance of the central point of the 2 km-long line

In this Subsection the same three-conductor line is considered with sets of three surge arresters installed at different distance intervals. The voltage-current characteristic of the adopted 15-kV class surge arresters is the same as in previous section and is shown in Figure 2-6. The considered phase-to-phase voltage at the utility frequency is 13.8 kV.

The distance between subsequent poles is 50 m. Also the parameters of the disruptive effect criterion (adopted for the representation of the flashovers in the line insulators) are the same of previous section and are reported in table 2-2. These parameters have been obtained in (De Conti et al., 2010) from the results of laboratory tests performed on a 15 kV pin-type ceramic insulator.

The presence of a transformer in the middle point of the line is assumed. The withstand voltage of the transformers is assumed to be constant and equal to 150 kV. In (Lopes et al., 2013) a procedure able to take into account the withstand probability distribution of transformer insulation is described.

Figure 2-24 shows the top view of the line; the position of the transformer is denoted by the cross in the middle of the line while the blue circles indicate the surge arrester locations. Distance d defines the interval between subsequent surge arresters. The length of the line is 2 km and the number of generated events in the Monte Carlo procedure is again 20,000. Table 2-10 and Table 2-11 show the MTBF values relevant to a transformer connected to the middle of the line for the two different insulators described in table 2-2, namely 165 kV and 100 kV, respectively. The results are reported for the three different current waveforms and for different distances between consecutive SAs, namely 100 m, 200 m, 300 m and 400 m.

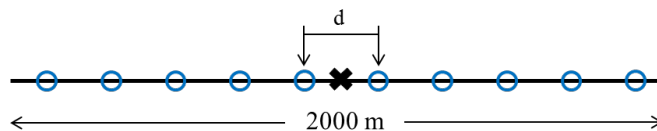


Figure 2-24 – Top view of the line with the indication of the observation point in the middle of the line and the position of the SAs.

TABLE 2-10 - MTBF (IN YEARS) AT MIDPOINT OF THE LINE FOR DIFFERENT DISTANCES BETWEEN CONSECUTIVE SURGE ARRESTERS, WITHSTAND VOLTAGE OF 150 kV. CFO OF THE INSULATORS = 165 kV.

| current waveform | without SA | | | with SA | | | | | | | | | | | |
|------------------|------------|----------|------|--------------------|----------|------|--------------------|----------|------|--------------------|----------|------|--------------------|----------|------|
| | | | | $d = 100\text{ m}$ | | | $d = 200\text{ m}$ | | | $d = 300\text{ m}$ | | | $d = 400\text{ m}$ | | |
| | direct | indirect | both | direct | indirect | both | direct | indirect | both | direct | indirect | both | direct | indirect | both |
| Trapezoidal | 4.28 | 6.55 | 2.59 | 35.5 | Inf | 35.5 | 15.5 | 1250 | 15.3 | 10.3 | 294 | 10.0 | 7.33 | 125 | 6.92 |
| Cigré | 4.28 | 6.70 | 2.61 | 37.3 | Inf | 37.3 | 16.0 | 1250 | 15.8 | 10.7 | 313 | 10.3 | 7.91 | 105 | 7.36 |
| Heidler | 4.28 | 6.86 | 2.64 | 39.7 | Inf | 39.7 | 16.6 | 1250 | 16.4 | 10.7 | 250 | 10.3 | 7.84 | 114 | 7.34 |

TABLE 2-11 - MTBF (IN YEARS) AT MIDPOINT OF THE LINE FOR DIFFERENT DISTANCES BETWEEN CONSECUTIVE SURGE ARRESTERS, WITHSTAND VOLTAGE OF 150 kV. CFO OF THE INSULATORS = 100 kV.

| current waveform | without SA | | | with SA | | | | | | | | | | | |
|------------------|------------|----------|------|--------------------|----------|------|--------------------|----------|------|--------------------|----------|------|--------------------|----------|------|
| | | | | $d = 100\text{ m}$ | | | $d = 200\text{ m}$ | | | $d = 300\text{ m}$ | | | $d = 400\text{ m}$ | | |
| | direct | indirect | both | direct | indirect | both | direct | indirect | both | direct | indirect | both | direct | indirect | both |
| Trapezoidal | 4.28 | 13.3 | 3.24 | 53.2 | Inf | 53.2 | 16.9 | 1250 | 16.7 | 11.9 | 357 | 11.5 | 9.0 | 147 | 8.48 |
| Cigré | 4.28 | 12.8 | 3.21 | 57.5 | Inf | 57.5 | 17.4 | 1250 | 17.2 | 12.0 | 313 | 11.6 | 8.98 | 122 | 8.36 |
| Heidler | 4.28 | 12.8 | 3.21 | 54.3 | Inf | 54.3 | 17.2 | 1250 | 17.0 | 12.0 | 250 | 11.5 | 8.94 | 119 | 8.32 |

The adoption of a different current waveform generally results in slight differences between the MTBF. The higher differences, concerning the direct events only, appear to be the ones relevant to the case with $d = 100$ m and CFO = 165 kV, for which the adoption of the Heidler and the Cigré turn out in a 10% and 6% increase of the MTBF, respectively. By increasing the distance between SAs these differences tend to be negligible. Concerning the indirect events only, the differences are negligible for the cases of $d = 100$ m and $d = 200$ m due to the very low probability of exceeding the withstand voltage of the transformer. The differences turn out to be appreciable, instead, by increasing d , while again they are negligible if the line is unprotected. These variations in the results are ascribed to the effect of non-linearity introduced by SAs and flashover model that enhance the effect of the difference among the chosen current waveshapes and in particular of their front.

The computational cost due to the assumption of more realistic current waveforms rather than the trapezoidal one is quite heavy. The time required to obtain the results of both Table 2-10 and Table 2-11 relevant to indirect strikes for the case of trapezoidal current waveform is about 8 h and about twice the time for the two other currents waveforms. The time needed for the direct strikes calculation is independent of the current waveform if the induced effects of the LEMP are disregarded. The simulations have been carried out by a computer with two 2.6 GHz Intel Xeon E5 eight-core processors and 64 GB of RAM, running 64-bit Windows (both CPU and RAM usage is lower than 30%).

Conclusion

This section has analyzed the influence of the choice of the function describing the current waveform at the base of the lightning channel on the lightning performance of power components connected to an overhead distribution line. To this purpose, a procedure able to extend the Monte Carlo method to the generation of a multivariate log-normal distribution of current parameters has been developed.

Whilst the influence of the current waveform on the perspective lightning performance (i.e. assuming no flashovers and no surge arresters) is somewhat limited, results with more significant differences are obtained when the presence of surge arresters and flashovers occurrence is taken into account. This is reflected in the reported calculations, see for instance the expected MTBF values of a transformer protected by surge arresters at the lowest distance considered in this section (50 m).

On the basis of the obtained results, it is possible to conclude that the simple trapezoidal current waveform represents a good compromise between computational effort and conservative assessment of the lightning performance, and therefore its use is recommended for insulation coordination studies, in particular if based on the Monte Carlo method.

2.4. Lightning Performance of a Real Distribution Network with Focus on Transformer Protection

The frequency of lightning-caused transformer failures in overhead distribution feeders may be of concern especially in areas characterized by a high keraunic level e.g. (*Plummer et al., 1994; Mikropoulos et al., 2014*), thus justifying specific studies in order to reduce the outage rate below the requested threshold. A joint research project between the Brazilian electric distribution utility AES Sul and two Universities, namely the Federal University of Itajubá and the University of Bologna, has focused on the assessment of the protection distance of surge arresters (SAs) in distribution networks with resonant grounding, in order to achieve the desired protection level of distribution transformers against lightning at affordable costs. The expected frequency of flashovers due to indirect strikes, i.e. lightning strikes hitting the ground nearby the lines, has been calculated for the case of medium voltage straight lines with different types of poles and the relevant results have been presented in (*Borghetti et al., 2012; Napolitano et al., 2014*).

The lightning induced voltage calculations is performed by using the LIOV-EMTP-rv code (*Napolitano et al., 2008; Nucci & Rachidi, 2014*); a Monte Carlo procedure adapted from the one presented in (*Borghetti et al., 2007*), also described in (*IEEE Std 1410-2010, 2011*), is applied in order to calculate the expected mean time between failures (MTBF) of the MV/LV transformers.

This section describes the development of such a procedure for the evaluation of the lightning performance of a real three-phase distribution medium voltage feeder located near Novo Hamburgo (Brazil). The feeder is characterized by a complex topology, with several multi-conductor lines, MV/LV transformers and surge protection devices.

In addition to the estimation of the indirect lightning performance (i.e. the lightning performance calculated only for the case of indirect strikes), in this section the analysis has been extended to include the effects of direct strikes.

The developed model of the distribution network represents the specific features of the real network, such as the network topology, the multi-conductor line and pole configurations, the presence of surge protective devices. The coupling model between the lightning electromagnetic pulse (LEMP) and the overhead conductors takes into account the

characteristics of the lightning current, the return stroke model, and the LEMP propagation above a lossy ground.

The Monte Carlo procedure adopted in this section includes a heuristic technique, designed and implemented in order to reduce the computational effort required for the analysis of large networks. The heuristic technique is able to deal with the non-linear response of the network due to the presence of SAs.

Calculation Method

The statistical procedure is based on the application of the Monte Carlo method and can be summarized as follows. A large number n_{tot} of lightning events is randomly generated. Each event is characterized by four parameters: lightning current amplitude I_p , time to peak t_f and stroke location with coordinates x and y .

The lightning current parameters are assumed to follow the Cigré log-normal probability distributions (*Anderson & Eriksson, 1980*), (*Cigré Working Group 33.01, 1991*) for negative first strokes, with a correlation coefficient between t_f and I_p equal to 0.47. The effects of the presence of positive flashes and of subsequent strokes in negative flashes on the lightning performance of the feeder are assumed to be negligible. The stroke locations are assumed to be uniformly distributed in a striking area, having a size large enough to contain the entire network and all the stroke locations of the indirect lightning events that could cause voltages larger than the minimum value of interest for the analysis.

In general, e.g. (*IEEE Std 1410-2010, 2011*), the lightning performance is expressed by means of a curve providing the expected annual numbers of lightning events F_p that cause voltages with amplitude larger than the insulation level reported in abscissa:

$$F_p = \frac{n}{n_{tot}} A N_g \quad (2.19)$$

where n is the number of events that cause voltages higher than the considered insulation level, A is the striking area and N_g is the annual ground flash density (assumed equal to 1 flash/km²/yr in this section).

If referred to a single straight line, the lightning performance is usually expressed in terms of number of events per year per unit length of line. However, the indirect lightning performance of a network with complex topology (e.g. a distribution feeder with several laterals) may significantly deviate by the one inferred from the results obtained for the case of a single

straight line (Borghetti *et al.*, 2009). Therefore, since the project that motivates the papers summarized in this section is focused on the protection of MV/LV transformers, the MTBF values are calculated by applying (2.19) to each MV bus where a transformer is connected. Value n is obtained by comparing the lightning voltages with the relevant withstand voltage of the transformer insulation that is assumed to be constant and known. In order to take into account the withstand probability distribution of transformer insulation a more complex procedure would need to be applied (Lopes *et al.*, 2013).

Indirect Lightning Performance

From the total set of n_{tot} lightning events, the ones relevant to indirect lightning are selected by using a lightning incidence model for the line. As done so far in this thesis the electro-geometric model suggested in (IEEE Std 1410-2010, 2011) is adopted. As already mentioned, the calculation of the induced voltages caused by indirect lightning strikes is performed by using the LIOV-EMTP-rv code. The LEMP is calculated by using the analytical formulation presented in (Napolitano, 2011) with the assumption that the lightning return stroke current propagates along a straight vertical channel according to the transmission line (TL) model. The assumed value for the return-stroke propagation speed is 1.5×10^8 m/s. The lightning current waveform at the channel base is approximated by a linear ramp up to the peak value I_p at time t_f , followed by a constant value. Two values of the ground conductivity σ_g are considered: 10^{-3} and 10^{-2} S/m. The lossy ground effect on the LEMP are accounted by means of the Cooray-Rubinstein formula (Cooray, 1992; Rubinstein, 1996). The bus voltage at the utility frequency is taken into account by using the procedure described in (Borghetti *et al.*, 2012).

In order to appraise the indirect lightning performance in a reasonably low computational time, a heuristic technique has been applied that avoids performing the time-domain simulation for events expected to be less harmful than previously calculated events that have not caused flashovers. The events that are believed to be not significant for the calculation of n without performing the corresponding time-domain simulations are those that are characterized by lower I_p , greater t_f and greater distance between the stroke location and the nearest SAs than a previously calculated event that causes a current in the SAs below a predefined minimum value, I_{sa} . The adopted value is $I_{sa} = 100$ A so that very similar results both with and without the application of the heuristic procedure are obtained for a test case composed by a straight three-conductor line with equally spaced SAs.

Direct Lightning Performance

In order to take into account the effects of direct events on the lightning performance of the network, the overvoltages corresponding to each of the Monte Carlo events classified as direct strikes to the line are calculated by using an LIOV-EMTP-rv model. A direct strike is represented by a current source connected to the pole closest to the randomly-generated stroke location coordinates. As for the calculation of the induced voltages, the waveshape of the lightning currents is represented by a linear front and a flat top. The surge impedance of the lightning channel is assumed much larger than that of the line and, therefore, neglected. The LEMP effect is accounted also in case of a direct strike, assuming the stroke location 10 m far from the line in order to avoid numerical singularities. This approximation is justified since, near the stroke location, the overvoltages due to the current injection prevail over those induced by the LEMP. Direct strikes to distribution overhead lines are always expected to cause flashovers at line insulators, unless very close SAs are installed (*IEEE Std 1410-2010*, 2011), even in presence of ground wires (*Nakada et al.*, 2003; *Miyazaki & Okabe*, 2009). A larger number of flashovers along the feeder would result in a worst lightning performance of the line, but in an increase of MTBF of the transformers not equipped by surge protective devices.

The implemented model represents the insulators flashovers by means of ideal switches that close according to the disruptive effect criterion (*Darveniza & Vlastos*, 1988): a flashover occurs if the time integral of the line-to-ground voltage exceeds a given value DE . The adopted DE values stand on the ones provided by *De Conti et al.* (2010), which are inferred from experimental tests on a pin-type ceramic insulator of the same type installed in the AES Sul networks. For the insulator of the central conductor, due to its vicinity to a metallic crossarm brace, the same values proposed in (*De Conti et al.*, 2010) for the insulator alone are assumed, i.e. $DE = 60.9 \text{ kV}\mu\text{s}$ and $V_0 = 90 \text{ kV}$, where V_0 is the minimum voltage for the initiation of the breakdown process. For the insulators of the two outer conductors the assumed values are: $DE = 255 \text{ kV}\mu\text{s}$ and $V_0 = 164 \text{ kV}$, taking into account that the insulators are in series with a 60 cm long wooden crossarm. The latter value, larger than the value proposed in (*De Conti et al.*, 2010) for insulators in series to 40 cm of wooden crossarm, has been obtained by assuming a per unit-length increase of the CFO due to the wood equal to 250 kV/m (as suggested in *IEEE Std 1410-2010* 2011) and a reducing factor equal to 0.7 for wet conditions (*Jacob et al.*, 1991).

Other assumptions: poles made of concrete with a grounding resistance equal to 400Ω and SAs grounded with a resistance R_g equal to 10Ω . The effect of the soil ionization at the grounded poles is accounted by using the Weck's approximation (*Cigré Working Group 33.01*, 1991).

The calculations have been repeated for three different values of the environmental shielding factor S_f , i.e. the per-unit portion of the distribution line shielded by nearby objects (*IEEE Std 1410-2010*, 2011): $S_f = 0$ (no shielding), $S_f = 0.91$ (that corresponds to the case of shielding provided by objects having the same height of the lines) and $S_f = 1$ (complete shielding provided by taller nearby objects). The effects on the lightning performance due the events that do not hit the line thanks to the environmental shielding are accounted by the calculation of the induced voltages caused by the associated LEMP. Multiple reflections of the current pulse along the stricken objects and the effects of the presence of the objects on the LEMP are neglected.

For the cases with S_f greater than 0, the shielding objects are assumed to be uniformly distributed in the whole area and placed at distance $d = 10$ m from the overhead lines. The events with a randomly-generated stroke location at a distance $d_i \leq d$ that are expected to hit a nearby object rather than the line are repositioned at a distance d from the line.

Distribution network and calculated lightning performances

The Novo Hamburgo distribution feeder is composed by three-phase overhead lines for a total length of almost 13.9 km. The mean length of the spans between subsequent poles is 40 m. The topology shown in Figure 2-25 has been acquired from the geographic information system (GIS) data of the network with only small changes so to have line lengths integer multiples of 5 m that is the spatial integration step adopted in the FDTD procedure. The primary substation is located at the origin of the coordinate system. The total number of MV/LV transformers is 80, 55 of which are utility transformers and 25 are of private users. Figure 2-25 also shows the ID numbers adopted to identify the transformers in in Table 2-12 and Table 2-13. All the lines are composed by three overhead conductors of diameter equal to 1 cm and assumed horizontally placed at 9.3 m above ground. The rated voltage of the network is 13.8 kV, whilst the withstand voltages (WV) of the transformers is assumed to be equal to 125 kV. The voltage-current characteristic of the SA is the one already adopted in the previous sections.

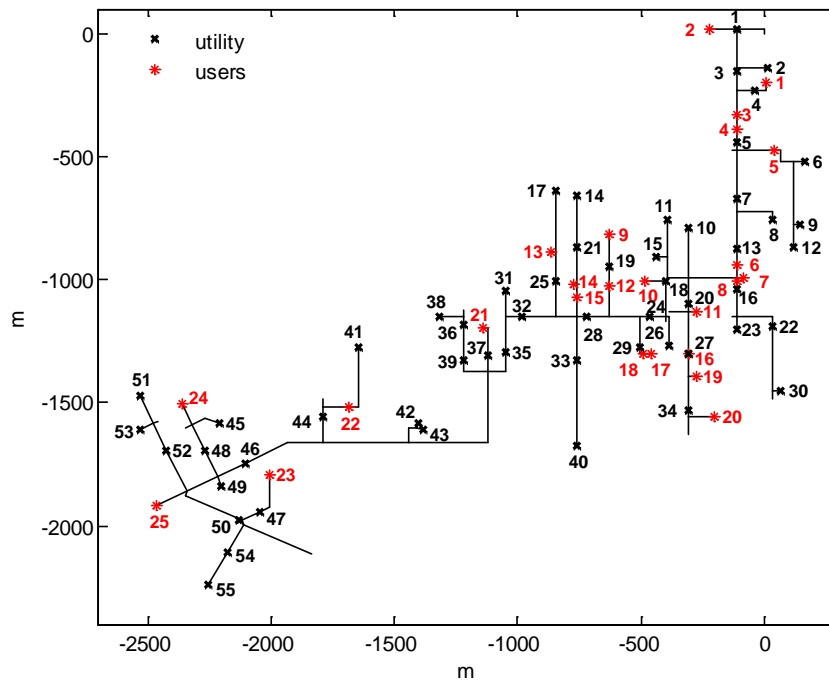


Figure 2-25 – Top view of the network topology, locations and identification number of the distribution transformers (with different notations for the utility substations and the private users' ones).

In (Borghetti *et al.*, 2014) the indirect lightning performance results obtained for the same network by assuming a rated voltage equal to 23.2 kV and $WV = 150$ kV are also reported.

Figure 2-26 shows the top view of the network together with the indication of the locations of both the direct and indirect strikes considered in the Monte Carlo simulation. The total number of Monte Carlo events is $n_{tot} = 200\,000$, 14 685 of which are direct strikes to line conductors. The events are generated uniformly over a striking area $A = 19$ km² with borders at least 1 km far from the network (only part of A is shown in Figure 2-26).

The number of time-domain simulated events is 60 471 out of the 185 315 indirect ones for the case of ground conductivity $\sigma_g = 0.001$ S/m and 25 409 for the case of $\sigma_g = 0.01$ S/m. The reduction in the number of simulations is due the application of the heuristic technique and the corresponding calculation time reduction is 67.4% and 86.3% for $\sigma_g = 0.001$ S/m and $\sigma_g = 0.01$ S/m, respectively.

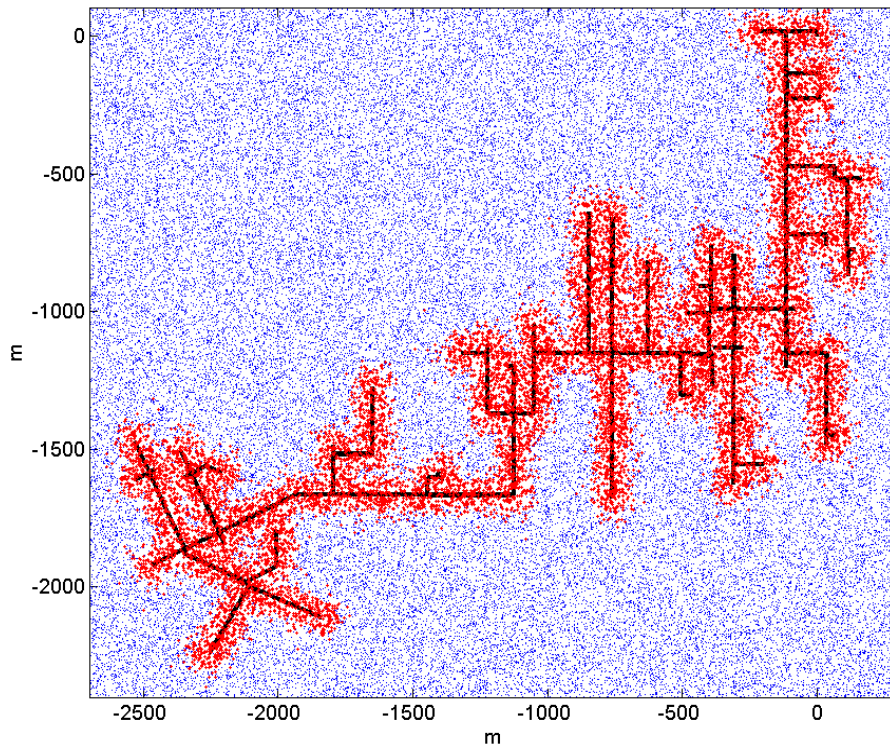


Figure 2-26 – Locations of the Monte Carlo events nearby the network (blue: indirect events, red: direct events).

The results of the calculations reported in what follows refer to the case of $\sigma_g = 0.001$ S/m and the calculations are repeated for two different configurations of the position of SAs:

- configuration A: the SAs are installed at the MV terminals of 31 of the 55 utility transformers;
- configuration B: the SAs are installed at the MV terminals of all the 25 users' transformers and of 16 of the 55 utility transformers.

Figure 2-27 and Figure 2-28 show the MTBF values due to indirect lightning events obtained for the transformers without SAs for configuration A and configuration B, respectively. The indications of the MTBF value is omitted if larger than 700. The indirect lightning performance of the unprotected transformers inferred for configuration A is more uniform than for configuration B as a consequence of a more uniform distribution of SAs in the network. In configuration B, with all users' transformers protected, some utility transformers are well protected against indirect lightning even without SAs.

Areas with high density of MV/LV transformers allow taking advantage of the protection distance of the surge protective devices in order to avoid or defer the installation of SAs at the connection of some distribution transformers. This is of particular interest when there is the need to upgrade of all the SAs due to the planned change of the neutral earthing method from

solidly earthed to resonant one, as for the case of the considered distribution network. However, as shown by the results obtained by taking into account both indirect and direct events, presented later in this Section, there is such a possibility only when the surrounding environment is expected to significantly shield the overhead lines against the direct lightning strikes.

The voltage stress on the transformers due to indirect lightning is highly dependent on the topological configuration of the distribution network. The indirect lightning performance of compact portions of the network, i.e. areas characterized by a larger number of laterals, is better in general than that of portions of the network with no laterals.

Figures 2-29 to 2-31 show the MTBF values calculated for configuration A, by taking into account both direct and indirect lightning, for the case of $S_f = 0$, $S_f = 1$, and $S_f = 0.91$, respectively.

In general, unprotected transformers installed at the ends of laterals suffer a worse lightning performance than that of transformers located in other parts of the network with the same distances from nearby SAs.

The comparison between the results of Figure 2-27 and Figure 2-29 shows that direct strikes to the line conductors yield much lower and more uniform MTBF values.

With $S_f = 1$ and $S_f = 0.91$, the MTBF values of several transformers are significantly increased, in particular for those near to SAs, as shown by Figure 2-30 and Figure 2-31. This confirms the possibility to avoid the installation of SAs at some transformers if the presence of nearby objects prevents, at least in part, direct strikes to the line, although the comparison between Figure 2-27 and Figure 2-30 shows that the MTBF values of several transformers are significantly affected also by the induced voltages due to indirect events to objects very close to a line.

Similar conclusions can be drawn from the corresponding results obtained for configuration B, shown in Figures 2-32 to 2-34. Figure 2-35 refers to the same case of Figure 2-29 but the response to direct strikes is evaluated without the LEMP. As expected, the MTBF values of Figure 2-35 are slightly higher than those of Figure 2-29, since the presence of the LEMP is in general expected to worsen the lightning performance (*Tossani et al., 2015a*).

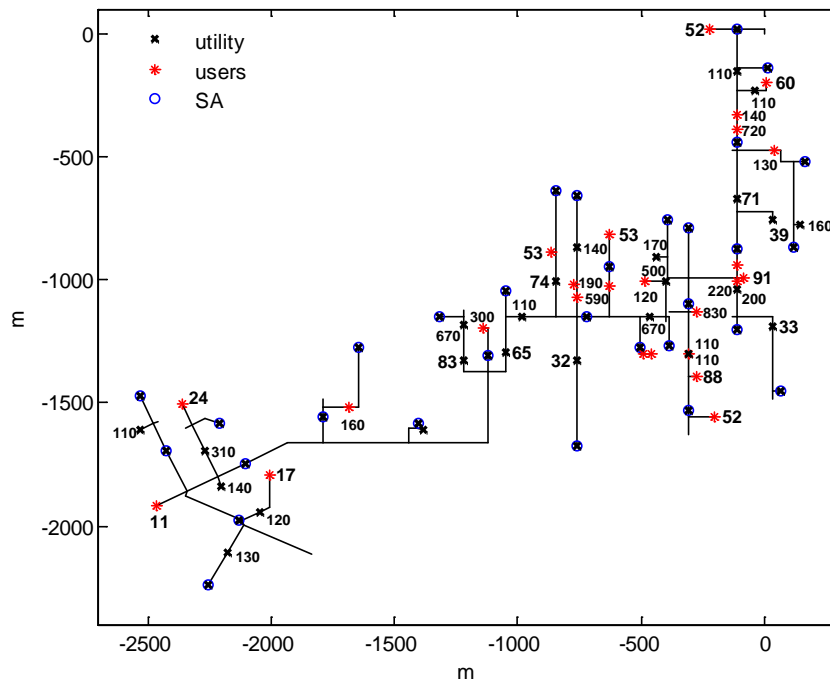


Figure 2-27 – Configuration A. MTBF values (in years) due to indirect lightning of transformers not equipped with SA. $\sigma_g=0.001$ S/m.

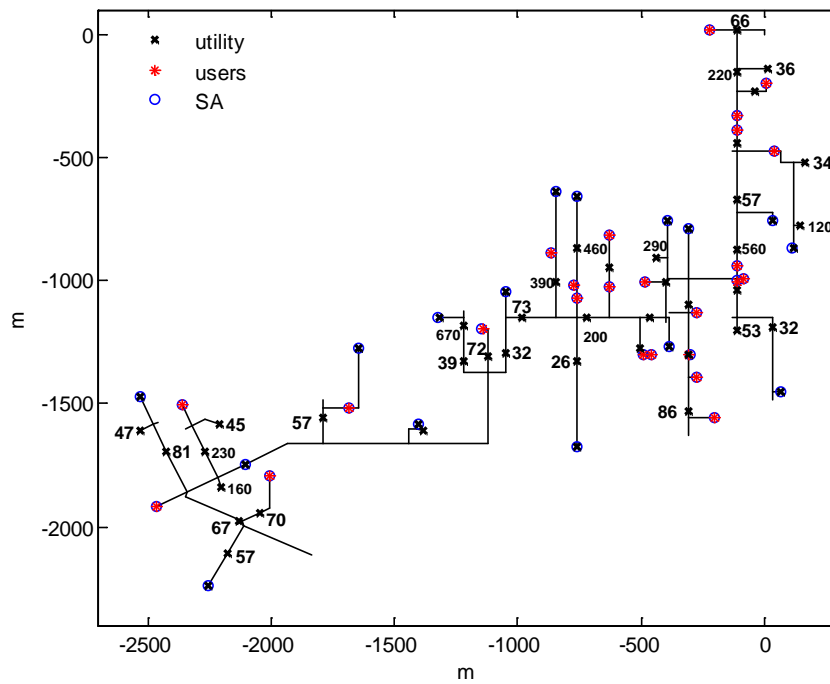


Figure 2-28 – Configuration B. MTBF values (in years) due to indirect lightning of transformers without SA. $\sigma_g = 0.001$ S/m.

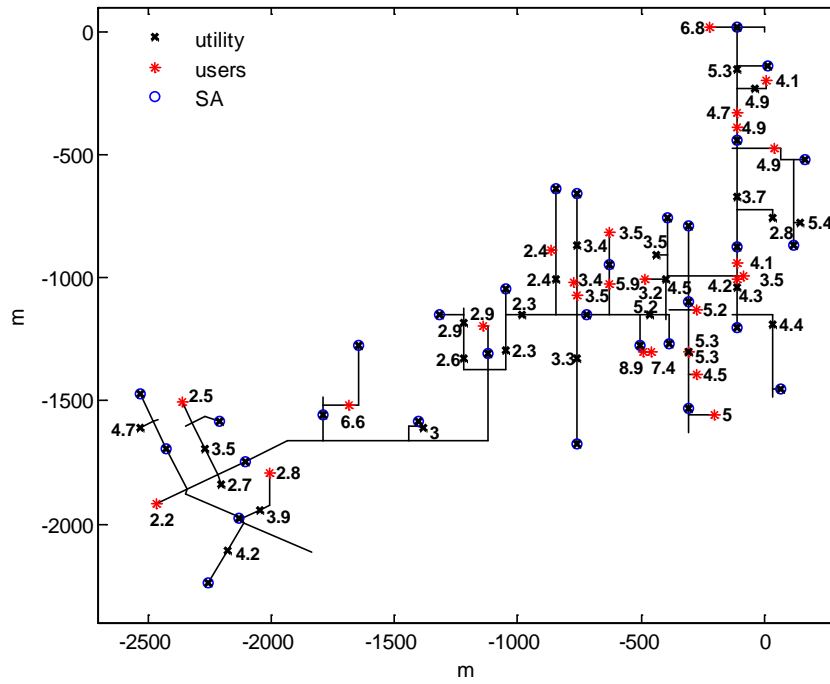


Figure 2-29 – Configuration A. MTBF (years) due to direct and indirect lightning of the transformers without SAs. $\sigma_g = 0.001$ S/m. $S_f = 0$.

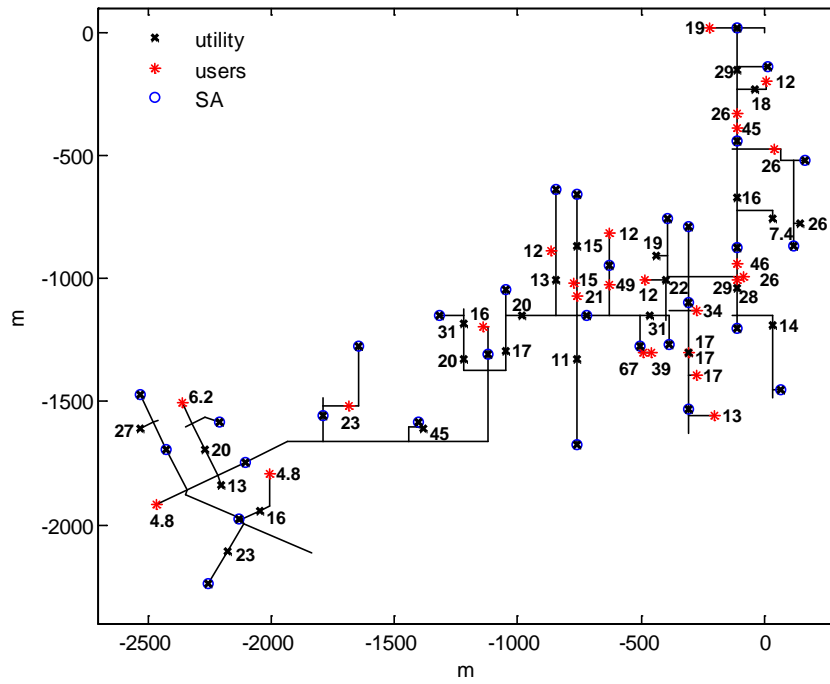


Figure 2-30 – Configuration A. MTBF (years) due to direct and indirect lightning of the transformers without SAs. $\sigma_g = 0.001$ S/m. $S_f = 1$.

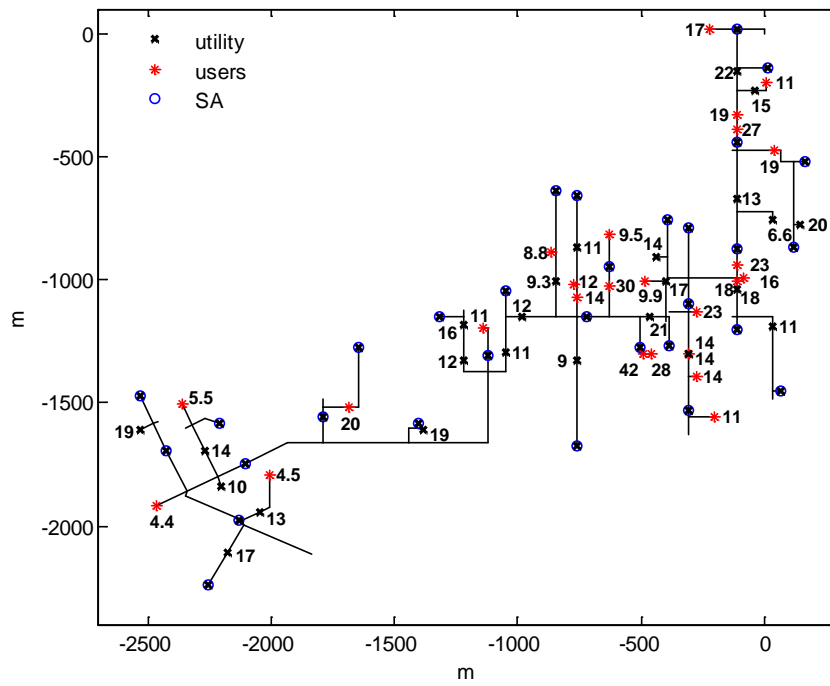


Figure 2-31 – Configuration A. MTBF (years) due to direct and indirect lightning of the transformers without SAs. $\sigma_g = 0.001$ S/m. $S_f = 0.91$.

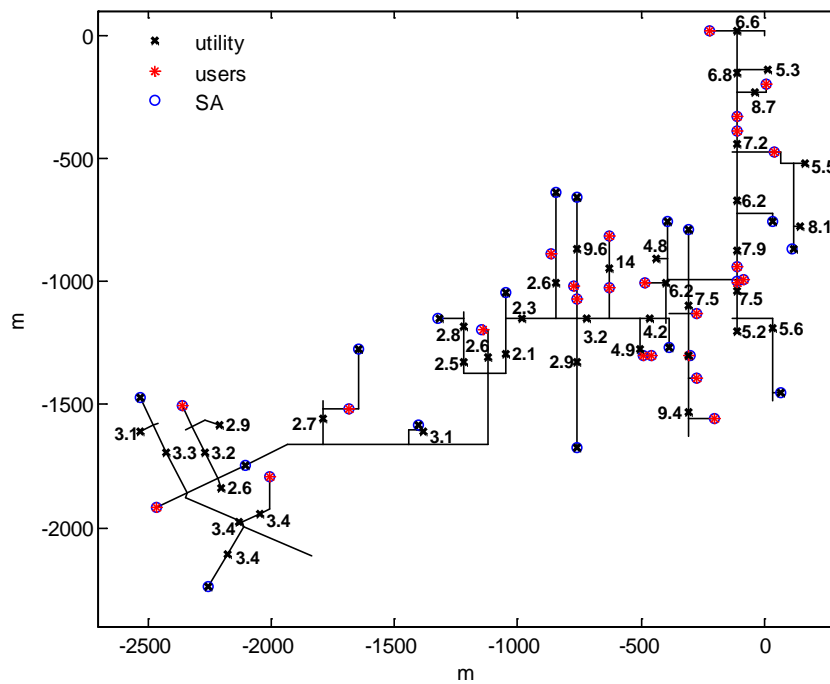


Figure 2-32 – Configuration B. MTBF (years) due to direct and indirect lightning of the transformers without SA. $\sigma_g = 0.001$ S/m. $S_f = 0$.

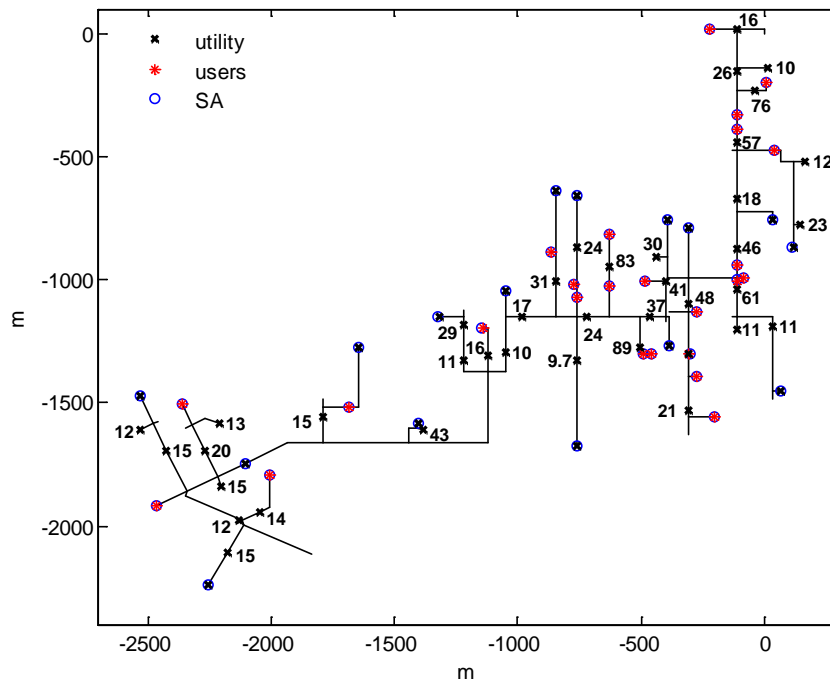


Figure 2-33 – Configuration B. MTBF (years) due to direct and indirect lightning of the transformers without SA. $\sigma_g = 0.001$ S/m. $S_f = 1$.

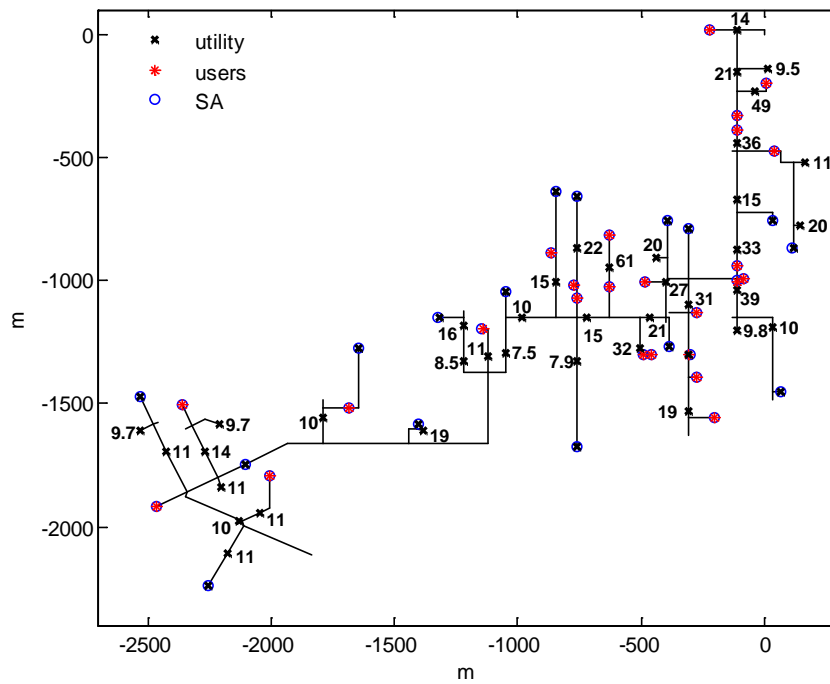


Figure 2-34 – Configuration B. MTBF (years) due to direct and indirect lightning of the transformers without SA. $\sigma_g = 0.001$ S/m. $S_f = 0.91$.

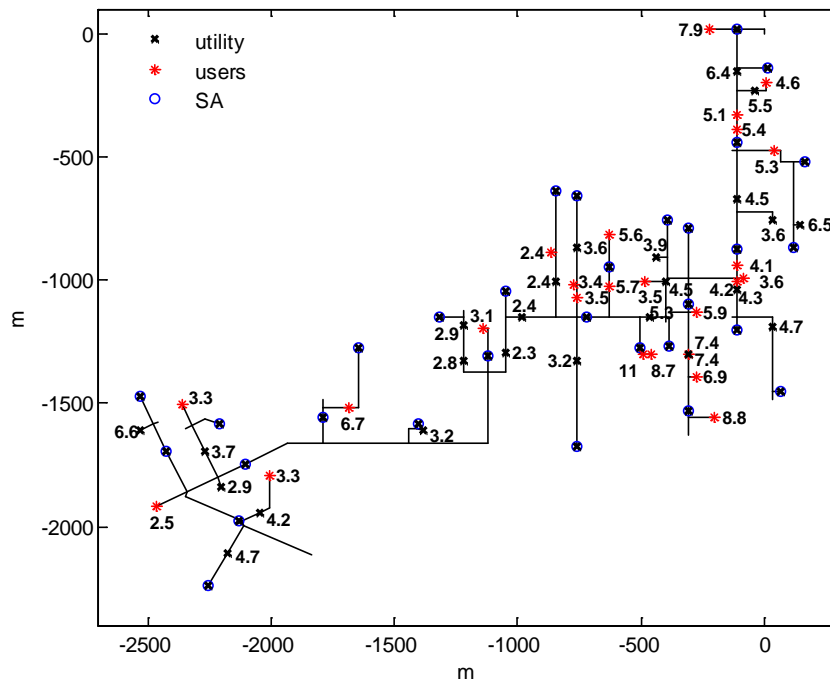


Figure 2-35 – MTBF (years) due to direct for the same case of Figure 2-29 but without taking into account the LEMP due to direct strikes.

The MTBF values relevant to configuration A and B calculated for the case of $\sigma_g = 0.001$ S/m are also reported in Table 2-12 and Table 2-13, respectively, together with the relevant confidence intervals. These values are compared with those obtained for $\sigma_g = 0.01$ S/m and with those obtained by including the effects of direct strikes to nearby objects ($S_f = 1$).

The tables show that, disregarding direct events, all the transformers are well protected for the case of $\sigma_g = 0.01$ S/m and almost all the transformers have MTBF values greater than 20 years for the case of $\sigma_g = 0.001$ S/m. If direct strikes to nearby objects are taken into account, almost all MTBF values are greater than 20 years only for the case of $\sigma_g = 0.01$ S/m.

The tables show that, disregarding direct events, all the transformers are well protected for the case of $\sigma_g = 0.01$ S/m and almost all the transformers have MTBF values greater than 20 years for the case of $\sigma_g = 0.001$ S/m. If direct strikes to nearby objects are taken into account, almost all MTBF values are greater than 20 years only for the case of $\sigma_g = 0.01$ S/m. Indeed, as already explained through this thesis, low soil conductivity significantly enhance the overvoltages due to indirect lightning events (Rachidi et al., 1996).

TABLE 2-12 – MEAN TIME BETWEEN FAILURES (YEARS) AND CONFIDENCE INTERVAL (CI). CONFIGURATION A.

| Obs. point | $\sigma_g = 0.001 \text{ S/m}$ | | | | $\sigma_g = 0.01 \text{ S/m}$ | | | | |
|------------|--------------------------------|--------|--|--------|-------------------------------|--------|--|--------|-----|
| | Indirect events only | | Indirect and direct events ($S_f = 1$) | | Indirect events only | | Indirect and direct events ($S_f = 1$) | | |
| | MTBF | CI (%) | MTBF | CI (%) | MTBF | CI (%) | MTBF | CI (%) | |
| Utility | 3 | 110 | 21 | 29 | 11 | inf | - | 71 | 16 |
| | 4 | 110 | 20 | 18 | 8.4 | 350 | 36 | 36 | 12 |
| | 7 | 71 | 16 | 16 | 7.9 | 320 | 35 | 36 | 12 |
| | 8 | 39 | 12 | 7.4 | 5.3 | 160 | 25 | 18 | 8.3 |
| | 9 | 160 | 25 | 26 | 9.9 | inf | - | 63 | 15 |
| | 15 | 170 | 26 | 19 | 8.4 | 770 | 54 | 35 | 12 |
| | 16 | 200 | 27 | 28 | 10 | inf | - | 64 | 16 |
| | 18 | 500 | 44 | 22 | 9.2 | inf | - | 37 | 12 |
| | 21 | 140 | 23 | 15 | 7.5 | inf | - | 34 | 11 |
| | 22 | 33 | 11 | 14 | 7.2 | 270 | 32 | 41 | 13 |
| | 24 | 670 | 51 | 31 | 11 | inf | - | 56 | 15 |
| | 25 | 74 | 17 | 13 | 7.1 | 260 | 31 | 26 | 10 |
| | 27 | 110 | 21 | 17 | 8.0 | 670 | 51 | 44 | 13 |
| | 32 | 110 | 20 | 20 | 8.8 | 720 | 52 | 48 | 14 |
| | 33 | 32 | 11 | 11 | 6.5 | 180 | 26 | 35 | 12 |
| | 35 | 65 | 16 | 17 | 8.0 | 480 | 43 | 41 | 13 |
| | 36 | 670 | 51 | 31 | 11 | inf | - | 53 | 14 |
| | 39 | 83 | 18 | 20 | 8.7 | 420 | 40 | 39 | 12 |
| | 43 | inf | - | 45 | 13 | inf | - | 130 | 22 |
| | 47 | 120 | 21 | 16 | 7.7 | inf | - | 41 | 12 |
| 48 | 310 | 35 | 20 | 8.8 | inf | - | 36 | 12 | |
| 49 | 140 | 23 | 13 | 7.1 | inf | - | 40 | 12 | |
| 53 | 110 | 20 | 27 | 10 | inf | - | 70 | 16 | |
| 54 | 130 | 23 | 23 | 9.5 | inf | - | 64 | 16 | |
| Users | 1 | 60 | 15 | 12 | 6.9 | 240 | 30 | 28 | 10 |
| | 2 | 52 | 14 | 19 | 8.4 | inf | - | 100 | 20 |
| | 3 | 140 | 23 | 26 | 9.9 | inf | - | 65 | 16 |
| | 4 | 720 | 52 | 45 | 13 | inf | - | 150 | 24 |
| | 5 | 130 | 22 | 26 | 10 | inf | - | 76 | 17 |
| | 6 | inf | - | 46 | 13 | inf | - | 130 | 22 |
| | 7 | 91 | 19 | 26 | 9.9 | 910 | 59 | 57 | 15 |
| | 8 | 220 | 29 | 29 | 11 | inf | - | 69 | 16 |
| | 9 | 53 | 14 | 12 | 6.7 | inf | - | 71 | 16 |
| | 10 | 120 | 22 | 12 | 6.9 | 830 | 57 | 26 | 10 |
| | 11 | 830 | 57 | 34 | 11 | inf | - | 95 | 19 |
| | 12 | inf | - | 49 | 14 | inf | - | 110 | 20 |
| | 13 | 53 | 14 | 12 | 6.9 | 160 | 25 | 23 | 9.4 |
| | 14 | 190 | 27 | 15 | 7.6 | inf | - | 39 | 12 |
| | 15 | 590 | 48 | 21 | 8.9 | inf | - | 63 | 16 |
| | 16 | 110 | 21 | 17 | 8.0 | 670 | 51 | 44 | 13 |
| | 17 | inf | - | 39 | 12 | inf | - | 110 | 20 |
| | 18 | inf | - | 67 | 16 | inf | - | 200 | 28 |
| | 19 | 88 | 18 | 17 | 8.1 | 670 | 51 | 45 | 13 |
| | 20 | 52 | 14 | 13 | 7.0 | 830 | 57 | 61 | 15 |
| | 21 | 300 | 34 | 16 | 7.8 | inf | - | 69 | 16 |
| | 22 | 160 | 25 | 23 | 9.4 | inf | - | 53 | 14 |
| | 23 | 17 | 8.0 | 4.8 | 4.2 | 190 | 27 | 19 | 8.6 |
| | 24 | 24 | 9.6 | 6.2 | 4.8 | 350 | 36 | 27 | 10 |
| | 25 | 11 | 6.5 | 4.8 | 4.3 | 76 | 17 | 20 | 8.8 |

TABLE 2-13 – MEAN TIME BETWEEN FAILURES (YEARS) AND CONFIDENCE INTERVAL (CI). CONFIGURATION B.

| Obs. point | $\sigma_g = 0.001 \text{ S/m}$ | | | | $\sigma_g = 0.01 \text{ S/m}$ | | | |
|------------|--------------------------------|--------|--|--------|-------------------------------|--------|--|--------|
| | Indirect events only | | Indirect and direct events ($S_f = 1$) | | Indirect events only | | Indirect and direct events ($S_f = 1$) | |
| | MTBF | CI (%) | MTBF | CI (%) | MTBF | CI (%) | MTBF | CI (%) |
| 1 | 66 | 16 | 16 | 7.7 | inf | - | 49 | 14 |
| 2 | 36 | 12 | 10 | 6.2 | 290 | 34 | 27 | 10 |
| 3 | 220 | 29 | 26 | 9.9 | 830 | 57 | 48 | 14 |
| 4 | inf | - | 76 | 17 | inf | - | 150 | 24 |
| 5 | inf | - | 57 | 15 | inf | - | 170 | 26 |
| 6 | 34 | 11 | 12 | 6.9 | 290 | 33 | 45 | 13 |
| 7 | 57 | 15 | 18 | 8.2 | 280 | 33 | 40 | 12 |
| 9 | 120 | 21 | 23 | 9.4 | inf | - | 58 | 15 |
| 13 | 560 | 46 | 46 | 13 | inf | - | 150 | 24 |
| 15 | 290 | 34 | 30 | 11 | inf | - | 55 | 15 |
| 16 | inf | - | 61 | 15 | inf | - | 160 | 25 |
| 18 | inf | - | 41 | 13 | inf | - | 85 | 18 |
| 19 | inf | - | 83 | 18 | inf | - | 200 | 28 |
| 20 | inf | - | 48 | 14 | inf | - | 110 | 21 |
| 21 | 460 | 42 | 24 | 9.6 | inf | - | 68 | 16 |
| 22 | 32 | 11 | 11 | 6.5 | 170 | 25 | 25 | 9.8 |
| 23 | 53 | 14 | 11 | 6.4 | 190 | 27 | 26 | 10 |
| 24 | inf | - | 37 | 12 | inf | - | 65 | 16 |
| 25 | 390 | 38 | 31 | 11 | inf | - | 63 | 16 |
| 28 | 200 | 28 | 24 | 9.7 | inf | - | 82 | 18 |
| 29 | inf | - | 89 | 19 | inf | - | 260 | 31 |
| 32 | 73 | 17 | 17 | 7.9 | 480 | 43 | 42 | 13 |
| 33 | 26 | 10 | 9.7 | 6.1 | 140 | 23 | 28 | 10 |
| 34 | 86 | 18 | 21 | 9.0 | inf | - | 73 | 17 |
| 35 | 32 | 11 | 10 | 6.3 | 180 | 26 | 26 | 9.9 |
| 36 | 670 | 51 | 29 | 10 | inf | - | 41 | 13 |
| 37 | 72 | 17 | 16 | 7.8 | inf | - | 47 | 13 |
| 39 | 39 | 12 | 11 | 6.5 | 210 | 28 | 24 | 9.6 |
| 43 | inf | - | 43 | 13 | inf | - | 130 | 22 |
| 44 | 57 | 15 | 15 | 7.6 | 500 | 44 | 46 | 13 |
| 45 | 45 | 13 | 13 | 7.0 | 220 | 29 | 26 | 9.9 |
| 47 | 70 | 16 | 14 | 7.2 | 560 | 46 | 30 | 11 |
| 48 | 230 | 30 | 20 | 8.8 | 910 | 59 | 39 | 12 |
| 49 | 160 | 25 | 15 | 7.5 | inf | - | 40 | 12 |
| 50 | 67 | 16 | 12 | 6.8 | 330 | 36 | 24 | 9.7 |
| 52 | 81 | 18 | 15 | 7.5 | 320 | 35 | 28 | 10 |
| 53 | 47 | 13 | 12 | 6.9 | 350 | 36 | 33 | 11 |
| 54 | 57 | 15 | 15 | 7.5 | 360 | 37 | 34 | 11 |

In order to illustrate the effects of the grounding resistance of SAs, the calculations have been repeated for the case of $R_g = 50 \Omega$ (configuration A and $\sigma_g = 0.001 \text{ S/m}$) instead of $R_g = 10 \Omega$ as in the previous calculations. Figure 2-36 compares the numbers of utility transformers (without SAs) that have MTBF values lower than abscissa, obtained by using the two different values of R_g . The comparison is carried out both for indirect events only and by taking into account also direct strikes ($S_f = 0$ and $S_f = 1$). As expected, since MTBF values decrease by increasing R_g , the number of transformers characterized by very low MTBF values increases: e.g. for the case of $S_f = 1$ the number of transformers with MTBF value lower than 20 years increases from 13 with $R_g = 10 \Omega$ to 17 with $R_g = 50 \Omega$.

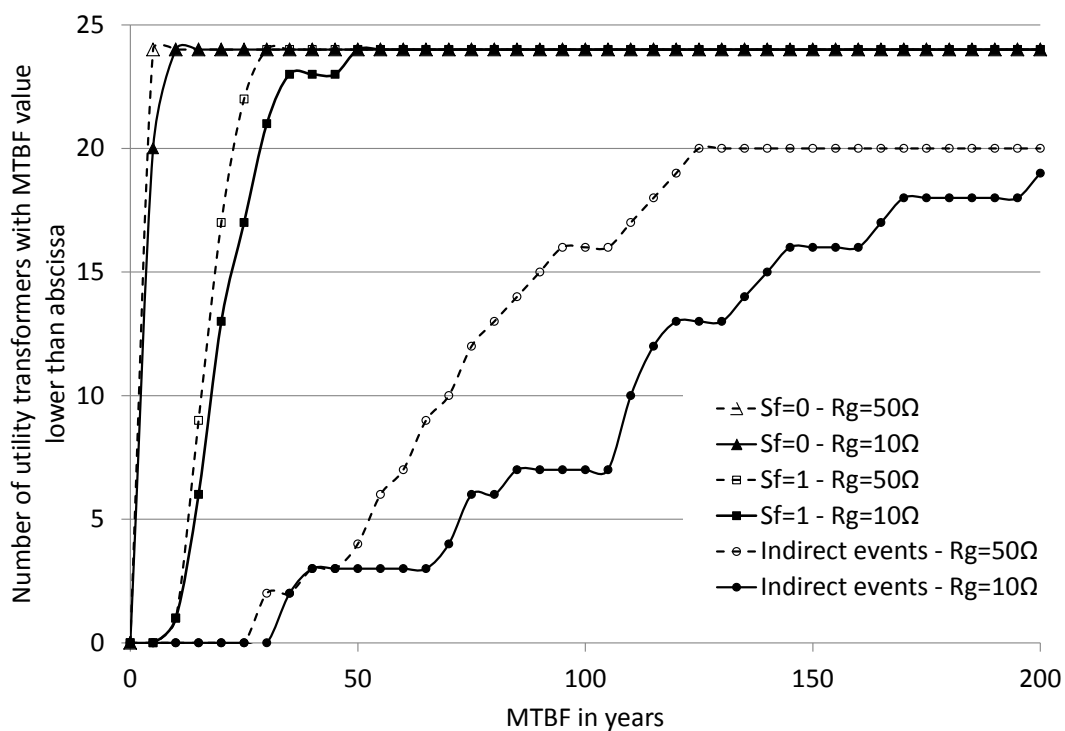


Figure 2-36 – Influence of grounding resistance R_g on the number of utility transformers with MTBF value lower than abscissa calculated for configuration A and $\sigma_g = 0.001 \text{ S/m}$.

Conclusion

This section has presented the application of a Monte Carlo procedure based on the accurate calculation of the induced voltages provided by the LIOV-EMTP-rv code for the evaluation of the lightning performance of an entire real distribution feeder. The analysis includes the effects of direct strikes to the line conductors, taking into account also the shielding provided by the presence of elevated objects nearby the lines (e.g. trees and buildings). The developed model, which accurately represents the complex network topology and its highly non-linear

response due to the presence of SAs, insulation breakdown and soil ionization, allows for the estimation of the MTBF values of each MV/LV transformer not equipped with SAs.

In case of open terrain lines, without shielding provided by nearby objects, the lightning performance is mainly determined by the direct strikes and low MTBF values are in general obtained for the unprotected transformers, almost independently from the network configuration and the distance from contiguous SAs. In case of shielding provided by nearby objects, which prevents direct strikes to the line, the lightning performance improves significantly even in case of partial shielding. In this case the LEMP effect of shielded strikes, i.e. strikes that would hit the line in open terrain, has a significant effect on the lightning performance. In particular the worst performances are those of the transformers connected at the end of laterals.

The presented methodology appears a useful tool in order to select the most appropriate strategies for the installation of SAs in order to achieve the desired lightning performance at affordable costs. This is of peculiar interest for the case of the network chosen for the analysis in which all the SAs needs to be replaced in view of the planned change of the neutral earthing method from solidly earthed to resonant one.

3. Conclusion

This final chapter is devoted to the main conclusions of this research activity.

Concerning the analysis carried out on the field to line coupling to transmission lines, two new analytical expressions for the evaluation of the inverse Laplace transform of the ground impedance matrix elements of a multiconductor overhead line have been derived. The first expression consists of the inverse Laplace transform of Sunde's logarithmic formula, and for it two equivalent forms have been proposed, namely a series expression, which is slowly converging at late times, and an integral one, which instead converges fairly quickly for any value of time. The second expression is the inverse Laplace transform of the general integral expression given by Sunde.

It has been proven that the proposed formulas are not affected by any singularity at the early times, contrary to the previously proposed low frequency expressions such as the one by Timotin and its derivations. The proposed series expression has been used for the evaluation of lightning-induced transients along a multi-conductor line. In order to assess the advantages of the proposed formulation with respect to other ones recently proposed for fixing the low frequency singularity, a comparison between the overvoltages induced on a lossy line according to the approach used by Rachidi et al., with those calculated using the proposed approach has been carried out. It is shown that for fast electromagnetic sources, and/or poor ground conductivities, the proposed expression provides more accurate results compared to the approach used by Rachidi et al. The observed difference on the peak of the induced voltages can reach 20%. The same conclusion applies also for the other two formulas proposed, namely the sum of the series and the inverse Laplace transform of Sunde's integral.

Further, the mathematical derivation of Sunde's integral inverse Laplace transform has been extended to the classical case of a multiconductor buried line taking into account also the displacement currents. A discussion on the ground transient resistance behavior of buried cables by using these new expressions is beyond the scopes of this thesis and therefore will be subject of future investigations.

The second chapter has dealt with the lightning performance of distribution networks. A Monte Carlo procedure based on the accurate calculation of the induced voltages provided by the LIOV-EMTP-rv code for the evaluation of the lightning performance of a large, real, distribution feeder has been proposed. The analysis includes the effects of direct strikes to the line conductors, taking into account also the shielding provided by the presence of elevated objects nearby the lines (e.g. trees and buildings). The developed model accurately represents the complex network topology and its highly non-linear response due to the presence of SAs, insulation breakdown and soil ionization. Furthermore, an analysis on the influence of the choice of the function describing the current waveform at the base of the lightning channel on the lightning performance of power components connected to an overhead distribution line has been carried out. At this purpose, a procedure able to extend the Monte Carlo method to the generation of a multivariate log-normal distribution of current parameters has been developed. On the basis of the obtained results, it is possible to conclude that the simple trapezoidal current waveform represents a good compromise between computational effort and accurate/conservative assessment of the lightning performance, and therefore its use is recommended for insulation coordination studies, in particular if based on the Monte Carlo method.

The proposed model allows for the estimation of the MTBF values of each MV/LV transformer not equipped with SAs. In case of open terrain lines, without shielding provided by nearby objects, the lightning performance is mainly determined by the direct strikes and low MTBF values are in general obtained for the unprotected transformers, almost independently from the network configuration and the distance from contiguous SAs. In case of shielding provided by nearby objects, which prevents direct strikes to the line, the lightning performance improves significantly even in case of partial shielding. In this case the LEMP effect of shielded strikes, i.e. strikes that would hit the line in open terrain, has a significant influence on the lightning performance. In particular the worst performances are those of the transformers connected at the end of laterals.

The presented methodology appears a useful tool in order to select the most appropriate strategies for the installation of SAs in order to achieve the desired lightning performance at affordable costs. This is of peculiar interest for the case of the network chosen for the analysis in which all the SAs needs to be replaced in view of the planned change of the neutral earthing method from solidly earthed to resonant one.

4. Appendix 1 – Inverse Laplace transform of Ground Impedance Matrix – case 1: Sunde's Logarithmic formula

Let us seek the time domain expression for the ground resistance starting from the following inverse Laplace transform

$$\xi'_{g,ij}(t) = L^{-1} \left\{ \frac{Z_{g,ij}}{s} \right\} \quad (\text{A.1})$$

Diagonal terms

The Sunde logarithmic expression for the diagonal terms of the ground matrix can be written as

$$Z'_{g,ii}(s) = \frac{s\mu_0}{2\pi} \ln(1+z) \quad (\text{A.2})$$

where

$$z = \frac{1}{h_i \cdot \gamma_g} = \frac{1}{b_i} [s(s+a)]^{\frac{1}{2}} \quad (\text{A.3})$$

$$a = \frac{\sigma_g}{\epsilon_0 \epsilon_{rg}} \quad \text{and} \quad b_i = h_i \sqrt{\mu_0 \epsilon_0 \epsilon_{rg}} .$$

Taking $|z| < 1$, it is possible to adopt the following series expansion

$$\ln(1+z) = \sum_{n=1}^{\infty} (-1)^{n+1} \frac{z^n}{n} \quad (\text{A.4})$$

and to express (A.2) as

$$Z'_{g,ii}(s) = \frac{s\mu_0}{2\pi} \sum_{n=1}^{\infty} (-1)^{n+1} \frac{[s(s+a)]^{\frac{n}{2}}}{nb_i^n} \quad (\text{A.5})$$

From (Abramowitz & Stegun, 1964), equation (29.3.50)

$$L^{-1}[s(s+a)]^{-k} = \frac{\sqrt{\pi}}{\Gamma(k)} \left(\frac{t}{a}\right)^{k-\frac{1}{2}} \exp\left(-\frac{at}{2}\right) \cdot I_{k-\frac{1}{2}}\left(\frac{at}{2}\right); k > 0 \quad (\text{A.6})$$

in which

$\Gamma(k)$ is Euler Gamma function of the real argument k ;

$I_{k-1/2}(at/2)$ is the modified Bessel function of the first kind, of the order $(k - 1/2)$ and of the real argument $at/2$.

From (Gustav Doetsch, 1974) theorem 30.1, the inverse transform (A.1) of (A.7) is

$$\xi'_{g,ii}(t) = \frac{\mu_0}{2\pi} \sum_{n=1}^{\infty} (-1)^{n+1} \frac{1}{nb_i^n} \frac{\sqrt{\pi}}{\Gamma\left(\frac{n}{2}\right)} \left(\frac{t}{a}\right)^{\frac{n-1}{2}} I_{\frac{n-1}{2}}\left(\frac{at}{2}\right) e^{-\frac{at}{2}} \quad (\text{A.7})$$

Off-diagonal terms

The Sunde logarithmic equation for the off-diagonal terms (Rachidi et al., 1999) can be written as

$$Z'_{g,ij} = \frac{s\mu_0}{4\pi} \left[\ln \frac{1 + \gamma_g \hat{h}_{ij}}{\gamma_g \hat{h}_{ij}} + \ln \frac{1 + \gamma_g \hat{h}_{ij}^*}{\gamma_g \hat{h}_{ij}^*} \right] \quad (\text{A.8})$$

Note that in (A.9) the only term that depends on h_i is b_i , thus, adopting (A.7) for each term of (A.8) leads to

$$\xi'_{g,ij}(t) = \frac{\mu_0}{4\pi} \sum_{n=1}^{\infty} (-1)^{n+1} \frac{1}{n} \left[\frac{1}{\hat{b}_{ij}^n} + \frac{1}{\hat{b}_{ij}^{*n}} \right] \frac{\sqrt{\pi}}{\Gamma\left(\frac{n}{2}\right)} \left(\frac{t}{a}\right)^{\frac{n-1}{2}} \exp\left(-\frac{at}{2}\right) \cdot I_{\frac{n-1}{2}}\left(\frac{at}{2}\right) \quad (\text{A.9})$$

where $\hat{b}_{ij} = \sqrt{\mu_0 \varepsilon_0 \varepsilon_{rg}} \hat{h}_{ij}$ and \hat{b}_{ij}^* is its complex conjugate.

After some mathematical manipulation one finally gets

$$\xi'_{g,ij}(t) = \frac{\mu_0}{2\pi} \sum_{n=1}^{\infty} (-1)^{n+1} \frac{1}{n} \frac{1}{|\hat{b}_{ij}|^n} \cos(n\delta_{ij}) \frac{\sqrt{\pi}}{\Gamma\left(\frac{n}{2}\right)} \left(\frac{t}{a}\right)^{\frac{n-1}{2}} \exp\left(-\frac{at}{2}\right) \cdot I_{\frac{n-1}{2}}\left(\frac{at}{2}\right) \quad (\text{A.10})$$

where $\delta_{ij} = \text{Arg}(\hat{b}_{ij})$.

5. Appendix 2 – Inverse Laplace transform of Ground Impedance Matrix – case 2: Sunde's Integral formula

Diagonal elements

Sunde's formula can be rewritten as follows:

$$\begin{aligned}
 Z'_{g,ii}(s) &= \frac{s\mu_0}{\pi} \int_0^{\infty} \frac{\exp(-2h_i x)}{\sqrt{x^2 + \gamma_g^2} + x} dx = \frac{s\mu_0}{\pi} \int_0^{\infty} \exp(-2h_i x) \frac{\sqrt{x^2 + \gamma_g^2} - x}{x^2 + \gamma_g^2 - x^2} dx = \\
 &= \frac{s\mu_0}{\pi\gamma_g^2} (Int_1 - Int_2)
 \end{aligned} \tag{A2.1}$$

where

$$Int_1 = \gamma_g \int_0^{\infty} \exp(-2h_i x) \sqrt{1 + \left(\frac{x}{\gamma_g}\right)^2} dx \tag{A2.2}$$

$$Int_2 = \int_0^{\infty} \exp(-2h_i x) x dx = \frac{1}{4h_i^2} \tag{A2.3}$$

The inverse transform of the second integral is trivial then it is left to the reader.

By performing the substitution $y = x / \gamma_g$

$$Int_1 = \gamma_g^2 \int_0^{\infty} \exp(-2h_i \gamma_g y) \sqrt{1 + y^2} dy \tag{A2.4}$$

Recalling that

- $\gamma_g = \sqrt{s\mu_0(\sigma_g + s\varepsilon_0\varepsilon_{rg})} = \sqrt{\mu_0\varepsilon_0\varepsilon_{rg}} \sqrt{s} \sqrt{a + s}$;
- $2h_i\gamma_g = 2b_i\sqrt{s} \sqrt{a + s}$;
- and $a = \sigma_g / \varepsilon_g$, $b_i = h_i\sqrt{\mu_0\varepsilon_g}$

$$\begin{aligned}
 L^{-1} \left\{ \frac{\mu_0}{\pi \gamma_g^2} Int_1 \right\} &= L^{-1} \left\{ \frac{\mu_0}{\pi} \int_0^\infty \exp(-2h_i \gamma_g y) \sqrt{1+y^2} dy \right\} \stackrel{2h_i \gamma_g = 2b_i \sqrt{s} \sqrt{s+a}}{=} \\
 &= \frac{\mu_0}{\pi} \int_0^\infty \sqrt{1+y^2} L^{-1} \left\{ \exp(-2b_i y \sqrt{s} \sqrt{s+a}) \right\} dy
 \end{aligned} \tag{A2.5}$$

From (Prudnikov et al., 1992) vol. 5 eq 2.2.5 - 2

$$L^{-1} \left\{ \frac{\exp(-k \sqrt{s} \sqrt{s+a})}{\sqrt{s} \sqrt{s+a}} \right\} = \theta(t-k) e^{-\frac{at}{2}} I_0 \left(\frac{a}{2} \sqrt{t^2 - k^2} \right) \tag{A2.6}$$

from which follows that

$$\begin{aligned}
 L^{-1} \left\{ \exp(-k \sqrt{s} \sqrt{s+a}) \right\} &= -\frac{\partial}{\partial k} \left[\theta(t-k) e^{-\frac{at}{2}} I_0 \left(\frac{a}{2} \sqrt{t^2 - k^2} \right) \right] = \\
 &= e^{-\frac{at}{2}} \left[\delta(t-k) I_0 \left(\frac{a}{2} \sqrt{t^2 - k^2} \right) + \theta(t-k) \frac{\frac{ak}{2} I_1 \left(\frac{a}{2} \sqrt{t^2 - k^2} \right)}{\sqrt{t^2 - k^2}} \right]
 \end{aligned} \tag{A2.7}$$

The Heaviside and Dirac function are null unless $k = t$, and therefore, k in (A2.6) and (A2.7) must be real.

By substituting (A2.7) in (A2.5) one gets

$$\begin{aligned}
 L^{-1} \left\{ \frac{\mu_0}{\pi \gamma_g^2} Int_1 \right\} &\stackrel{k=2b_i y}{=} \frac{\mu_0}{\pi} \frac{e^{-\frac{at}{2}}}{2b_i} \left[\int_0^\infty \delta(t-k) \sqrt{1 + \frac{k^2}{4b_i^2}} I_0 \left(\frac{a}{2} \sqrt{t^2 - k^2} \right) dk + \right. \\
 &\quad \left. + \int_0^\infty \theta(t-k) \sqrt{1 + \frac{k^2}{4b_i^2}} \frac{\frac{ak}{2} I_1 \left(\frac{a}{2} \sqrt{t^2 - k^2} \right)}{\sqrt{t^2 - k^2}} dk \right]
 \end{aligned} \tag{A2.8}$$

Hence, being $I_0(0) = 1$

$$L^{-1} \left\{ \frac{\mu_0}{\pi \gamma_g^2} Int_1 \right\} \stackrel{k=2b_i y}{=} \frac{\mu_0}{\pi} \frac{e^{-\frac{at}{2}}}{2b_i} \left[\sqrt{1 + \frac{t^2}{4b_i^2}} + \int_0^t \frac{ak}{2} \sqrt{1 + \frac{k^2}{4b_i^2}} \frac{I_1 \left(\frac{a}{2} \sqrt{t^2 - k^2} \right)}{\sqrt{t^2 - k^2}} dk \right] \tag{A2.9}$$

And finally

$$\begin{aligned}
 L^{-1} \left\{ \frac{Z'_{g,ii}(s)}{s} \right\} &= \frac{\mu_0}{\pi} L^{-1} \left\{ \int_0^{\infty} \frac{\exp(-2h_t x)}{\sqrt{x^2 + \gamma_g^2} + x} dx \right\} = \\
 &= \frac{\mu_0}{\pi} \frac{e^{-\frac{at}{2}}}{2b_i} \left[\sqrt{1 + \frac{t^2}{4b_i^2}} + \int_0^t \frac{ak}{2} \sqrt{1 + \frac{k^2}{4b_i^2}} \frac{I_1 \left(\frac{a}{2} \sqrt{t^2 - k^2} \right)}{\sqrt{t^2 - k^2}} dk \right] - \frac{\mu_0}{\pi} \frac{1}{4b_i^2 a} (1 - e^{-at}) \quad (A2.10)
 \end{aligned}$$

The integral presents some numerical instability issues at very late times (more than 10 μ s for the physical cases considered so far); therefore we rewrite it as follows:

$$\int_0^t \frac{ak}{2} \sqrt{1 + \frac{k^2}{4b_i^2}} \frac{I_1 \left(\frac{a}{2} \sqrt{t^2 - k^2} \right)}{\sqrt{t^2 - k^2}} dk \stackrel{x=k/t}{=} \frac{at}{2} \int_0^1 x \sqrt{1 + x^2} \frac{t^2}{4b_i^2} \frac{I_1 \left(\frac{at}{2} \sqrt{1 - x^2} \right)}{\sqrt{1 - x^2}} dx$$

One can bring variable x inside the square root, so that the integrand becomes an even function:

$$\frac{at}{4} \int_{-1}^1 \sqrt{x^2 + x^4} \frac{t^2}{4b_i^2} \frac{I_1 \left(\frac{at}{2} \sqrt{1 - x^2} \right)}{\sqrt{1 - x^2}} dx$$

The integration can now be performed by using Chebyshev-Gauss quadrature formula:

$$\begin{aligned}
 \int_{-1}^1 \frac{f(x)}{\sqrt{1 - x^2}} dx &= \frac{\pi}{n} \sum_{i=1}^n f \left(\cos \frac{(2i-1)\pi}{2n} \right) \\
 f(x) &= \sqrt{x^2 + x^4} \frac{t^2}{4b_i^2} I_1 \left(\frac{at}{2} \sqrt{1 - x^2} \right)
 \end{aligned}$$

To avoid numerical instabilities at late times one can include the exponential $\exp(-at/2)$ inside the integral and we multiply and divide for the coefficient $\exp(-at/2\sqrt{1-x^2})$:

$$f(x) = \sqrt{x^2 + x^4} \frac{t^2}{4b_i^2} I_1 \left(\frac{at}{2} \sqrt{1 - x^2} \right) e^{-at/2} \frac{e^{-at/2\sqrt{1-x^2}}}{e^{-at/2\sqrt{1-x^2}}} = \sqrt{x^2 + x^4} \frac{t^2}{4b_i^2} I_1 \left(\frac{at}{2} \sqrt{1 - x^2} \right) e^{-at/2\sqrt{1-x^2}} \frac{e^{-at/2}}{e^{-at/2\sqrt{1-x^2}}}$$

which allows for the use of more accurate routines available for the function $I_1 \left(\frac{at}{2} \sqrt{1 - x^2} \right) e^{-at/2\sqrt{1-x^2}}$ rather than evaluate the Bessel and the exponential separately (see Abramowitz).

Off-diagonal elements

Again the integral can be split in two parts.

$$Z'_{g,ii}(s) = \frac{s\mu_0}{\pi} \int_0^{\infty} \frac{e^{-(h_i+h_j)x}}{\sqrt{x^2 + \gamma_g^2} + x} \cos(r_{ij}x) dx = \frac{s\mu_0}{\pi\gamma_g^2} (Int_1 - Int_2) \quad (A2.11)$$

and as the inverse transform of the second one is trivial is left to the reader.

By using $\hat{b}_{ij} = \sqrt{\mu_0\epsilon_0\epsilon_{rg}} \left(\frac{h_i + h_j}{2} + j \frac{r_{ij}}{2} \right) = \sqrt{\mu_0\epsilon_0\epsilon_{rg}} \hat{h}_{ij}$, as done so far, the first integral can be rewritten as

$$L^{-1} \left\{ \frac{\mu_0}{\pi\gamma_g^2} Int_1 \right\} = \frac{\mu_0}{\pi} \operatorname{Re} \left\{ \int_0^{\infty} \exp(-2\hat{h}_{ij}\gamma_g y) \sqrt{1+y^2} dy \right\} \quad (A2.12)$$

Setting $k = 2\hat{b}_{ij}y$ and reminding that k must be real, lead to a semi-infinite integral of the real variable k , letting y become the complex variable $k/2\hat{b}_{ij}$. One can now use again (A2.7) to evaluate the inverse Laplace transform of the exponential, and (A2.12) becomes

$$\begin{aligned} L^{-1} \left\{ \frac{\mu_0}{\pi\gamma_g^2} Int_1 \right\} & \stackrel{k=2\hat{b}_{ij}y}{=} \operatorname{Re} \left\{ \frac{\mu_0}{\pi} \frac{e^{-\frac{at}{2}}}{2\hat{b}_{ij}} \left[\int_0^{\infty} \delta(t-k) \sqrt{1 + \frac{k^2}{4\hat{b}_{ij}^2}} I_0 \left(\frac{a}{2} \sqrt{t^2 - k^2} \right) dk + \right. \right. \\ & \left. \left. + \int_0^{\infty} \theta(t-k) \sqrt{1 + \frac{k^2}{4\hat{b}_{ij}^2}} \frac{ak}{2} \frac{I_1 \left(\frac{a}{2} \sqrt{t^2 - k^2} \right)}{\sqrt{t^2 - k^2}} dk \right] \right\} = \\ & = \frac{\mu_0}{\pi} \operatorname{Re} \left\{ \frac{e^{-\frac{at}{2}}}{2\hat{b}_{ij}} \left[\sqrt{1 + \frac{t^2}{4\hat{b}_{ij}^2}} + \int_0^t \frac{ak}{2} \sqrt{1 + \frac{k^2}{4\hat{b}_{ij}^2}} \frac{I_1 \left(\frac{a}{2} \sqrt{t^2 - k^2} \right)}{\sqrt{t^2 - k^2}} dk \right] \right\} \end{aligned} \quad (A2.13)$$

Finally, the inverse Laplace transform for the off-diagonal elements reads:

$$\begin{aligned}
 L^{-1} \left\{ \frac{Z'_{g,ij}(s)}{s} \right\} &= \frac{\mu_0}{\pi} L^{-1} \left\{ \int_0^{\infty} \frac{e^{-(h_i+h_j)x}}{\sqrt{x^2 + \gamma_g^2} + x} \cos(r_{ij}x) dx \right\} = \\
 &= \frac{\mu_0}{\pi} \operatorname{Re} \left\{ \frac{e^{-\frac{at}{2}}}{2\hat{b}_{ij}} \left[\sqrt{1 + \frac{t^2}{4\hat{b}_{ij}^2}} + \int_0^t \frac{ak}{2} \sqrt{1 + \frac{k^2}{4\hat{b}_{ij}^2}} \frac{I_1\left(\frac{a}{2}\sqrt{t^2 - k^2}\right)}{\sqrt{t^2 - k^2}} dk \right] \right\} + \\
 &- \frac{\mu_0}{\pi} \frac{(h_1 + h_2)^2 - r_{ij}^2}{\left[(h_1 + h_2)^2 + r_{ij}^2 \right]^2} \frac{1}{\mu_0 \varepsilon_g \cdot a} (1 - e^{-at})
 \end{aligned} \tag{A2.14}$$

Buried Cables – Integral component

The procedure is similar to the case of overhead lines

$$L^{-1} \left\{ \frac{J_{ij}(s)}{s} \right\} = L^{-1} \left\{ \frac{\mu_0}{\pi} \int_0^{\infty} \frac{\exp\left(-2h_{ij}\sqrt{x^2 + \gamma_g^2}\right)}{\sqrt{x^2 + \gamma_g^2} + x} \cos(r_{ij}x) dx \right\} = \frac{\mu_0}{\pi} L^{-1} \left\{ \frac{1}{\gamma_g^2} (Int_1 - Int_2) \right\} \tag{A2.15}$$

where, after the same substitution as before, the two integral read:

$$\begin{aligned}
 Int_1 &= \gamma_g^2 \operatorname{Re} \left\{ \int_0^{\infty} \exp \left[-2h_i \left(\sqrt{1 + y^2} + j \frac{yr_i}{2h_i} \right) \gamma_g \right] \sqrt{1 + y^2} dy \right\} \\
 Int_2 &= \gamma_g^2 \operatorname{Re} \left\{ \int_0^{\infty} \exp \left[-2h_i \left(\sqrt{1 + y^2} + j \frac{yr_i}{2h_i} \right) \gamma_g \right] y dy \right\}
 \end{aligned} \tag{A2.16}$$

This time, the substitution to be performed in order to make possible the inversion through formula (A2.7), is the following

$$k = 2b_i \left(\sqrt{1 + y^2} + j \frac{yr_i}{2h_i} \right) \tag{A2.17}$$

from which, after some mathematical manipulation, one gets:

$$y(k) = \frac{-jkr_{ij} + 2\sqrt{h_{ij}^2 k^2 - b_{ij}^2 (4h_{ij}^2 + r_{ij}^2)}}{\sqrt{\mu_0 \varepsilon_g} (4h_{ij}^2 + r_{ij}^2)} \tag{A2.18}$$

Following the same procedure adopted for the overhead lines one gets the final expression for the inverse Laplace transform of the integral J_{ij}

$$\begin{aligned}
 L^{-1} \left[\frac{J_{ij}(s)}{s} \right] &= L^{-1} \left[\frac{\mu_0}{\pi} \int_0^{\infty} \frac{\exp(-2h_{ij}\sqrt{x^2 + \gamma_g^2})}{\sqrt{x^2 + \gamma_g^2} + x} \cos(r_{ij}x) dx \right] = \\
 &= \frac{\mu_0}{\pi} \frac{e^{-\frac{at}{2}}}{2b_{ij}} \theta(t - 2b_{ij}) \operatorname{Re} \left\{ \left[\sqrt{1 + y^2(t)} - y(t) \right] \left[\frac{y(t)}{\sqrt{1 + y^2(t)}} + j \frac{r_{ij}}{2h_{ij}} \right]^{-1} \right. \\
 &\quad \left. + \int_{2b_{ij}}^t \left(\sqrt{1 + y^2(k)} - y(k) \right) \left[\frac{y(k)}{\sqrt{1 + y^2(k)}} + j \frac{r_{ij}}{2h_{ij}} \right]^{-1} \frac{\frac{ak}{2} I_1 \left(\frac{a}{2} \sqrt{t^2 - k^2} \right)}{\sqrt{t^2 - k^2}} dk \right\}
 \end{aligned} \tag{A2.19}$$

To avoid numerical issues, one should first evaluate the real part of the function being integrated.

Buried Cables – Bessel component

Let us consider the integral representation of the modified Bessel Function of the Second Kind (Abramowitz & Stegun, 1964) eq. 9.6.24 (Note that $|\arg(z)| < \pi/2$ is satisfied by the fact that the ILT integration path lays on the right semi-plane, $\operatorname{Re}(s) > 0$)

$$L^{-1} \left[\frac{\mu_0}{2\pi} K_0(\gamma_g d_{ij}) \right] = \frac{\mu_0}{2\pi} L^{-1} \left[\int_0^{\infty} \exp(-d_{ij}\gamma_g \cosh(x)) dx \right] \tag{A2.20}$$

The procedure is the same as before, but the substitution to be performed is the following

$$k = d_{ij} \sqrt{\mu_0 \varepsilon_g} \cosh(x) \tag{A2.21}$$

This leads to the final expression for the inverse Laplace transform of the difference between the two Bessel functions

$$\begin{aligned}
 & \frac{\mu_0}{2\pi} L^{-1} \left[\mathbf{K}_0(\gamma_g d_{ij}) - \mathbf{K}_0(\gamma_g D_{ij}) \right] = \\
 & \frac{\mu_0}{2\pi} e^{-\frac{at}{2}} \theta(t - d_{ij} \sqrt{\mu_0 \epsilon_g}) \left[\frac{1}{\sqrt{t^2 - d_{ij}^2 \mu_0 \epsilon_g}} + \int_{d_{ij} \sqrt{\mu_0 \epsilon_g}}^t \frac{\frac{ak}{2} I_1\left(\frac{a}{2} \sqrt{t^2 - k^2}\right)}{\sqrt{t^2 - k^2}} \frac{1}{\sqrt{k^2 - d_{ij}^2 \mu_0 \epsilon_g}} dk \right] + \\
 & -\frac{\mu_0}{2\pi} e^{-\frac{at}{2}} \theta(t - D_{ij} \sqrt{\mu_0 \epsilon_g}) \left[\frac{1}{\sqrt{t^2 - D_{ij}^2 \mu_0 \epsilon_g}} + \int_{D_{ij} \sqrt{\mu_0 \epsilon_g}}^t \frac{\frac{ak}{2} I_1\left(\frac{a}{2} \sqrt{t^2 - k^2}\right)}{\sqrt{t^2 - k^2}} \frac{1}{\sqrt{k^2 - D_{ij}^2 \mu_0 \epsilon_g}} dk \right]
 \end{aligned} \tag{A2.22}$$

6. References

- Abramowitz, M. & Stegun, I. (1964). *Handbook of mathematical functions*.
- Agrawal, A.K., Price, H.J. & Gurbaxani, S.H. (1980). Transient Response of Multiconductor Transmission Lines Excited by a Nonuniform Electromagnetic Field. *IEEE Transactions on Electromagnetic Compatibility*. EMC-22 (2). p.pp. 119–129.
- Akbari, M., Sheshyekani, K., Pirayesh, A., Rachidi, F., Paolone, M., A., B., Nucci, C.A., Borghetti, A. & Nucci, C.A. (2013). Evaluation of Lightning Electromagnetic Fields and Their Induced Voltages on Overhead Lines Considering the Frequency Dependence of Soil Electrical Parameters. *IEEE Transactions on Electromagnetic Compatibility*. 55 (6). p.pp. 1210–1219.
- Allan J. Macleod (1996). Algorithm 757, MISCFUN: A software package to compute uncommon special functions. *ACM Transactions on Mathematical Software*. 22 (3). p.pp. 288–301.
- Allan J. Macleod (1993). Chebyshev Expansions for Modified Struve and Related Functions. *Mathematics of Computation*. 60 (202). p.pp. 735–747.
- Anderson, R.B. & Eriksson, A.J. (1980). Lightning parameters for engineering applications. *ELECTRA*. 69. p.pp. 65–102.
- Andreotti, A., Martinis, U. De, Maffucci, A. & Verolino, L. (1998). Lightning induced overvoltages on lossy multiconductor power lines with non linear loads. In: *24th International Conference on Lightning Protection*. 1998, Birmingham, England.
- Andreotti, A., Pierno, A. & Rakov, V.A. (2015). A New Tool for Calculation of Lightning-Induced Voltages in Power Systems—Part I: Development of Circuit Model. *IEEE Transactions on Power Delivery*. 30 (1). p.pp. 326–333.
- Andreotti, A., Pierno, A., Rakov, V.A. & Verolino, L. (2013). Analytical Formulations for Lightning-Induced Voltage Calculations. *IEEE Transactions on Electromagnetic Compatibility*. 55 (1). p.pp. 109–123.
- Araneo, R. & Celozzi, S. (2001). Direct time-domain analysis of transmission lines above a lossy ground. *IEE Proceedings - Science, Measurement and Technology*. 148 (2). p.p. 73.
- Barbosa, C.F. & Paulino, J.O.S. (2010). A time-domain formula for the horizontal electric field at the earth surface in the vicinity of lightning. *IEEE Transactions on Electromagnetic Compatibility*. 52 (3).
- Berger, K., Anderson, R.B. & Kroninger, H. (1975). Parameters of lightning flashes. *Electra*. 41. p.pp. 23–37.
- Berger, K. & Garbagnati, E. (1984). Lightning Current Parameters. Results Obtained in Switzerland and Italy. In: *Proc. URSI Conf.* 1984, Florence, Italy.
- Bermudez, J.L., Pena-Reyes, C.A., Rachidi, F. & Heidler, F. (2002). Use of genetic algorithms to extract primary lightning current parameters. In: *Proceedings of Int. Symp. EMC Europe*. 2002.

- Borghetti, A., Gutierrez, J.A., Nucci, C.A., Paolone, M., Petrache, E. & Rachidi, F. (2004). Lightning-induced voltages on complex distribution systems: models, advanced software tools and experimental validation. *Journal of Electrostatics*. 60 (2-4). p.pp. 163-174.
- Borghetti, A., Napolitano, F., Nucci, C.A., Martinez, M.L.B., Lopes, G.P. & Uchoa, J.I.L. (2012). Protection systems against lightning-originated overvoltages in resonant grounded power distribution systems. In: *31st International Conference on Lightning Protection*. 2012, Vienna, Austria.
- Borghetti, A., Napolitano, F., Nucci, C.A., Paolone, M. & Rachidi, F. (2013). Use of the full-wave Finite Element Method for the numerical electromagnetic. *Electric Power Systems Research*. 94. p.pp. 24-29.
- Borghetti, A., Nucci, C.A. & Paolone, M. (2007). An improved procedure for the assessment of overhead line indirect lightning performance and its comparison with the IEEE Std. 1410 method. *IEEE Transactions on Power Delivery*. 22 (1). p.pp. 684-692.
- Borghetti, A., Nucci, C.A. & Paolone, M. (2009). Indirect-Lightning Performance of Overhead Distribution Networks With Complex Topology. *IEEE Transactions on Power Delivery*. 24 (4). p.pp. 2206-2213.
- Borghetti, A., Dos Santos, G.J.G., Fagundes, D.R., Lopes, G.P., Martinez, M.L.B., Napolitano, F., Nucci, C.A., Tossani, F., Fagundes, D.R., Lopes, G.P. & Martinez, M.L.B. (2014). Indirect Lightning Performance of a Real Distribution Network With Focus on Transformer Protection. In: *32nd International Conference on Lightning Protection*. 2014, Shanghai, China.
- Bruce, C.E.R. & Golde, R.H. (1941). The Lightning Discharge. *J. Inst. Electr. Eng.* 88. p.pp. 487-505.
- Carson, J.R. (1926). Wave Propagation in Overhead Wires with Ground Return. *Bell System Technical Journal*. (5). p.pp. 539-554.
- Chandrasekaran, K. & Puneekar, G.S. (2014). Use of Genetic Algorithm to Determine Lightning Channel-Base Current-Function Parameters. *IEEE Transactions on Electromagnetic Compatibility*. 56 (1). p.pp. 235-238.
- Chen, J. & Zhu, M. (2014). Calculation of Lightning Flashover Rates of Overhead Distribution Lines Considering Direct and Indirect Strokes. *IEEE Transactions on Electromagnetic Compatibility*. 56 (3). p.pp. 668-674.
- Chowdhuri, P. (1990). Lightning-induced voltages on multiconductor overhead lines. *IEEE Transactions on Power Delivery*. 5 (2). p.pp. 658-667.
- Chowdhuri, P. (1969). Voltages induced on overhead multiconductor lines by lightning strokes. *Proc IEE*. 116 (4). p.pp. 561-565.
- CIGRE WG C4.407 (2013). *Lightning parameters for engineering applications (TB 549)*. TB 549. Paris, France.
- Cigré Working Group 33.01 (1991). *Guide to procedures for estimating the lightning performance of transmission lines (TB 63)*. Paris: CIGRE.
- Cinieri, E. & Fumi, A. (1979). Effetto della presenza di più conduttori e di funi di guardia sulle sovratensioni atmosferiche indotte nelle linee elettriche. *L'Energia Elettrica*. 11-12. p.pp. 595-601.
- Cinieri, E. & Muzi, F. (1996). Lightning Induced Overvoltages . Improvement in Quality of Service in MV Distribution Lines by Addition of Shield Wires. *IEEE Transactions on Power Delivery*. 11 (1).

- De Conti, A., Perez, E., Soto, E., Silveira, F.H., Visacro, S.S. & Torres, H. (2010). Calculation of Lightning-Induced Voltages on Overhead Distribution Lines Including Insulation Breakdown. *IEEE Transactions on Power Delivery*. 25 (4). p.pp. 3078–3084.
- De Conti, A. & Visacro, S. (2007). Analytical representation of single- and double-peaked lightning current waveforms. *IEEE Transactions on Electromagnetic Compatibility*. 49 (2). p.pp. 448–451.
- Cooray, V. (2010). Horizontal Electric Field Above- and Underground Produced by Lightning Flashes. *IEEE Transactions on Electromagnetic Compatibility*. 52 (4). p.pp. 936–943.
- Cooray, V. (1992). Horizontal fields generated by return strokes. *Radio Science*. 27 (4). p.pp. 529–537.
- Cooray, V. (2008). On the accuracy of several approximate theories used in quantifying the propagation effects on lightning generated electromagnetic fields. *Antennas and Propagation, IEEE Transactions on*. 56 (7). p.pp. 1960–1967.
- Cooray, V. (2002). Some considerations on the Cooray-Rubinstein formulation used in deriving the horizontal electric field of lightning return strokes over finitely conducting ground. *IEEE Transactions on Electromagnetic Compatibility*. 44 (4). p.pp. 560–566.
- Cooray, V. & De la Rosa, F. (1986). Shapes and amplitudes of the initial peaks of lightning-induced voltage in power lines over finitely conducting earth: Theory and comparison with experiment. *IEEE Transactions on Antennas and Propagation*. 34 (1). p.pp. 88–92.
- Darveniza, M. (2007). A practical extension of Rusck's formula for maximum lightning-induced voltages that accounts for ground resistivity. *IEEE Transactions on Power Delivery*. 22 (1). p.pp. 605–612.
- Darveniza, M. & Vlastos, A.E. (1988). The generalized integration method for predicting impulse volt-time characteristics for non-standard wave shapes—a theoretical basis. *IEEE Transactions on Electrical Insulation*. 23 (3). p.pp. 373–381.
- Delfino, F., Procopio, R. & Rossi, M. (2008a). Lightning return stroke current radiation in presence of a conducting ground: 1. Theory and numerical evaluation of the electromagnetic fields. *Journal of Geophysical Research*. 113 (D5).
- Delfino, F., Procopio, R., Rossi, M., Rachidi, F. & Nucci, C.A. (2008b). Lightning return stroke current radiation in presence of a conducting ground: 2. Validity assessment of simplified approaches. *Journal of Geophysical Research*. 113 (D5).
- Diendorfer, G. (1990). Induced voltage on an overhead line due to nearby lightning. *IEEE Transactions on Electromagnetic Compatibility*. 32 (4). p.pp. 292–299.
- Eriksson, A., Stringfellow, M. & Meal, D. (1982). Lightning - Induced Overvoltages on Overhead Distribution Lines. *IEEE Transactions on Power Apparatus and Systems*. PAS-101 (4). p.pp. 960–968.
- Gary, C. (1976). Approche complète de la propagation multifilaire en haute fréquence par l'utilisation des matrices complexes. *EDF Bulletin de la direction des études et recherches*. B (3/4). p.pp. 5–20.
- Guerrieri, S., Ianoz, M., Nucci, C.A. & Rachidi, F. (1996). Lightning-induced voltages on an overhead line above a

- lossy ground: a sensitivity analysis. In: *23rd International Conference on Lightning Protection*. 1996, Florence, Italy.
- Gustav Doetsch (1974). *Introduction to the Theory and Application of the Laplace Transformation*. Springer-Verlag.
- Heidler, F. (1985). Analytische blitzstromfunktion zur LEMP-berechnung. In: *Proc. 18th Int. Conf. Lightning Protection*. 1985, pp. 63–66.
- Høidalen, H.K. (2003). Analytical formulation of lightning-induced voltages on multiconductor overhead lines above lossy ground. *IEEE Transactions on Electromagnetic Compatibility*. 45 (1). p.pp. 92–100.
- IEEE Std 1410-2010 (2011). IEEE guide for improving the lightning performance of electric power overhead distribution lines. *IEEE Std 1410-2010 (Revision of IEEE Std 1410-2004)*. p.pp. 1–73.
- Ishii, M., Michishita, K., Hongo, Y. & Oguma, S. (1994). Lightning-induced voltage on an overhead wire dependent on ground conductivity. *IEEE Transactions on Power Delivery*. 9 (1). p.pp. 109–118.
- Jacob, P.B., Grzybowski, S. & Ross, E.R. (1991). An estimation of lightning insulation level of overhead distribution lines. *IEEE Transactions on Power Delivery*. 6 (1). p.pp. 384–390.
- Javor, V. (2012). Multi-peaked functions for representation of lightning channel-base currents. In: *31st International Conference on Lightning Protection*. 2012, Vienna, Austria.
- Javor, V. & Rancic, P.D. (2011). A channel-base current function for lightning return-stroke modeling. *IEEE Transactions on Electromagnetic Compatibility*. 53 (1). p.pp. 245–249.
- Jones, R.D. (1977). On the Use of Tailored Return-Stroke Current Representations to Simplify the Analysis of Lightning Effects on Systems. *IEEE Transactions on Electromagnetic Compatibility*. EMC-19 (2). p.pp. 95–96.
- Kannu, P.D. & Thomas, M.J. (2005). Lightning induced voltages on multiconductor power distribution line. *IEE Proc.-Gener. Transm. Distrib.* 152 (6).
- Liew, A.C. & Mar, S.C. (1986). Extension of the Chowdhuri-Gross Model for Lightning Induced Voltage on Overhead Lines. *IEEE Power Engineering Review*. PER-6 (4). p.pp. 51–51.
- Lima, S. De & Portela, C. (2007). Inclusion of Frequency-Dependent Soil Parameters in Transmission-Line Modeling. *IEEE Transactions on Power Delivery*. 22 (1). p.pp. 492–499.
- Lopes, G.P., Martinez, M.L.B., Borghetti, A., Napolitano, F., Nucci, C.A., Uchoa, J.I.L., Dos Santos, G.J.G. & Fagundes, D.R. (2013). A procedure to evaluate the risk of failure of distribution transformers insulation due to lightning induced voltages. *22nd International Conference and Exhibition on Electricity Distribution (CIRED 2013)*. 2013 (615 CP). p.pp. 1484–1484.
- Loyka, S. & Kouki, A. (2001). Early-time behavior of the ground transient resistance of overhead lines. In: *2001 IEEE International Symposium on Electromagnetic Compatibility*. 2001, IEEE, pp. 222–226.
- Loyka, S.L. (1999). On calculation of the ground transient resistance of overhead lines. *IEEE Transactions on Electromagnetic Compatibility*. 41 (3). p.pp. 193–195.
- Luke, Y.L. (1975). *Mathematical Functions and their Approximations*. New York: Academic Press Inc.

- Master, M. & Uman, M. (1984). Lightning Induced Voltages on Power Lines: Theory. *IEEE Transactions on Power Apparatus and Systems*. PAS-103 (9). p.pp. 2502–2518.
- Master, M.J. & Uman, M.A. (1983). Transient electric and magnetic fields associated with establishing a finite electrostatic dipole. *American Journal of Physics*. 51. p.p. 118.
- Mikropoulos, P.N. & Tsovilis, T.E. (2013). Statistical method for the evaluation of the lightning performance of overhead distribution lines. *IEEE Transactions on Dielectrics and Electrical Insulation*. 20 (1). p.pp. 202–211.
- Mikropoulos, P.N., Tsovilis, T.E. & Koutoula, S.G. (2014). Lightning Performance of Distribution Transformer Feeding GSM Base Station. *IEEE Transactions on Power Delivery*. 29 (6). p.pp. 2570–2579.
- Miyazaki, T. & Okabe, S. (2009). A detailed field study of lightning stroke effects on distribution lines. *IEEE Transactions on Power Delivery*. 24 (1). p.pp. 352–359.
- Munhoz Rojas, P.E. (2009). The Effect of Discontinuities in a Multiconductor Line on Lightning-Induced Voltages. *IEEE Transactions on Electromagnetic Compatibility*. 51 (1). p.pp. 53–66.
- Nakada, K., Sugimoto, H. & Yokoyama, S. (2003). Experimental facility for investigation of lightning performance of distribution lines. *IEEE Transactions on Power Delivery*. 18 (1). p.pp. 253–257.
- Napolitano, F. (2011). An Analytical Formulation of the Electromagnetic Field Generated by Lightning Return Strokes. *IEEE Transactions on Electromagnetic Compatibility*. 53 (1). p.pp. 108–113.
- Napolitano, F., Borghetti, A., Nucci, C.A., Martinez, M.L.B., Lopes, G.P. & Dos Santos, G.J.G. (2014). Protection against lightning overvoltages in resonant grounded power distribution networks. *Electric Power Systems Research*. 113. p.pp. 121–128.
- Napolitano, F., Borghetti, A., Nucci, C.A.A., Paolone, M., Rachidi, F., Mahseredjian, J., Mahserejian, J. & Mahseredjian, J. (2008). An advanced interface between the LIOV code and the EMTP-RV. In: *29th Int. Conf. on Lightning Protection, ICLP*. 2008, Uppsala, Sweden, pp. 1–12.
- Napolitano, F., Tossani, F., Nucci, C.A. & Rachidi, F. (2015). On the Transmission-Line Approach for the Evaluation of LEMP Coupling to Multiconductor Lines. *IEEE Transactions on Power Delivery*. 30 (2). p.pp. 861–869.
- Newman, J.N. (1984). Approximations for the Bessel and Struve functions. *Mathematics of Computation*. 43 (168). p.pp. 551–551.
- Nucci, C.A., Bardazzi, V., Iorio, R., Mansoldo, A. & Porrino, A. (1994). A code for the calculation of lightning-induced overvoltages and its interface with the electromagnetic transient program. In: *22nd International Conference on Lightning Protection*. 1994, Budapest, Hungary.
- Nucci, C.A., Diendorfer, G., Uman, M.A., Rachidi, F., Ianoz, M. & Mazzetti, C. (1990). Lightning return stroke current models with specified channel-base current: a review and comparison. *Journal of Geophysical Research*. 95 (D12). p.pp. 20395–20408.
- Nucci, C.A., Mazzetti, C., Rachidi, F. & Ianoz, M. (1988). On lightning return stroke models for LEMP calculations. In: *19th International Conference on Lightning Protection*. 1988, Graz, Austria.

- Nucci, C.A. & Rachidi, F. (1989). Experimental validation of a modification to the transmission line model for LEMP calculations. In: *8th Int. Zurich Symp. EMC. 1989, Zurich; Switzerland*, pp. 389–394.
- Nucci, C.A. & Rachidi, F. (2014). Interaction of electromagnetic fields generated by lightning with overhead electrical networks. In: V. Cooray (ed.). *The Lightning Flash. 2nd Edition*. IET - Power and Energy Series 69, pp. 559–610.
- Nucci, C.A. & Rachidi, F. (2003). Interaction of electromagnetic fields with electrical networks generated by lightning. In: V. Cooray (ed.). *The Lightning Flash: Physical and Engineering Aspects*. IEE - Power and Energy Series 34, pp. 425–478.
- Nucci, C.A. & Rachidi, F. (1995). On the contribution of the Electromagnetic field components in field-to-transmission lines interaction. *IEEE Transactions on Electromagnetic Compatibility*. 37 (4). p.pp. 505–508.
- Nucci, C.A., Rachidi, F., Ianoz, M. & Mazzetti, C. (1995). Comparison of two coupling models for lightning-induced overvoltage calculations. *IEEE Transactions on Power Delivery*. 10 (1). p.pp. 330–339.
- Nucci, C.A., Rachidi, F., Ianoz, M. V & Mazzetti, C. (1993). Lightning-Induced Voltages on Overhead Lines. *IEEE Transactions on Electromagnetic Compatibility*. 35 (1). p.pp. 75–86.
- Nucci, C.A., Rachidi, F. & Rubinstein, M. (2012). Interaction of lightning-generated electromagnetic fields with overhead and underground cables. In: V. Cooray (ed.). *Lightning Electromagnetics*. pp. 667–718.
- Oliver, J. (1977). An error analysis of the modified Clenshaw method for evaluating Chebyshev and Fourier series. *Journal of the IMA*. 20. p.pp. 379–391.
- Orzan, D. (1997). Time-Domain Low Frequency Approximation for the Off-Diagonal Terms of the Ground Impedance Matrix. *IEEE Transactions on Electromagnetic Compatibility*. 9375 (February). p.p. 9375.
- Orzan, D., Baraton, P., Ianoz, M. & Rachidi, F. (1996). Comparaison entre deux approches pour traiter le couplage entre un champ EM et des réseaux de lignes. In: *8ème Colloque International sur la Compatibilité Electromagnétique*. 1996.
- Paolone, M., Nucci, C.A., Petrache, E. & Rachidi, F. (2004). Mitigation of Lightning-Induced Overvoltages in Medium Voltage Distribution Lines by Means of Periodical Grounding of Shielding Wires and of Surge Arresters: Modeling and Experimental Validation. *IEEE Transactions on Power Delivery*. 19 (1). p.pp. 423–431.
- Paolone, M., Nucci, C.A. & Rachidi, F. (2001). A new finite difference time domain scheme for the evaluation of lightning induced overvoltages on multiconductor overhead lines. In: *5th international conference on Power system transients, Rio de Janeiro, Brazil*. 2001.
- Paolone, M., Rachidi, F., Borghetti, A., Nucci, C.A., Rubinstein, M., Rakov, V.A. & Uman, M.A. (2009). Lightning Electromagnetic Field Coupling to Overhead Lines: Theory, Numerical Simulations, and Experimental Validation. *IEEE Transactions on Electromagnetic Compatibility*. 51 (3). p.pp. 532–547.
- Paulino, J.O.S., Barbosa, C.F., Lopes, I.J.S. & Boaventura, W.C. (2015). Assessment and analysis of indirect lightning performance of overhead lines. *Electric Power Systems Research*. 118. p.pp. 55–61.

- Perez, E., Delgadillo, A., Urrutia, D. & Torres, H. (2007). Optimizing the Surge Arresters Location for Improving Lightning Induced Voltage Performance of Distribution Network. In: *2007 IEEE Power Engineering Society General Meeting*. June 2007, IEEE, pp. 1–6.
- Petrache, E., Rachidi, F., Paolone, M., Nucci, C.A.A., Rakov, V.A. & Uman, M.A. (2005). Lightning induced disturbances in buried cables - Part I: Theory. *IEEE Transactions on Electromagnetic Compatibility*. 47 (3). p.pp. 498–508.
- Piantini, A. & Janiszewski, J.M. (2009). Lightning-Induced Voltages on Overhead Lines—Application of the Extended Rusck Model. *IEEE Transactions on Electromagnetic Compatibility*. 51 (3). p.pp. 548–558.
- Piantini, A., Janiszewski, J.M., Borghetti, A., Nucci, C.A. & Paolone, M. (2007). A Scale Model for the Study of the LEMP Response of Complex Power Distribution Networks. *IEEE Transactions on Power Delivery*. 22 (1). p.pp. 710–720.
- Plummer, C.W., Goedde, G.L., Pettit, E.L., Godbee, J.S. & Hennessey, M.G. (1994). Reduction in distribution transformer failure rates and nuisance outages using improved lightning protection concepts. In: *Proceedings of IEEE/PES Transmission and Distribution Conference*. 1994, IEEE, pp. 411–416.
- Pollaczek, F. (1931). On the field produced by an infinitely long wire carrying alternating current. *Elektrische Nachrichten Technik*. 3 (9). p.pp. 339–359.
- Pollaczek, F. (1926). Über das feld einer unendlichen langenwechsel stromdurchflossenen einfachleitung. *Elect. Nachr. Tech*. 3 (9). p.pp. 339–360.
- Prudnikov, A.P., Brychkov, Y.A. & Marichev, O.I. (1992). *Integrals and Series (vol.5: Inverse Laplace Transforms)*. Gordon & Breach (eds.). New York.
- Rachidi, F. (1993). Formulation of the field-to-transmission line coupling equations in terms of magnetic excitation field. *IEEE Transactions on Electromagnetic Compatibility*. 35 (3). p.pp. 404–407.
- Rachidi, F., Loyka, S.L., Nucci, C.A. & Ianoz, M. (2003). A new expression for the ground transient resistance matrix elements of multiconductor overhead transmission lines. *Electric Power Systems Research*. 65 (1). p.pp. 41–46.
- Rachidi, F. & Nucci, C.A. (1990). On the Master, Uman, Lin, Standler and the Modified Transmission Line lightning return stroke current models. *Journal of Geophysical Research*. 95.
- Rachidi, F., Nucci, C.A. & Ianoz, M. (1999). Transient Analysis of Multiconductor Lines Above a Lossy Ground. *IEEE Transactions on Power Delivery*. 14 (January 1999). p.pp. 294–302.
- Rachidi, F., Nucci, C.A., Ianoz, M. & Mazzetti, C. (1996). Influence of a lossy ground on lightning-induced voltages on overhead lines. *IEEE Transactions on Electromagnetic Compatibility*. 38 (3). p.pp. 250–264.
- Rachidi, F., Nucci, C.A.A., Ianoz, M., Mazzetti, C. & Rachidi et al (1997). Response of multiconductor power lines to nearby lightning return stroke electromagnetic fields. *IEEE Transactions on Power Delivery*. 12 (3). p.pp. 14041–1411.
- Rakov, V.A. & Uman, M.A. (1998). Review and evaluation of lightning return stroke models including some

- aspects of their application. *IEEE Transactions on Electromagnetic Compatibility*. 40 (4). p.pp. 403–426.
- Rubinstein, M. (1996). An Approximate Formula for the Calculation of the Horizontal Electric Field from Lightning at Close, Intermediate, and Long Range. *IEEE Transactions on Electromagnetic Compatibility*. 38 (3). p.pp. 531–535.
- Rubinstein, M., Tzeng, A.Y., Uman, M.A., Medelius, P.J. & Thomson, E.M. (1989). An experimental test of a theory of lightning-induced voltages on an overhead wire. *IEEE Transactions on Electromagnetic Compatibility*. 31 (4). p.pp. 376–383.
- Rusck, S. (1958a). Induced lightning overvoltages on power transmission lines with special reference to the overvoltage protection of low voltage networks. *Transactions of the Royal Institute of Technology*. (120). p.pp. 1–118.
- Rusck, S. (1958b). Induced lightning overvoltages on power transmission lines with special reference to the overvoltage protection of low voltage networks. *Transactions of the Royal Institute of Technology*. 120.
- Rusck, S. (1977). Protection of distribution lines. In: R. H. & Golde (eds.). *Lightning*. New York: Academic.
- Semlyen, A. (1981). Ground Return Parameters of Transmission Lines an Asymptotic Analysis for Very High Frequencies. *IEEE Transactions on Power Apparatus and Systems*. PAS-100 (3). p.pp. 1031–1038.
- Silveira, F.H., De Conti, A. & Visacro, S. (2014). Evaluation of Lightning-Induced Voltages over Lossy Ground with Frequency-dependent Soil Parameters. In: *32nd International Conference on Lightning Protection*. October 2014, Shanghai, China.
- Silveira, F.H., De Conti, A. & Visacro, S. (2011). Voltages Induced in Single-Phase Overhead Lines by First and Subsequent Negative Lightning Strokes: Influence of the Periodically Grounded Neutral Conductor and the Ground Resistivity. *IEEE Transactions on Electromagnetic Compatibility*. 53 (2). p.pp. 414–420.
- Sommerfeld, A. (1949). *Partial Differential Equations in Physics*. New York: Elsevier.
- Sommerfeld, A. (1909). Über die ausbreitung der wellen in der drahtlosen telegraphie. *Ann. Phys.* 28. p.pp. 665–665.
- Sunde, E.D.D. (1968). *Earth conduction effects in transmission systems*. D. Van Nostrand Company (ed.). New York: Dover publications.
- Taylor, C., Satterwhite, R. & Harrison, C. (1965). The response of a terminated two-wire transmission line excited by a nonuniform electromagnetic field. *IEEE Transactions on Antennas Propagation*. 13 (6). p.pp. 987–989.
- Tesche, F.M., Ianoz, M. & Karlsson, T. (1997). *EMC Analysis Methods and Computational Models*.
- Thang, T.H., Baba, Y., Member, S., Piantini, A., Member, S. & Rakov, V.A. (2015). Lightning-Induced Voltages in the Presence of Nearby Buildings: FDTD Simulation Versus Small-Scale Experiment. *IEEE Transactions on Electromagnetic Compatibility*. p.pp. 1–7.
- Timotin, A. (1967). Longitudinal transient parameters of a unifilar line with ground return. *Rev. Roum. Se. Techn., Electrotechn. et Energie*. 12 (4). p.pp. 523–535.
- Tossani, F., Napolitano, F., Borghetti, A., Nucci, C.A., Lopes, G.P., Martinez, M.L.B. & dos Santos, G.J.G. (2015a).

- Estimation of the influence of direct strokes on the lightning performance of overhead distribution lines. In: *2015 IEEE Eindhoven PowerTech*. June 2015, Endhoven: IEEE, pp. 1–7.
- Tossani, F., Napolitano, F., Rachidi, F. & Nucci, C.A. (2015b). An Improved Approach for the Calculation of the Transient Ground Resistance Matrix of Multiconductor Lines. *IEEE Transactions on Power Delivery*. PP. p.pp. 1–1.
- Vance, E. (1978). *Coupling to shielded cables*. Florida: R.E. Krieger Publishing Company.
- Visacro, S. & Alipio, R. (2012). Frequency Dependence of Soil Parameters: Experimental Results, Predicting Formula and Influence on the Lightning Response of Grounding Electrodes. *IEEE Transactions on Power Delivery*. 27 (2). p.pp. 927–935.
- Wait, J.R. (1997). Concerning the horizontal electric field of lightning. *IEEE Transactions on Electromagnetic Compatibility*. 39 (2). p.p. 186.
- Yokoyama, S. (1984). Calculation of Lightning-Induced Voltages on Overhead Multiconductor Systems. *IEEE Transactions on Power Apparatus and Systems*. PAS-103 (1). p.pp. 100–108.
- Yokoyama, S., Miyake, K. & Fukui, S. (1989). Advanced observations of lightning induced voltage on power distribution lines (II). *IEEE Transactions on Power Delivery*. 4 (4). p.pp. 2196–2203.
- Yokoyama, S., Miyake, K., Mitani, H. & Takanishi, A. (1983). Simultaneous Measurement of Lightning Induced Voltages with Associated Stroke Currents. *IEEE Power Engineering Review*. PER-3 (8). p.pp. 24–25.
- Yokoyama, S., Miyake, K., Mitani, H. & Yamazaki, N. (1986). Advanced Observations of Lightning-Induced Voltage on Power Distribution Lines. *IEEE Power Engineering Review*. PER-6 (4). p.pp. 40–41.
- Zeddani, A. & Degauque, P. (1990). Current and voltage induced on a telecommunication cable by a lightning stroke. In: R. L. Gardner (ed.). *Lightning Electromagnetics*. Hemisphere Publ. Corp., pp. 377–400.